Excitatory and inhibitory calcium activity during sleep

Dissertation

der Mathematisch-Naturwissenschaftlichen Fakultät

der Eberhard Karls Universität Tübingen

zur Erlangung des Grades eines

Doktors der Naturwissenschaften

(Dr. rer. nat.)

Vorgelegt von

Mag. rer. nat. Niels Niethard

aus Kirchheimbolanden (Rheinland-Pfalz)

Tübingen

2019

Gedruckt mit Genehmigung der Mathematisch-Naturwissenschaftlichen Fakultät der Eberhard Karls Universität Tübingen.

Tag der mündlichen Qualifikation:	20.12.2019
Dekan:	Prof. Dr. Wolfgang Rosenstiel
1. Berichterstatter:	Prof. Dr. Jan Born
2. Berichterstatter:	Prof. Dr. Hartmut Leuthold
3. Berichterstatter:	Prof. Dr. Dr. h.c. Onur Güntürkün

'Sleep is indeed a delicious invention!'

Heinrich Heine

Kurzfassung

Von der Schnecke über die Fliege und Echse bis hin zum Menschen, nahezu alle Organismen schlafen. Da der Organismus während dieser Phasen äußerst vulnerabel ist, muss Schlaf aus evolutionsbiologischer Sicht einer lebensnotwendigen Funktion dienen. Eine Funktion, die in den letzten Jahren zunehmend Beachtung gefunden hat, ist die potentielle Rolle des Schlafes für synaptische Plastizität. Hierbei hat die bisherige Forschung einerseits Belege für eine unspezifische, allgemeine Abschwächung der synaptischen Übertragungsstärke während des Schlafes gefunden, die möglicherweise der energieeffizienten Erhaltung der synaptischen Erregbarkeit dient. Andererseits untermauern viele Studien den positiven Effekt von Schlaf auf das Gedächtnis und die Verstärkung und Bildung neuer Synapsen während des Schlafs. Diese Befunde deuten auf eine komplexe, multidirektionale Dynamik der synaptischen Plastizität während des Schlafes hin.

Für exzitatorische Synapsen konnte bereits gezeigt werden, dass sich während des Schlafs die Expression der Glutamatrezeptoren - und somit die Stärke erregender synaptischer Verbindungen - verändert und stark von der jeweiligen intrazellulären Kalziumkonzentration abhängt. Neuronale Schaltkreise bestehen allerdings zu rund einem Drittel aus inhibitorischen Zellen, deren Rolle für die synaptische Plastizität während des Schlafs bisher nur wenig untersucht wurde.

Die vorliegende Arbeit zielt daher darauf ab, schlafspezifische Veränderungen der Aktivität sowohl von exzitatorischen Pyramidenzellen als auch von verschiedenen Untergruppen von inhibitorischen Zellen zu charakterisieren, um ein möglichst umfassendes Bild der neuronalen Schaltkreise während des Schlafs zu gewinnen. In insgesamt drei Studien wurde hierzu die Kalziumaktivität gentechnisch veränderter Mauslinien mithilfe der *in vivo* Zwei-Photonen-Mikroskopie im Schlaf- und im Wachzustand gemessen. Die gleichzeitige Aufzeichnung von EEG-Signalen ermöglichte zusätzlich die Klassifizierung verschiedener Schlafstadien und schlafspezifischer EEG-Wellen. Studie I konzentrierte sich auf schlafstadienspezifische Veränderungen und zeigte, dass die Aktivität der exzitatorischen Zellen während des Tiefschlafs (SWS) und während des paradoxen Schlafs (REM) stetig abnimmt, während die Aktivität der inhibitorischen, Parvalbumin-positiven Interneurone (PV-In) während des REM-Schlafes ansteigt.

Studie II untersuchte die Aktivität während verschiedener EEG-Rhythmen im Schlaf. Die hyperpolarisierte Phase der slow oscillation (SO) war von einer Zunahme der Aktivität der Somatostatin-positiven Interneurone (SOM-In) und einer gleichzeitigen Abnahme der PV-In Aktivität begleitet. Das entgegengesetzte Muster zeigte sich während der Schlaf-

Spindeln. Hier wiesen die PV-In erhöhte Kalziumaktivität auf, während die Aktivität der SOM-In unverändert blieb. Exzitatorische Zellen zeigten nur dann eine erhöhte Aktivität, wenn Schlaf-Spindeln gekoppelt mit SOs auftraten.

In Studie III wurden alle Zelltypen basierend auf ihrer Aktivität während der Schlaf-Spindeln gruppiert. Dies ermöglichte es zu testen, ob exzitatorische Zellen, die eine erhöhte Aktivität während der Schlaf-Spindeln aufweisen, ihre Erregbarkeit dauerhaft erhöhen. Diese Hypothese bestätigte sich. Darüber hinaus konnte festgestellt werden, dass die Erregbarkeit der Zellen, die während der Spindeln inaktiv sind, abnimmt.

Zusammengenommen zeigen die Ergebnisse, dass Schlaf durch einzigartige Veränderungen der Balance zwischen neuronaler Erregung und Hemmung gekennzeichnet ist. Darüber hinaus weisen sie darauf hin, dass die Zellaktivierung während der Schlaf-Spindeln zu Veränderungen der synaptischen Übertragung, die die Erregbarkeit der Zelle dauerhaft verändern, beiträgt. Die Ergebnisse liefern die Grundlage für gezielte Manipulationen der jeweiligen Zellen zur Überprüfung kausaler Zusammenhänge in zukünftigen Studien.

Abstract

From the snail to the fly and the lizard to humans, almost every organism sleeps. Since the organism is extremely vulnerable during these phases, from an evolutionary point of view sleep must serve a vital function to justify such a high risk. One function that has been receiving increased attention during the recent years is sleep's potential role in synaptic plasticity. On the one hand, this line of research, has found evidence for an unspecific, general weakening of synaptic strength during sleep, which may serve the energy-efficient stabilization of synaptic excitability. On the other hand, it not only has shown beneficial effects of sleep on memory but also on strengthening and formation of synapses suggesting a variety of neuronal plasticity dynamics during sleep.

For excitatory synapses, it has already been shown that over sleep the glutamate receptor expression and thus the excitatory synaptic connectivity changes and depends strongly on intracellular calcium concentrations. However, about one third of neuronal circuits consists of inhibitory cells, whose role for synaptic plasticity during sleep has so far received less attention.

Therefore, the present work aims at characterizing sleep-specific changes in the activity of excitatory pyramidal cells as well as of different sub-groups of inhibitory cells in order to obtain a comprehensive picture of the neuronal circuits during sleep. In total three studies using in vivo two-photon microscopy combined with genetically modified mice were performed to record calcium activity of the different cell types. Simultaneous EEG recordings allowed the classification of different sleep stages and sleep-specific EEG oscillations. In study I we focused on sleep stage-specific changes and found that excitatory activity constantly reduces from wakefulness over slow wave sleep (SWS) to rapid eye movement (REM) sleep, whereas Parvalbumin-positive interneurons (PV-In) increased their activity during REM sleep.

In study II we measured the calcium activity during distinct EEG rhythms. During SWS the hyperpolarized downstate of slow oscillations (SO) was accompanied by an increase in the activity of Somatostatin-positive interneurons (SOM-In) and a simultaneous decrease in PV-In activity. The opposite pattern was observed during sleep spindles. Here the PV-in showed increased calcium activity, while the activity of the SOM-in remained unchanged. Excitatory cells only showed increased activity when sleep spindles occurred coupled with SOs.

In study III we clustered all cell types based on their activity during sleep spindles to test whether excitatory cells showing increased activity during spindles show permanently enhanced excitability. Indeed, we confirmed this hypothesis and furthermore found that the excitability of cells, which are inactive during spindles, decreased.

Taken together, the results show that sleep is characterized by unique changes in the balance between neuronal excitation and inhibition. In addition, they indicate that cell activation during sleep spindles contributes to changes in synaptic plasticity, which permanently alter the excitability of the neural network. These findings provide the basis for targeted manipulations of the respective cells to validate causal relationships in future studies.

Content

List of figures

List of tables

Abbreviations

AMPA	α-amino-3-hydroxy-5-methyl-4-isoxazolepropionic-acid
Ca^{2+}	Calcium
CCD	Charge-coupled device
Cre	cyclization recombination
EEG	Electroencephalogram
E/I	Excitation/inhibition
EMG	Electromyogram
EOG	Electrooculogram
GABA	γ-aminobutyric acid
GCaMP6f	Genetically encoded calcium indicator 6th generation fast
NMDA	N-methyl-D-aspartate
Non-REM	Non rapid eye movement
PV	Parvalbumin
PV-In	Parvalbumin positive interneuron
REM	Rapid eye movement
RMS	Root mean square
SEM	Standard error of the mean
SO	Slow oscillation
SOM	Somatostatin
SOM-In	Somatostatin positive interneuron
SWS	Slow wave sleep
VIP	Vasoactive intestinal peptide

List of relevant publications

This dissertation is based on the following research papers:

I.   **Niethard, N**., Hasegawa, M., Itokazu, T., Oyanedel, C.N., Born, J., and Sato, T.R. (2016). Sleep-stage-specific regulation of cortical excitation and inhibition. Current Biology 26, 2739–2749.

II. **Niethard, N**., Ngo, H.-V. V, Ehrlich, I., and Born, J. (2018). Cortical circuit activity underlying sleep slow oscillations and spindles. Proceedings of the National Academy of Science U. S. A. 115, E9220–E9229

III. **Niethard, N**., Brodt, S., Born, J.: How sleep balances cortical circuit activity. *Submitted*

1 Introduction

1.1 General introduction

Why do we need to sleep? This question is not only the subject of many modern scientific investigations but reaches back to ancient times. In both the Greek and Roman mythology, sleep was personified as the brother of death, together inhabiting the underworld. This close relationship emphasizes on two important features of sleep: the disconnection from the environment and the resulting high vulnerability of the organism. Therefore, from an evolutionary perspective sleep must serve an important function worth such a high risk. In our daily lives, we constantly notice that we become tired after being awake for a long time and that we feel rested and refreshed after sleeping. There are plenty of explanations for the interplay between wakefulness and sleep, such as the degradation of metabolic waste products. However, from a neurobiological perspective, this can be considered as follows.

In order to use information from past experiences to show adaptive behavior in the future, our brain needs to accomplish two seemingly opposing tasks. On the one hand, it needs to be able to store new information in a long-lasting and stable way and it is assumed that information storage in the brain is achieved via an increase in synaptic weights between those cells representing the encoded information. On the other hand, over time this process would lead to a saturation of the neural network's ability to increase its excitability, preventing the brain from remaining plastic in order to guarantee the storage of new information at all times. The need for a homeostatic process countering this continuous potentiation has been acknowledged for a long time. However, it took until almost half a century ago, when Borbély's (1982) definition of sleep as a homeostatic process provided the fundament for a subfield of sleep research investigating a potential regulatory role of sleep in synaptic potentiation and depotentiation. In the early two-thousands this concept built the basis for the synaptic homeostasis theory (SHY), which proposes sleep as a key factor for synaptic downscaling to maintain neuronal connectivity and activity within an optimal range (Tononi and Cirelli, 2003).

Five years later Vyazovskiy et al. (2008) backed up this theory with seminal empirical evidence by combining molecular and electrophysiological methods in rats. On the molecular level, they measured the expression of GluR1-containing AMPA receptors as an indicator for synaptic strength in cortex and hippocampus. Additionally, they measured electrically evoked local field potentials within the frontal cortex as a correlate for synaptic strength. Both measures consistently showed that wakefulness is associated with an increase and sleep with a decrease of intra-cortical net connectivity. The authors discussed that the measured AMPA receptor levels could not differentiate between surface and internal receptors. However, newer studies confirmed that synaptic AMPA receptor levels and their phosphorylation are reduced during sleep (Diering et al., 2017).

Ca^{2+} is a key element for the regulation of neuronal plasticity. Synaptic potentiation as well as depotentiation strongly depend on Ca^{2+} influx and intracellular Ca^{2+} concentrations (Kawamoto et al., 2012). It acts as a second messenger and has been shown to affect gene expression (Berridge et al., 1998), dendrite development (Lohmann and Wong, 2005), synaptogenesis (Michaelsen and Lohmann, 2010) and several other processes involved in neuronal plasticity. During the depolarization of the cell, NMDA and AMPA receptors open leading to high intra cellular Ca^{2+} concentrations, which triggers intracellular cascades such as gene expression and finally synaptic plasticity. However, so far intracellular Ca^{2+} has never been measured during natural sleep.

To shed some light on this we conducted a set of experiments, which are part of the present thesis. Besides measuring intracellular Ca^{2+} transients in all cells, we discriminated between excitatory and inhibitory activity to be able to distinguish potential opposing dynamics. To obtain both measures, we used *in vivo* two-photon microscopy that allowed the discrimination of excitatory and inhibitory calcium activity in a combination of electro encephalogram (EEG) recordings for discriminating different sleep stages as well as specific EEG oscillations. Therefore, the second main aim was to investigate how specific neuronal cell populations are involved in the etiology of these phenomena and how they relate to neuronal plasticity during sleep. Parts of the present work have been already published in *Current Biology* and *Proceedings of the National Academy of Sciences of the United States of America* (Study I: Niethard et al., 2016 and Study II: Niethard et al., 2018) or have been submitted for publication (Study III; Niethard et al., 2019).

1.2 Sleep

Sleep is often referred to as a recurring state of mind, characterized by unconsciousness. Scientifically, four main attributes have been used to define sleep in different types of organisms: Immobility, increased arousal threshold, a specific posture and homeostatic regulation (longer sleep following sleep deprivation)(Cirelli and Tononi, 2008; Hartse, 2011). Based on those criteria extensive research during the last decades showed that sleep can not only be found in humans and other mammals but also in animals with low complexity nervous systems such as e.g. the sea slug *Aplysia californica* (Vorster and Born, 2015), the worm *Caenorhabditis elegans* (Raizen et al., 2008), the fruit fly *Drosophila melanogaster* (Huber et al., 2004) or the lizard *Pogona vitticeps* (Shein-Idelson et al., 2016).

In 1924, the pioneering work of Hans Berger, discovering different EEG rhythms between sleeping and awake brains, laid the foundation for modern sleep research. 28 years later, when Aserinsky and Kleitman discovered a unique pattern of eye movements during certain sleep episodes, the discrimination of rapid eye movement (REM) and Non-REM sleep was introduced (Aserinsky and Kleitman, 1953). However, Rechtschaffen and Kales (Kales and Rechtschaffen, 1968) were the first to publish a manual for EEG-based sleep scoring. The majority of sleep studies in humans still follows their sleep scoring rules dividing Non-REM sleep in 4 sub-stages (stage 1 - 4). The Non-REM stages 3 and 4 are often referred to as slow wave sleep (SWS) as they are characterized by slow rhythmic EEG activity. In non-human mammals, the discrimination of Non-REM and REM sleep is widely accepted but the subdivision of mammalian Non-REM sleep is often not applied and is still a matter of discussion (e.g. see Genzel et al., 2014). Therefore, here Non-REM sleep and SWS are used as an equivalent.

In humans normally a full night of sleep is characterized by four to five cycles of consecutive Non-REM and REM episodes, each cycle lasting for 70-90 minutes (Rasch and Born, 2013). In rodents, the duration of those cycles is reduced but they also show reoccurring alterations between Non-REM and REM sleep during their resting phase (Grosmark et al., 2012; Watson et al., 2016). Importantly, Non-REM and REM sleep are not equally distributed across a whole night or equivalent inactive period of night active mammals. While the beginning of each inactive period is dominated by Non-REM sleep

episodes, the density of REM episodes constantly increases over time, leading to more REM sleep episodes during the second half of the inactive period (Rasch and Born, 2013).

1.2.1 Slow wave sleep (SWS)

One hallmark of SWS are synchronized high amplitude EEG oscillations in frequencies ranging from 0.1 – 4 Hz called slow oscillations (SO). They are characterized by step-like fluctuating membrane potentials of cortical pyramidal cells. During the SO downstate these cells are hyperpolarized and show reduced action potential activity, whereas during the up state, the membrane potential of cortical pyramidal cells is depolarized and therefore shifted towards the spiking threshold leading to an overall increase in spiking probability. SOs often show a propagation pattern of a traveling wave in anterior-posterior directions (Luczak et al., 2007; Massimini, 2004). Even though SOs can persist without thalamic input (Steriade et al., 1993), recent work has demonstrated a strong negative effect of thalamic inactivation on the occurrence of active states of the SO (Lemieux et al., 2014). Interestingly, research showed that both transcranial current stimulation (Binder et al., 2014; Marshall et al., 2006) and acoustic stimulation (Ngo et al., 2013a) can systematically induce SOs. Those findings finally lead to the development of standalone EEG-based applications for improving SO density and amplitude as well as overall SWS duration (Debellemaniere et al., 2018).

Sleep spindles are another distinctive oscillatory feature of SWS. They are characterized by waxing and waning field potentials within frequency ranges of 7 - 15 Hz in rodents and 10 - 16 Hz in humans for timespans between 0.5 and 3 s. Rhythmogenesis of sleep spindles is initiated by intrathalamic circuits including GABAergic neurons within nucleus Reticularis thalami (nRT) and glutamatergic cells of thalamo-cortical projection neurons (For review Lüthi, 2013). Even though thalamic spindles have been recorded after decortication (Contreras et al., 1996; Steriade, 1995; Timofeev and Steriade, 1996), their initiation and termination critically depends on cortico-thalamic feedback (Bonjean et al., 2011; Gennaro and Ferrara, 2003).

Spindles tend to follow the initial depolarization of cortical upstates during SOs (Steriade et al., 1993) and can even be indirectly induced by auditory stimulation of SOs (Ngo et

al., 2013b, 2013a). Many studies showed beneficial effects of SOs and spindles on synaptic plasticity and memory consolidation during sleep (Diekelmann and Born, 2010; Rasch and Born, 2013; Ulrich, 2016). It has been proposed that the beneficial effect of SOs on memory consolidation derives from the grouping of faster brain rhythms especially of spindle activity (Mölle et al., 2002; Ngo et al., 2013b; Piantoni et al., 2013). Sejnowski and Destexthe (2000) hypothesized that the beneficial effect of sleep spindles on memory consolidation during sleep is caused by triggering Ca^{2+} influx into neocortical pyramidal cells, which in turn triggers the expression of NMDA receptors (Sabatini et al., 2001; Zucker, 1999).

1.2.2 REM sleep

The first criterion used to classify REM sleep was the bursting activity of oculomotor muscles during rapid eye movements, which also gave it its name. Furthermore, REM sleep is characterized by a very low muscle tone that originates from the active suppression of muscle activity only intermitted by brief muscle twitches and an increased brain temperature compared to Non-REM sleep. In mammals, one of the most consistent and pronounced features of REM sleep is hippocampal theta activity (4 - 10 Hz) of the local field potentials. It is initiated by medial septal inputs to the hippocampus and intrahippocampally it is then mediated via rhythmic activity of parvalbumin (PV)-positive interneurons (Ognjanovski et al., 2017, 2018). In humans, REM sleep-related theta activity is less obvious than in rodents, however a 4 – 8 Hz rhythm has been described in cortex and also hippocampus (Cantero et al., 2003; Vijayan et al., 2017).

Naturally, REM sleep always follows SWS. Base on this the "sequential hypothesis" postulates that REM sleep complements the prior memory consolidation during SWS (Giuditta et al., 1995). This idea was further supported by a study showing that the incidence of sleep spindles and hippocampal ripples predicted hippocampal firing rate changes during REM sleep (Miyawaki and Diba, 2016).

1.3 Cortical circuits

A fundamental characteristic of cortical networks is their vast level of diversity. A typical cortical pyramidal cell is equipped with about 10,000 synaptic inputs (Laughlin and Sejnowski, 2003) and the majority of those inputs consists of excitatory inputs arising from other cortical pyramidal cells. Typically, pyramidal cells mainly project on cells in the close vicinity, which leads to a high level of local, recurrent connectivity. Additionally, inhibitory interneurons interconnect with this excitatory network. A prominent connectivity pattern between excitatory and inhibitory cells within the cortex are excitatory connections onto inhibitory cells, which, in turn, project back onto the initial excitatory cell (Fino et al., 2012; Tremblay et al., 2016). One way to distinguish excitatory and inhibitory cells is according to the neurotransmitter they emit. While excitatory cells release glutamate, inhibitory cells release GABA. However, both cell types can be further discriminated into many distinct types based on morphological, physiological and molecular properties. In this thesis, only inhibitory cells will be further discriminated based on molecular markers.

1.3.1 Inhibitory cell types

On average, the cortex consists of 20 - 30% GABAergic cells (Douglas and Martin, 2004; Markram et al., 2004; Rudy et al., 2011). These cells are also called interneurons and can be further classified based on molecular markers that they express. The three most commonly employed molecular markers are parvalbumin (PV), somatostatin (SOM) and vasoactive intestinal peptide (VIP). Those subclasses of interneurons innervate their target cells by a stereotypic distribution of their synapses on select membrane domains (e.g. axon initial segment (AIS), somata, dendritic shafts and spines) (Douglas and Martin, 2004; Kubota et al., 2016; Markram et al., 2004; Yavorska and Wehr, 2016). Dependent on their input site they differentially affect the output of the targeted cell (Figure 1). PV-positive interneurons (PV-In) mainly target the AIS and somata of pyramidal cells. This local inhibition is optimally positioned to alter a neuron's output by precisely changing the temporal sequence of action potentials. Indeed, it is well established that PV-In play an important role in phasing neuronal activity (Ognjanovski et al., 2017, 2018). In con-

trast, SOM-positive interneurons (SOM-In) mainly target the apical dendrites of pyramidal cells. This enables these cells to selectively manipulate synaptic inputs either by local inhibition of single synapses, by interacting with back propagating action potentials or by affecting the generation and propagation of dendritic calcium spikes. Dendritic calcium influx plays a key role in the induction of dendritic plasticity (Zucker, 1999). Therefore, cell compartment-specific inhibitory input has a direct impact on plasticity at glutamatergic synapses. Indeed, synaptic plasticity during learning is accompanied by a reduction of projections from SOM-In onto pyramidal cells (Chen et al., 2015). Importantly interneurons not only project onto excitatory pyramidal cells but also onto other interneurons. This allows complex local changes of the Excitation/Inhibition (E/I) balance without compromising the network's overall excitability.
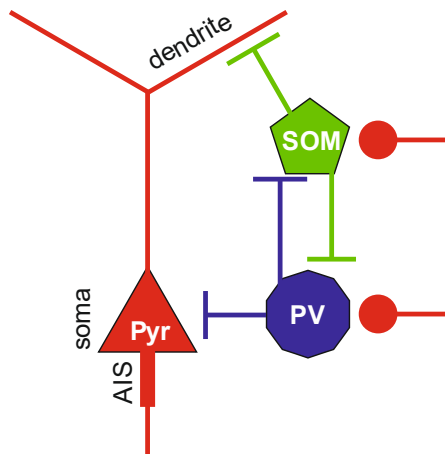

Figure 1: Cortical circuitry of excitatory pyramidal cells and inhibitory interneurons. SOM-positive interneurons (SOM, green) project to apical dendrites of excitatory pyramidal cells (Pyr, red) and to PV-positive interneurons (PV, blue). They receive excitatory inputs from pyramidal cells and inhibitory inputs from PV-positive interneurons. PV-positive interneurons project onto the soma and the axonal initial segment (AIS) of excitatory pyramidal cells. They in turn receive excitatory inputs from pyramidal cells. SOM-positive interneurons strongly mediate local calcium influx on dendritic compartments, while PV-positive interneurons mainly affect pyramidal cell output by changing the temporal dynamics of the action potential propagation.

1.4 Excitation/inhibition balance and synaptic plasticity

Research during the last decade has revealed the important role of GABAergic interneurons in information processing and neuronal plasticity during wakefulness (Liguz-Lecznar et al., 2016; Lovett-Barron et al., 2012, 2014; Scheyltjens and Arckens, 2016; van Versendaal and Levelt, 2016). Furthermore, they are crucially involved in triggering

the critical period of enhanced synaptic plasticity during development (Hensch, 2005; Levelt and Hübener, 2012). Following the Hebbian plasticity paradigm, activity-dependent competition of synapses and especially the spike timing of action potentials is crucial for synaptic plasticity. Especially fast spiking PV-In are known to be involved in the generation of specific brain rhythms through synchronized inhibitory inputs (e.g. theta, spindle or ripple activity) (Averkin et al., 2016; Né Dicte Amilhon et al., 2015; Ognjanovski et al., 2017; Peyrache et al., 2011; Royer et al., 2012). This synchronized inhibitory input in turn enforces precise timing of action potentials of excitatory cells (Higley, 2006; Isaacson and Scanziani, 2011; Wehr and Zador, 2003). Therefore, inhibitory activity is essential for coordinating spike timing that is necessary for the induction of Hebbian plasticity in the cortex.

Beside the function of synchronizing cortical activity GABA release also directly suppresses local dendritic calcium influx and thereby promotes the competitive selection of synapses. Interestingly, parallel *in vivo* imaging of excitatory and inhibitory postsynaptic sites of the same neuron revealed that the turnover of inhibitory synapses occurs on shorter timescales than that of excitatory synapses (Villa et al., 2016), suggesting that inhibitory activity is essential for the induction of local plastic changes on excitatory cells. This corresponds well with the finding that spine shrinkage or elimination at excitatory synapses goes hand in hand with the activation of nearby GABA receptors (Hayama et al., 2013).

1.5 Sleep and synaptic plasticity

Over the last century, researchers have identified sleep as a key mechanism for synaptic rescaling. On the one side, sleep was shown to promote consolidation of memories by strengthening memory-specific neuronal synapses (Puentes-Mestril et al., 2019; Rasch and Born, 2013). On the other side, sleep was proposed to facilitate the global homeostatic regulation of synaptic connections within the brain (Tononi and Cirelli, 2014). This theory assumes that during wakefulness the cortical excitability increases due to the continuous processing of incoming information, which in turn makes it necessary to counterbalance this increase during subsequent sleep.

According to this theory, cells that increase their activity during wakefulness must undergo stronger downregulation than cells with lower activity increases during wakefulness. Therefore, a cell's excitability during wakefulness determines its excitability during subsequent sleep. Interestingly, over the last decades several studies showed that, those brain areas and neurons, which are active during the encoding of new information during wakefulness, are reactivated during subsequent sleep (Chen and Wilson, 2017). This reactivation can predict the quality of memory consolidation during sleep and can even be facilitated or attenuated by targeted manipulation (Antony et al., 2012; Cairney et al., 2014; Oudiette and Paller, 2013; Rasch et al., 2007). The neuronal network must therefore constantly fulfil two opposing tasks. The first is that it must not lose connections that represent memories and the second is that it must dissolve unnecessarily potentiated connections in order to remain plastic.

To untangle the mechanisms underlying these opposing dynamics, researchers have started to look more intensively into sleep stage-specific differences of synaptic plasticity. Although SWS and REM sleep are both associated with memory consolidation, accumulating evidence suggests that they have different effects on synaptic renormalization. Electrophysiological experiments showed that REM sleep, but not SWS on average reduces firing rates within the hippocampus (Grosmark et al., 2012). On a structural level, Gan's group showed that REM sleep leads to synaptic pruning, i.e. removal of excess synaptic connections (Li et al., 2017). In contrast, SWS enables branch-specific spine formation, which is not disrupted by selective REM sleep deprivation (Yang et al., 2014). These studies also included a motor learning task and spine formation during SWS was accompanied by the reactivation of task-specific cell ensembles. Therefore, they not only show synaptic formation during SWS and synaptic pruning during REM sleep but also how these processes facilitate memory consolidation (Li et al., 2017; Yang et al., 2014). However, there are also contradictory findings, which showed that a subset of cells exhibiting visual evoked responses to repeatedly presented stimuli during wakefulness increase their firing rates over the course of following REM sleep, but not SWS epochs (Clawson et al., 2018). In summary, it can be said that during SWS as well as REM sleep divergent synaptic dynamics can be present.

Secondly, research has also focused on investigating homeostatic differences between different brain areas, e.g. motor cortex and sensory cortical areas during sleep. A recent

study using electron microscopy to investigate the changes of axon-spine interfaces provided evidence that during sleep synaptic connections are in average reduced or weakened in both primary motor and primary somatosensory cortex (de Vivo et al., 2017). Although a number of studies support this view, the current literature still does not present a consistent picture. Within visual cortex, neither wake-related increase nor sleep-related decrease in network activity was found in a familiar environment. Instead, after firing rates were depressed by monocular deprivation, they stayed stable during sleep and only returned to baseline by a sustained increase during following wakefulness (Hengen et al., 2016). In fact, firing rate responses to visual stimuli even show a select increase during subsequent sleep but not during wakefulness after stimulus presentation (Clawson et al., 2018; Durkin and Aton, 2016). Evidence from frontal and visual cortex recordings suggest that especially low active cells – presumably the cells most likely encoding new information (Grosmark and Buzsaki, 2016) – show an increase in activity and connectivity during sleep, while cells with high activity during wakefulness show a decrease during sleep (Clawson et al., 2018; Watson et al., 2016). These results suggest that synaptic scaling during sleep depends more on previous activity during wakefulness than on the observed brain region.

This idea is further supported by evidence showing that the novelty of encoded information also affects synaptic plasticity during REM sleep. While hippocampal place cells that encode a newly experienced place reactivate during the peaks of theta oscillations during REM sleep, the same cells change their discharge time point to the negative trough of the theta oscillation once the place becomes familiar (Poe et al., 2000). Importantly reactivation during the theta peak leads to synaptic potentiation while reactivation during the trough leads to depotentiation (Poe, 2017; Poe et al., 2000). Taking all the mentioned findings together, they support the theory of a global downscaling process during sleep. Concurrently, a small fraction of cells, potentially the ones storing newly encoded information, show selective upscaling during SWS, which then is preserved or even further strengthened during REM sleep (Figure 2).

For understanding, how synaptic plasticity during sleep subserves adaptive behavior and memory it is first essential to elucidate how inhibitory networks interact with excitatory networks and how they are involved in coding information. This is important because changes in inhibitory circuits trigger opposite dynamics in excitatory circuits and vice

versa. To shed some light on how sleep affects cortical excitation and inhibition the present work investigated cortical calcium activity of three main cortical cell types: excitatory pyramidal cells, PV-In and SOM-In.
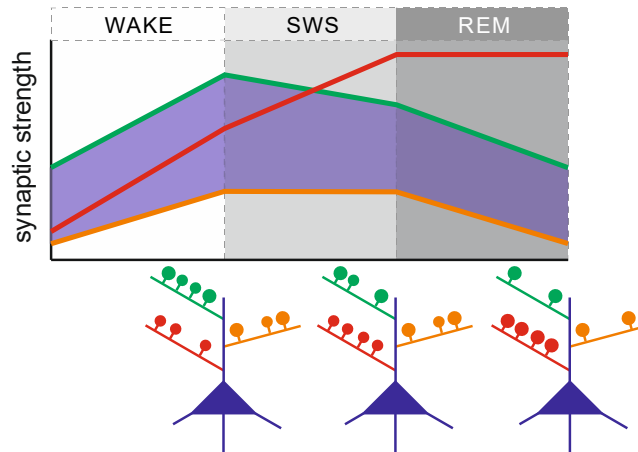

Figure 2: Synaptic strength dynamics during sleep. Top: Blue shaded area represents overall changes in synaptic strength over the course of wakefulness and sleep. Both core sleep stages, SWS and REM sleep can convey synaptic downscaling. However, contributions of SWS to synaptic downscaling appear to be more limited and restricted to cells highly active during wakefulness (green line) than cells with low activity during wakefulness (orange line). Recent studies have revealed signs of a global synaptic downscaling over periods of REM sleep more consistently than over SWS. A subset of synapses that are activated during spindles in SWS and are likely to carry fresh memory information, presumably undergo synaptic upscaling rather than downscaling during SWS and are preserved from pruning during REM sleep (red line). Bottom: Sleep-related downscaling spares synapses on dendritic branches carrying freshly encoded memory information and even strengthens them dependent on their reactivation during spindles (red; green and orange illustrates newly formed, wake active and inactive synapses, respectively; adapted from Niethard and Born, 2019).

1.6 Objectives and hypotheses

After learning, new spines grow locally on the apical dendrites of pyramidal cells while axonal boutons of SOM-In are eliminated. At the same time PV-In show increased numbers of axonal boutons (Chen et al., 2015). Importantly, SOM-In preferentially inhibit distal dendrites of excitatory neurons and PV-In mainly inhibit perisomatic regions (Douglas and Martin, 2004; Markram et al., 2004; Yavorska and Wehr, 2016). This

shifted inhibition provides a unique environment for the pyramidal cells to form new spines due to local dendritic disinhibition while the E/I balance is stable and hyperexcitability is avoided. These specific inhibition changes have so far only been shown during wakefulness.

The first study of this thesis investigated the activity changes within cortical circuits during natural sleep. To untangle changes in E/I balance during sleep *in vivo* two-photon calcium imaging was used. This technique allows the selective recording from cell subpopulations combined with surface EEG for classifying sleep stages. Two transgenic animal lines were used to label two major inhibitory cell types: PV-In and SOM-In. Additionally, wide field calcium imaging of excitatory cells was used to investigate region-specific calcium activity changes during sleep. Based on previous publications (Vyazovskiy et al., 2009) widespread high excitatory activity was expected during REM sleep.

The second study was conducted to investigate calcium activity of excitatory pyramidal cells, PV-In and SOM-In during SWS-specific oscillations. Therefore, slow oscillations, spindles and the co-occurrence of both events were detected based on cortical surface EEG. The calcium activity of pyramidal cells was expected to be highest during the upstate of SOs and during spindles while increased inhibitory activity was expected before and during the SO downstate.

The last study elucidated the role of sleep spindles on the long-lasting changes in cell excitability. Cells were clustered based on their activity during spindles to discriminate calcium activity changes during sleep of spindle-active and spindle-inactive pyramidal cells. It was hypothesized that cells being active during spindles undergo selective upscaling, meaning a persistent increase of their excitability during SWS, which is maintained during subsequent REM sleep.

2 Studies

2.1 General methods

The following section shortly introduces the general methods used for investigating cortical calcium activity during sleep.

2.1.1 *In vivo* two-photon calcium imaging

Two-photon imaging depends on the excitation of fluorescence. The important difference compared to single-photon imaging is that the wavelength of the used light source is twice as long as the excitation wavelength ideally would be. Therefore, for the actual excitation of the fluorescent molecules, the energy is only sufficient for the induction of light emission if two photons hit the same molecule simultaneously. Therefore, the excitation probability is highly limited to the area around the focus point and background excitation is dramatically reduced compared to single-photon imaging (Figure 3). Overall, this leads to an increased signal to noise ratio that allows the detection of signals coming from single cell somata or even single dendrites.
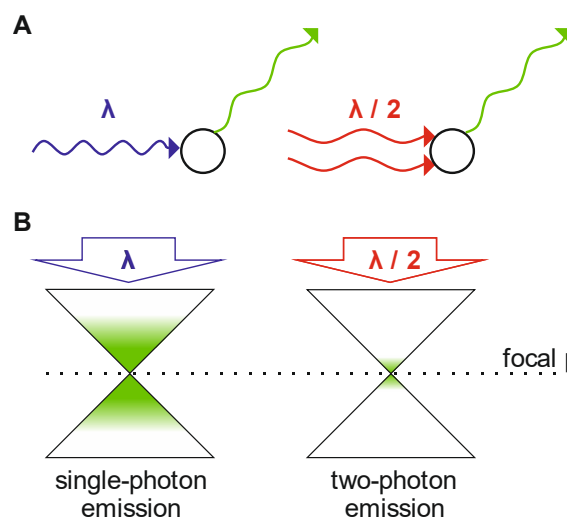

Figure 3. Basic principles of fluorescence microscopy. A Fluorescence microscopy is based on the ability of fluorophores to absorb light with a specific wavelength λ (blue wave) to emit the fluorescent light (green wave). Two-photon microscopy uses an excitation wavelength that is carrying half λ/2 (red wave) of the actually needed excitation energy. Therefore, the energy is only sufficient once two photons hit the fluorophore at nearly the same time point. **B** The probability of two photons arriving at the same time point is very rare and is limited to the area of the focal plane. This increases the overall signal to noise ratio because the out of focus background illumination is kept at a minimum compared to single-photon microscopy.

The expression of fluorescent proteins can be either cell type unspecific or dependent on genetic markers of transgenic animals. For the present studies using two-photon microscopy we used two different genetically modified mice strains: PV-Cre and SOM-Cre animals. Those strains express the Cre recombinase either in all PV-positive cells or in all SOM-positive cells. After the injection of a Cre specific virus the expression of a red fluorescent protein is exclusive for one or the other cell type. Additionally, to monitor the cytosolic calcium activity of the cells a second virus leading to the expression of a genetically encoded calcium indicator (GECI) must be injected into the same brain area. This calcium indicator is not Cre-dependent and therefore all cells around the injection site will express it. Importantly the GECI emits green light while the molecule for the Cre dependent labeling of the PV- or SOM-positive cell population emits red light. Highly sensitive photomultipliers detect the emitted light, which is separated by filters between red and green wavelengths. This then allows using the red signal for the detection of PV-In or SOM-In while the green signal allows the detection of intracellular calcium of all cells (including PV-In and SOM-In) in the imaging area independent of their cell type (Figure 4).
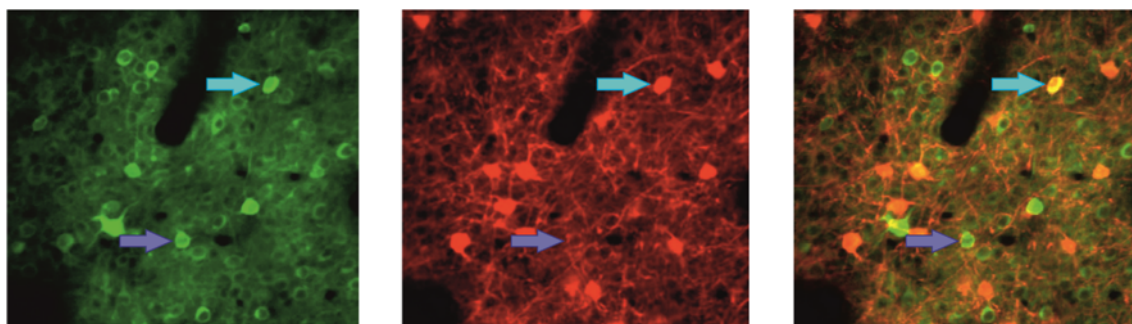
Figure 4. Fluorescence signal recorded from an example PV-Cre animal expressing the green fluorescence calcium indicator GCaMP6f (left) and the PV-In specific red fluorescent protein tdTomato (middle). Overlaying both simultaneously recorded channels allows the discrimination of calcium signals coming from red PV-In (example cell marked with light blue arrow) and unlabeled cells, which are primarily pyramidal cells (example cell marked with dark blue arrow).

2.1.2 *In vivo* wide field imaging

In vivo wide field imaging is only using single photons for exciting the fluorophores (see Figure 3). In the present work, a blue high-power LED (λ 570nm) was used as excitation light source. Transgenic animals expressing the calcium indicator GCaMP6f in all pyramidal cells were used for monitoring cortical activity. The emission light was detected with a high sensitive CCD camera that allowed frame rates up to 60 frames per second. The size of the imaging area was around 1 cm^2. Even though the transgenic animals express GCaMP6f in the entire brain, the majority of the recorded fluorescence signal originated from the cortical surface, because the excitation light does not penetrate into deep tissue (see Figure 5).
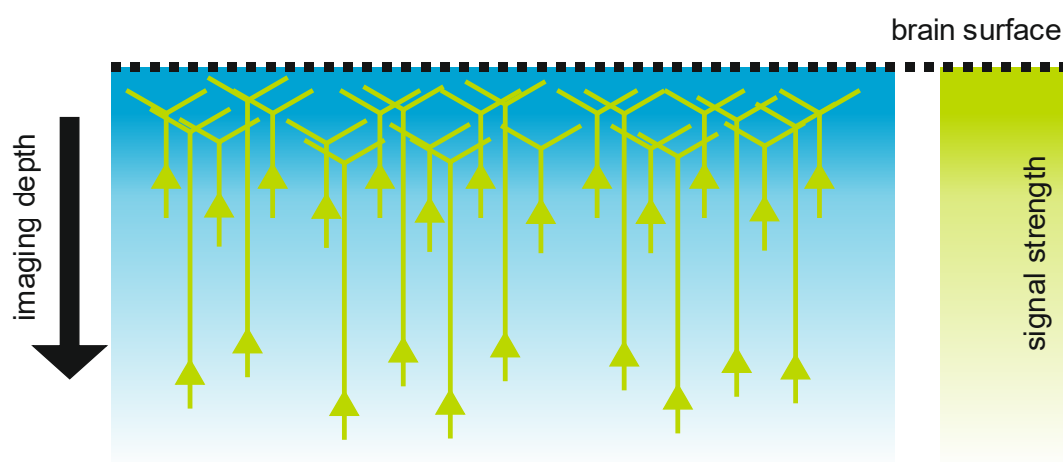
Figure 5. Excitation and emission during wide field imaging. With increased imaging depth, the excitation light gets scattered and less intensive (blue shaded area) this leads to weaker excitation in deeper tissues. Additionally, also the emission light (green shaded area) gets scattered after emitting from cell soma and dendrites leading to even weaker signals from deeper layers. Therefore, the majority of the wide field calcium signal originates from superficial layers, mainly containing apical dendrites.

2.1.3 Sleep scoring

To discriminate the different sleep stages (wakefulness, SWS and REM sleep), every ten seconds of the recording session were manually classified. The criteria for the classification were the frequency bands of the frontal EEG together with the EMG power. In brief,

wakefulness was characterized by high frequencies in EEG and high EMG power. SWS was scored whenever the EMG showed low activity together with high amplitude slow oscillations (0.5 - 4 Hz) and sleep spindles (7 - 15 Hz) in the EEG signal. High power in the theta frequency band (6 - 10 Hz) together with very low muscle activity were used as criteria for scoring REM sleep. Episodes, where the EEG signal saturated or movement artefacts were present were excluded from any further analysis. To ensure that all animals showed natural sleep under head fixation we only included animals that showed alterations between SWS and REM sleep.

2.2 Study I: Sleep-stage-specific regulation of cortical excitation and inhibition

Published as:

Niethard, N., Hasegawa, M., Itokazu, T., Oyanedel, C.N., Born, J., and Sato, T.R. (2016). Sleep-stage-specific regulation of cortical excitation and inhibition. Current Biology 26, 2739–2749.

Author contributions study I

Author	Author position	Scientific ideas %	Data generation %	Analysis & interpretation %	Paper writing %
Niels Niethard	1st	33.3	90	33.3	33.3
Masashi Hasegawa	2nd	0	8	0	0
Takahide Itokazu	3rd	0	1	0	0
Carlos Oyanedel	4th	0	1	0	0
Jan Born	5th Corresponding.	33.3	0	33.3	33.3
Takashi Sato	Last Corresponding.	33.3	0	33.3	33.3
Title of paper:		Sleep-stage-specific regulation of cortical excitation and inhibition.			
Status in publication process		Published in: Current Biology 26, 2739–2749.			

Sleep-Stage-Specific Regulation of Cortical Excitation and Inhibition

Highlights

- Cortical activity is suppressed globally during sleep, being lowest during REM sleep

- During REM sleep, a subset of PV+ interneurons increase their activity

- Neurons that are active during wake tend to show higher activity during REM sleep

Authors

Niels Niethard, Masashi Hasegawa, Takahide Itokazu, Carlos N. Oyanedel, Jan Born, Takashi R. Sato

Correspondence

jan.born@uni-tuebingen.de (J.B.), takashi.sato@cin.uni-tuebingen.de (T.R.S.)

In Brief

Niethard et al. show that REM sleep is associated with a global suppression of cortical neural activity, which is accompanied by a specific activation of parvalbumin-positive inhibitory interneurons.

Sleep-Stage-Specific Regulation of Cortical Excitation and Inhibition

Niels Niethard,[1] Masashi Hasegawa,[2] Takahide Itokazu,[2] Carlos N. Oyanedel,[1] Jan Born,[1,2,*] and Takashi R. Sato[2,3,4,*]

[1]Institute for Medical Psychology and Behavioral Neurobiology, University of Tübingen, 72076 Tübingen, Germany
[2]Center for Integrative Neuroscience, University of Tübingen, 72076 Tübingen, Germany
[3]PRESTO, Japan Science and Technology, 332-0012 Saitama, Japan
[4]Lead Contact
*Correspondence: jan.born@uni-tuebingen.de (J.B.), takashi.sato@cin.uni-tuebingen.de (T.R.S.)
http://dx.doi.org/10.1016/j.cub.2016.08.035

SUMMARY

Sleep is characterized by unique patterns of cortical activity alternating between the stages of slow-wave sleep (SWS) and rapid-eye movement (REM) sleep. How these patterns relate to the balanced activity of excitatory pyramidal cells and inhibitory interneurons in cortical circuits is unknown. We investigated cortical network activity during wakefulness, SWS, and REM sleep globally and locally using in vivo calcium imaging in mice. Wide-field imaging revealed a reduction in pyramidal cell activity during SWS compared with wakefulness and, unexpectedly, a further profound reduction in activity during REM sleep. Two-photon imaging on local circuits showed that this suppression of activity during REM sleep was accompanied by activation of parvalbumin (PV)+ interneurons, but not of somatostatin (SOM)+ interneurons. PV+ interneurons most active during wakefulness were also most active during REM sleep. Our results reveal a sleep-stage-specific regulation of the cortical excitation/inhibition balance, with PV+ interneurons conveying maximum inhibition during REM sleep, which might help shape memories in these networks.

INTRODUCTION

Sleep induces specific activity patterns in brain and neocortex. These patterns alternate in a clearly distinguishable manner, as measured by electroencephalogram (EEG), between the stages of slow-wave sleep (SWS) and rapid-eye movement (REM) sleep. Whereas SWS, which is characterized by high-amplitude, low-frequency (0.5–4 Hz) EEG activity, is a state of generally reduced cortical activity, REM sleep with dominant theta activity (4–11 Hz) is considered an active state of sleep accompanied by enhanced cortical neural activity [1, 2]. Consequently, these two sleep stages have been associated with quite different ways in which information is processed in the cortex [3–5]. However, it is not clear how the two sleep stages influence network activity in cortical circuits to ultimately emboss a stage-specific mode of information processing.

The activity in cortical networks is mediated through the local circuits that constitute the network and are composed of excitatory pyramidal cells and inhibitory interneurons. Cortical interneurons can be classified into diverse subtypes based on molecular, structural, and electrophysiological properties [6], and each of these subtypes has been associated with distinct functional roles in brain-state-dependent cortical information processing [7–9]. For example, specific subtypes of interneurons modulate processing of cortical information during wakefulness, depending on whether the animal is in an active state (whisking and running) or in a quiet state with each state linked to specific changes in the excitation/inhibition balance of the local circuits [10–13]. Thus, the investigation of how specific subtypes of interneurons contribute to the excitation/inhibition balance appears to be likewise a critical step toward an understanding of how brain states like SWS and REM sleep shape the processing of information in cortical networks.

In this study, we investigated the activity of cortical circuits during spontaneous wakefulness, SWS, and REM sleep using in vivo calcium imaging. Using wide-field calcium imaging, we found that SWS is associated with a global reduction in pyramidal cell activity. Surprisingly, during REM sleep, this global reduction in network activity was even more profound. Using specific Cre-mouse lines, we then examined activity of parvalbumin-positive and somatostatin-positive interneurons (PV-INs and SOM-INs). We found that the reduced cortical activity during REM sleep is accompanied by the activation of PV-INs, but not of SOM-INs. We conclude that, during REM sleep, PV-INs mediate a distinct shift in the excitation/inhibition balance of cortical network activity toward an enhanced inhibitory control of information processing.

RESULTS

We first investigated how sleep influences the global cortical network activity using wide-field calcium imaging (Figure 1). This imaging method can monitor neural activity with high sensitivity over a large portion of the cerebral cortex [14, 15]. We performed the calcium imaging, covering almost the entire dorsal cortical surface of transgenic mice expressing genetically encoded calcium indicator (GCaMP6f) in the majority of cortical pyramidal neurons across all layers (CaMKII-GCaMP6f; Figure 1B). High-speed imaging (∼60 frames/s) revealed spontaneous changes of the normalized fluorescence signal (F_{norm}) that corresponded to local population activity (Movie S1) [14].
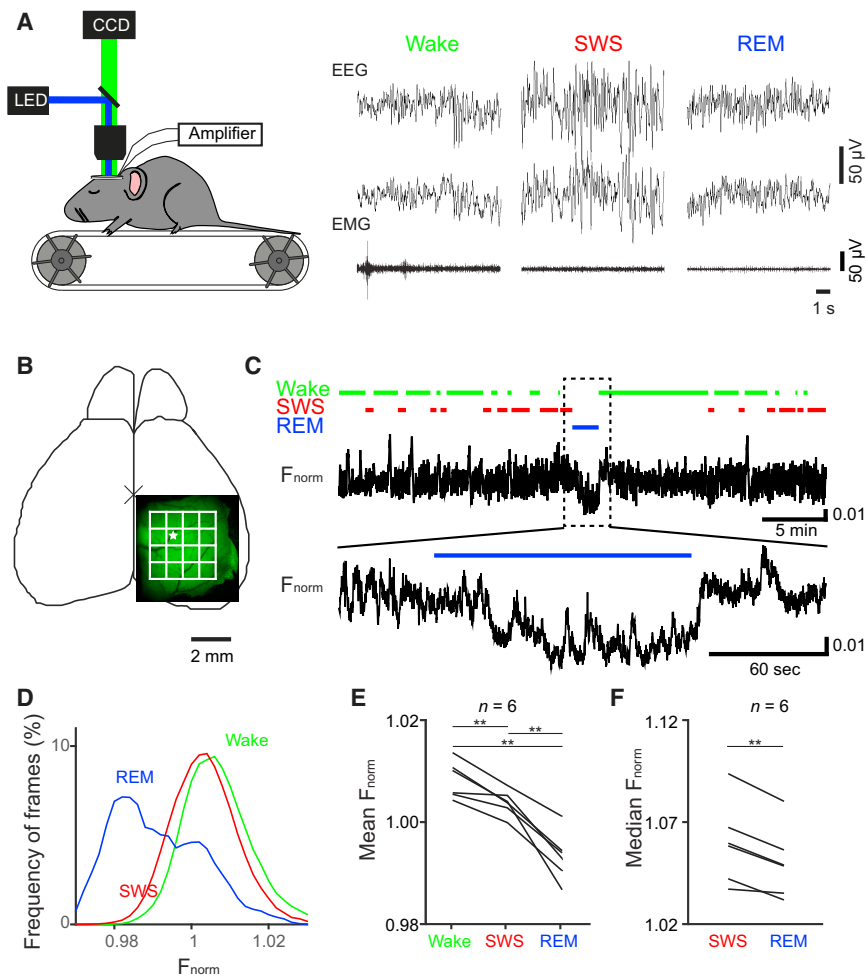
Figure 1. Global Suppression of Cortical Activity during REM Sleep

(A) Procedure for wide-field imaging experiments (n = 6 mice). A head-fixed mouse was placed on a treadmill (left). EEG and EMG were recorded simultaneously to distinguish brain states of wake, SWS, and REM sleep (right).

(B) (Left) An imaging window was placed over the posterior cortex of one hemisphere. "x" indicates bregma. The 4 × 4 grid shows the 16 ROIs in which fluorescence signal (F_{norm}) was analyzed. The star indicates the ROI for which the fluorescence signal is shown in (C) and (D).

(C) An example recording of F_{norm} and concurrent epochs of wake (green bars), SWS (red), and REM sleep (blue) during one imaging session. Dotted box corresponds to the time window shown enlarged in bottom trace. Note that F_{norm} signal decreases shortly after transition into REM sleep (blue bar) and increases again at the end of the REM sleep epoch.

(D) The distribution of F_{norm} signal during wake (229,993 frames), SWS (140,213 frames), and REM sleep (21,932 frames) for the ROI shown in (B) and (C).

(E) Mean F_{norm} during wake, SWS, and REM sleep for six mice. In all ROIs, the F_{norm} signal is highest during wake, intermediate during SWS, and lowest during REM sleep (p < 0.001).

(F) Median F_{norm} activity during REM sleep and a 40-s pre-REM sleep baseline after high pass filtering at 0.1 Hz.

**p < 0.001. See also Figures S1, S2, and S5.

Simultaneously, the EEG and electromyogram (EMG) were recorded to classify sleep stages (wake, SWS, and REM sleep) [16, 17]. We found that sleep stages were consistently associated with changes in population activity; i.e., F_{norm} was largest when the mouse was awake, lower during SWS, and lowest when the animal was in REM sleep (p < 0.001 for all pairwise comparisons of mean F_{norm} during each stage). Especially, REM sleep was typically identifiable based on fluorescence traces alone (Figures 1C and S1). The sleep-stage-dependent change in activity held over the entire imaging area encompassing parietal and occipital cortices (p < 0.001 for all pairwise comparisons between sleep stages and all 16 subregions; Figures 1D, 1E, and S1; n = 6 mice). These sleep-stage-induced changes were further confirmed in mice that expressed GCaMP6f in sensorimotor, barrel, and visual cortices by viral injection (AAV-syn-GCaMP6f). Simultaneous imaging and standard sleep recordings in these animals revealed the fluorescence signal to be similarly reduced to a minimum during REM sleep in the three cortical areas (p < 0.001 for all pairwise comparisons between brain states and for all three areas; Figure S2; n = 6 mice).

The low activity during REM sleep was unexpected, given that REM sleep is considered an active sleep stage with increased neural firing [18, 19]. In order to distinguish whether this reduction in activity originated from neurons in the supra-granular (superfi-

cial) layers or from deeper infra-granular layers, we injected a virus that expresses GCaMP6f (AAV2.1-syn-GCaMP6f) locally to superficial layers and deep layers of the sensorimotor cortex, respectively (Figure 2). Injection into superficial layers resulted in the labeling of neurons in both superficial layers together with smaller numbers of neurons labeled in deep layers. The injection of virus into deep layers, on the other hand, resulted in an expression confined to the deep layers. This is presumably because the virus in the superficial layers infects layer V neurons via the apical dendrites, whereas the dendritic arbors of layer II/III neurons do not penetrate into the deep layers (e.g., [20]). In both injection conditions, the fluorescence signal was easily detectable from the cortical surface (Figures 2B and 2F), and the fluorescence signal (F_{norm}) exhibited distinct changes depending on the brain state (Figures 2C and 2G). In both injection conditions, activity was lowest during REM sleep (p < 0.001 for all pairwise comparisons with the mean F_{norm} during wake and SWS; Figures 2D and 2H; n = 3 mice for both experiments). During SWS, activity in most cases was at an intermediate level (p < 0.001 compared to activity during wake). These experiments suggest that activity during REM sleep is minimal in both superficial and deep cortical layers.

In order to further clarify, in particular, the unexpected finding of strongly reduced activity across cortical layers during REM sleep, we examined activity of local circuits using in vivo two-photon calcium imaging (Figure 3) [21–23]. In these experiments, we focused on the activity of different classes of interneurons,
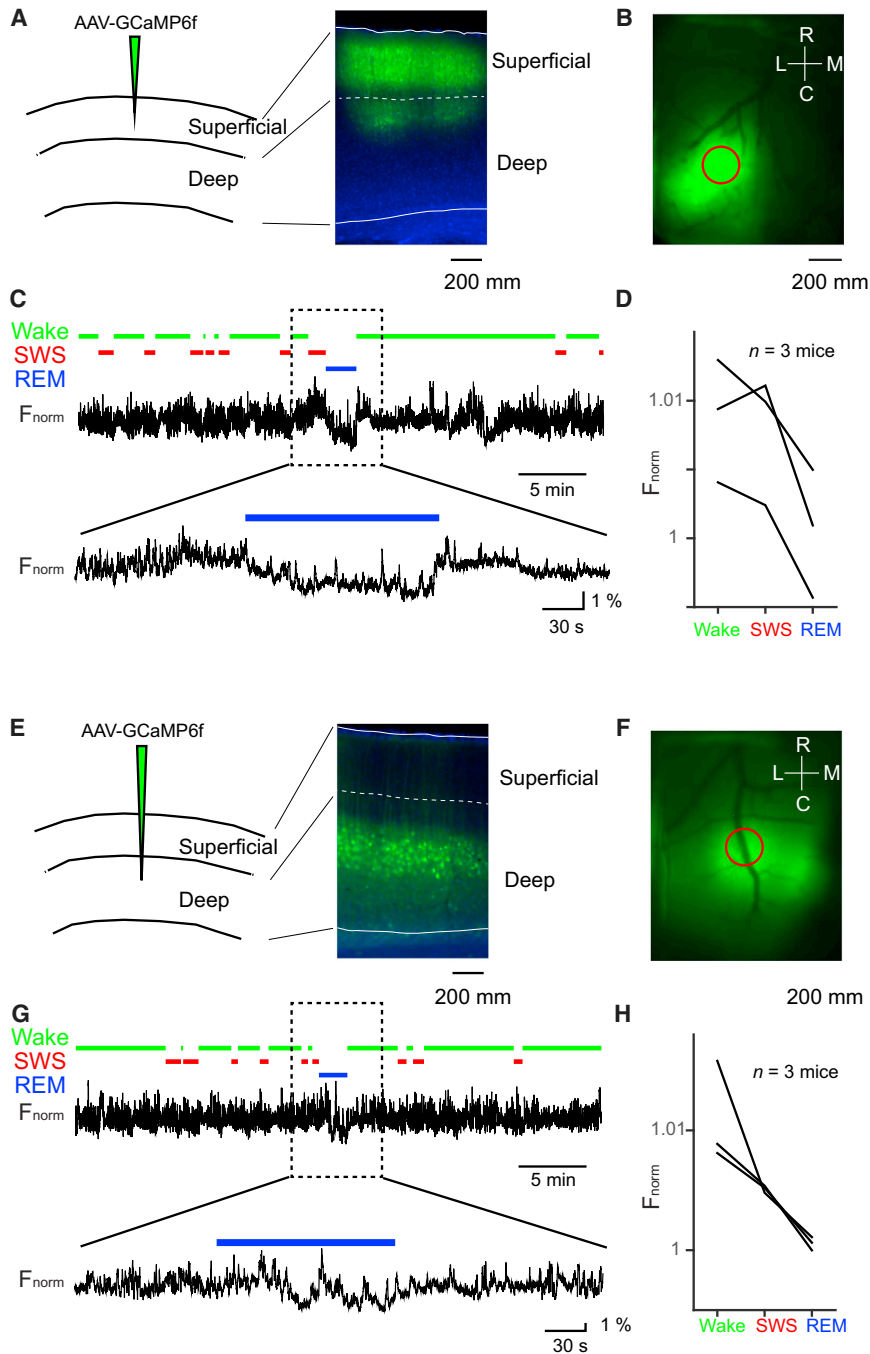
Figure 2. Fluorescence Signal from Neurons in Superficial and Deep Cortical Layers

(A) Experimental procedures. The virus was injected into superficial layers of the sensorimotor cortex (left), which led to the expression of GCaMP6f in neurons of both superficial and deep layers (right).

(B) The signal from GCaMP6f in the neurons can be detected from the dorsal surface. Red circle indicates ROI for which fluorescence signal is indicated in (C).

(C) Recording of fluorescence signal (F_{norm}) and concurrent epochs of wake (green bars), SWS (red), and REM sleep (blue) during one imaging session. Dotted box corresponds to the time interval shown enlarged in bottom trace. Note decrease in F_{norm} signal during REM sleep (blue bar).

(D) Mean F_{norm} during wake, SWS, and REM sleep in three different mice.

(E–H) Panels correspond to (A)–(D) but with the virus injected into the deep layers of the sensorimotor cortex (three mice). Note that expression of GCaMP6f here was confined to the deep layers. See also Figure S5.

neously with that of surrounding unlabeled neurons. The surrounding neurons that do not express tdTomato can be assumed to comprise a substantial number of pyramidal cells, although they likely include also other types of interneurons, particularly in superficial cortex layers [25, 26]. Most of the PV-IN, SOM-IN, and unlabeled cells showed spontaneous fluorescence changes that corresponded to spontaneous action potentials (Figure 3D; Movie S2) [21]. When a neuron showed $\Delta F/F$ greater than the mean +2 SD signal during a sliding 6-min window, the neuron was considered to be active at the time of the respective 169-ms imaging frame (frame rate 5.92 Hz; see Experimental Procedures). We quantified the activity of individual neurons using either the frequency of the active frames or the $\Delta F/F$, with both procedures yielding essentially the same results (Figure S3).

The sleep stages affected the frequency of the spontaneous activity in a cell-type-specific fashion. For unlabeled cells, the frequency of active neurons was highest during the wake state, lower during SWS (p < 0.001), and lowest during REM sleep (p < 0.001 for pairwise comparisons of mean activity across the cells; n = 2,042; Figures 4A and 4B), mirroring progressive decrease across the sleep stages, which we observed for pyramidal cells in our wide-field imaging experiments (Figures 1 and 2). Of the interneurons, PV-INs also showed highest activity during the wake state and lower activity during SWS (p < 0.001). However, during REM sleep, activity increased again to levels only slightly lower than those during wakefulness (p < 0.001 for comparison with SWS; p < 0.05 for comparison with

PV-INs and SOM-INs. For this goal, a mixture of two types of viruses was injected into the sensorimotor cortex of PV-Cre or SOM-Cre transgenic mice: a virus that expresses a genetically encoded calcium indicator (GCaMP6f) pan-neuronally (AAV-syn-GCaMP6f) [24] and a virus expressing tdTomato in a Cre-dependent manner (AAV-FLEX-tdTomato). At the time of imaging, GCaMP6f was expressed in most neurons within ~200 μm around the injection sites (Figures 3B and 3C), whereas tdTomato was expressed selectively in the specific types of interneurons in the same area (Figures 3B and 3C). This allowed us to investigate activity of the specific interneurons simulta-

A

B

GCaMP   tdTomato

C

D

REM

cell 1

cell 2

cell 3

cell 4

10 s   50 %

E
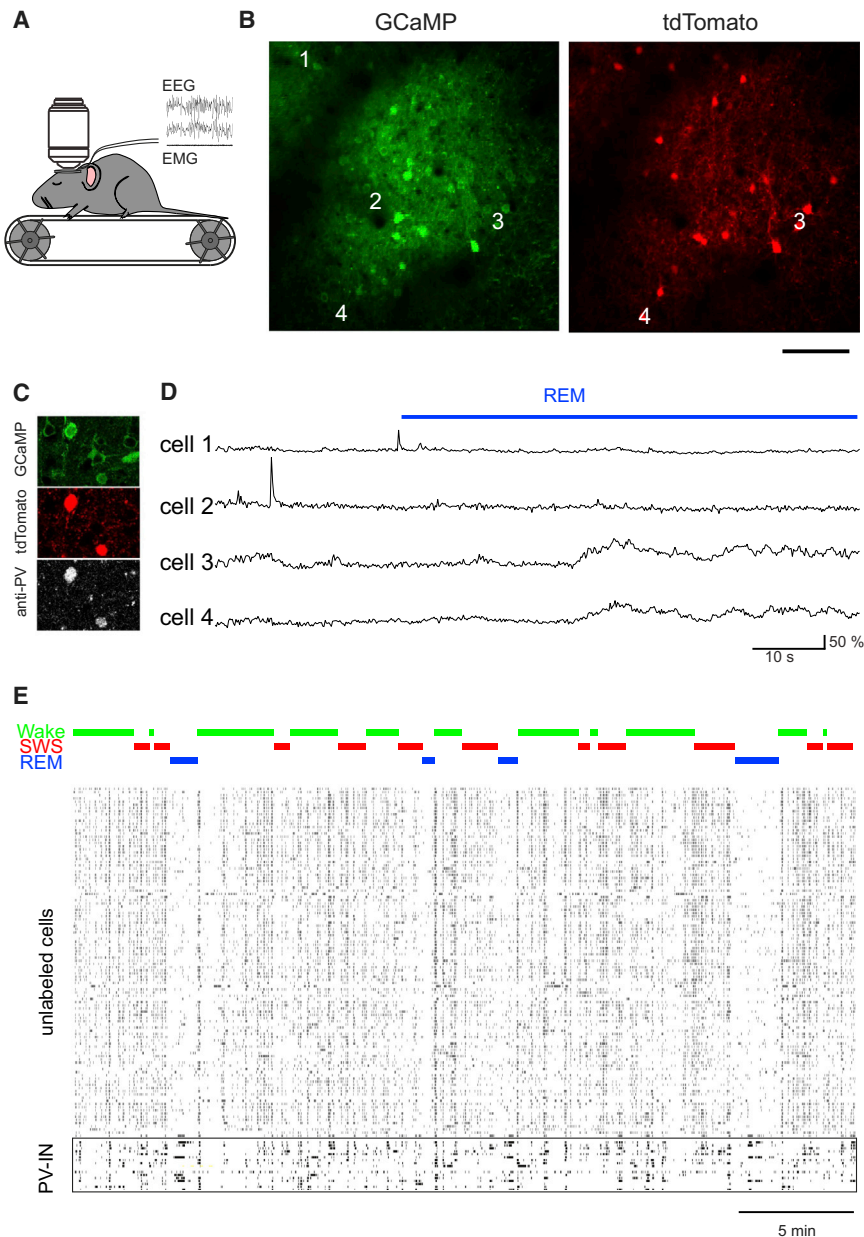
Wake
SWS
REM

unlabeled cells

PV-IN

5 min

Figure 3. In Vivo Two-Photon Calcium Imaging during Sleep

(A) In vivo two-photon imaging was performed on a head-fixed mouse that repeatedly went through periods of wake, SWS, and REM sleep during one imaging session. Sleep stages were identified by EEG and EMG.

(B) Representative in vivo two-photon images of neurons labeled with GCaMP6f (left) and tdTomato (right) in a PV-Cre mouse. GCaMP6f was expressed pan-neuronally, whereas tdTomato was expressed in a Cre-dependent manner. The scale bar indicates 100 μm.

(C) Expression of GCaMP6f (left column) and tdTomato (middle column) was confirmed through histological sectioning. In PV-Cre mice, the expression of tdTomato was confined to PV+ interneurons (PV-INs). Arrows indicate colocalization of Alexa-Fluor-647-conjugated antibody and tdTomato signals.

(D) Example recordings of $\Delta F/F$ from four neurons indicated in (C). Cells 3 and 4 are labeled with tdTomato, indicating that they are PV-INs. Note that these two PV-INs increased their activity during REM sleep (horizontal bar).

(E) The activity (for 169-ms frames; see Experimental Procedures) of 110 unlabeled cells, including mainly putative pyramidal cells, and 17 PV-INs that were imaged simultaneously. The activity of unlabeled neurons, but not PV-INs, is substantially decreased during REM sleep.

28]. We suspected that the discrepancy might be due to the selection bias inherent to extracellular unit recording, i.e., neurons that are active during the wake period might be more likely to be selected for extracellular recordings and only those neurons might also show higher activity during REM sleep than SWS. To test this possibility, we examined the relationship between the activity a neuron showed during the wake stage and the difference in activity between REM sleep and SWS (REM − SWS). Indeed, these two values were positively correlated in all three types of neurons (pyramidal, $r = 0.20$, $p < 0.001$; PV-INs, $r = 0.35$, $p < 0.001$; SOM-INs, $r = 0.25$, $p < 0.01$; Figures 5A–5C). The effect of wake activity was further demonstrated by analyzing subsets of neurons with high activity during the wake state. The pyramidal cells with wake activity within the top 20% showed similar activity during SWS and REM ($n = 408$; $p > 0.05$; Figure 5A, middle), and those within the top 5% were even more active during REM sleep than SWS ($n = 102$; $p < 0.05$; Figure 5A, right). This relationship was even more pronounced for PV-INs, i.e., PV-INs with high wake activity were substantially more active during REM sleep compared to SWS ($n = 42$, $p < 0.001$ for the top 20%; $n = 11$, $p < 0.001$ for the top 5%; Figure 5B). SOM-INs with wake activity within the top 20% showed lower activity during REM sleep than SWS ($n = 24$; $p < 0.05$ for the top 20%), but those few within the top 5%

wake; n = 211; Figure 4; see also Figure S4). This increase in the mean activity during REM sleep appeared to be due to a subset of interneurons that exhibited quite high activity. In contrast, SOM-INs displayed a pattern of activity similar to that of pyramidal cells, with highest activity during wake, lower activity during SWS ($p < 0.001$), and lowest activity during REM sleep ($p < 0.001$; n = 117; Figure 4). These data demonstrate the specific activation of PV-INs during REM sleep, which is accompanied by the suppression of both pyramidal neural and SOM-IN activity, which suggests that the shift in the overall excitation/inhibition balance toward predominant inhibition during REM sleep is conveyed by a subset of REM sleep-active PV-INs.

Our data appear to be at odds with past studies using extracellular unit recordings, showing that cortical activity is enhanced during REM sleep compared to SWS [18, 19, 27,
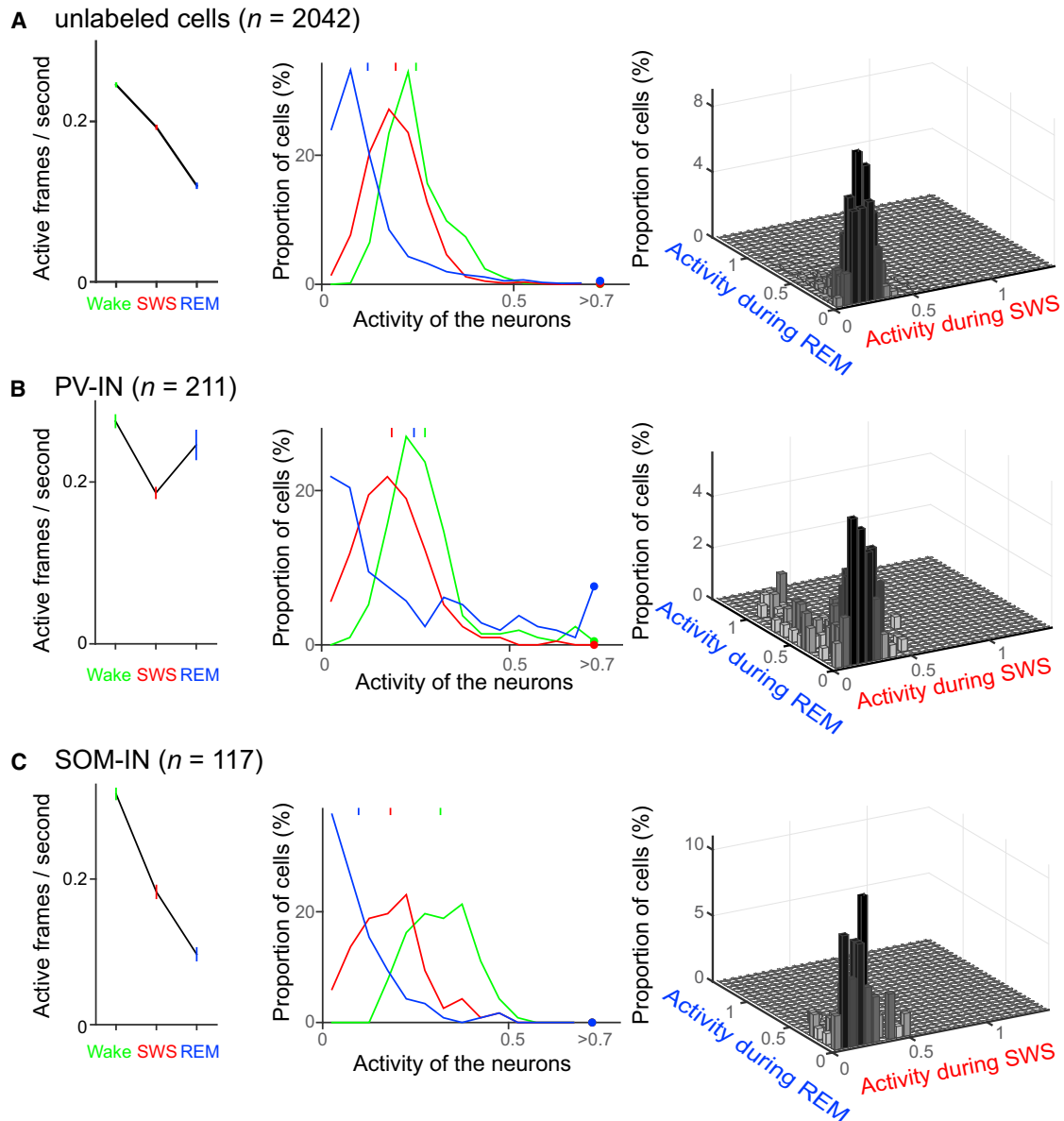
Figure 4. Cell-type-Specific Changes in Neural Activity during Wake, SWS, and REM Sleep

Left panels: mean ± SEM activity of (A) unlabeled cells (n = 2,042), (B) PV-INs (n = 211), and (C) SOM-INs (n = 117) during wake, SWS, and REM sleep. Middle panels: the distributions of activity for the three cell-types are shown. Note that the distribution for PV-INs during REM sleep contains a long tail, indicating that only a subset of PV-INs contribute to the increased activity during REM. Tick marks at the top of each graph indicate the mean activity. Right panels: three-dimensional histograms indicating the distribution of activity for the cell-types across SWS and REM sleep are shown. x and y axes indicate active frames per seconds during SWS and REM, respectively. z axis indicates the proportion of cells relative to the total number of a cell type. The increased proportion of PV-INs only active during REM sleep, but not during SWS, is shown. See also Figures S3 and S4 and Table S1.

exhibited similar activity in the two sleep stages (n = 6; p > 0.3 for the top 5%; Figure 5C). Overall, these data indicate that the neurons with higher activity during wake also show higher activity during REM sleep, compared to SWS. The analysis not only reconciles the discrepancy between previous studies based on electrophysiological recordings of unit activity and the current findings but also provides further support to the view that the high activity of PV-INs during REM sleep mainly originates from a subset of neurons that were also active during the wake period.

The increased PV-IN activity together with decreased activity of unlabeled cells and of identified pyramidal cell activity in our wide field imaging data suggests that the network excitatory/inhibitory balance shifts during REM sleep toward maximum network inhibition. We used the ratio between the proportion of active PV-INs and the sum of the proportion of active PV-INs and unlabeled cells (i.e., PV-IN %/[PV-IN % + Unl %]) as an estimate of inhibition in this balance. Indeed, this ratio was maximal during REM sleep (0.66 ± 0.03), intermediate during

A unlabeled cells

Wake active cells (top 20 %)

Wake active cells (top 5 %)
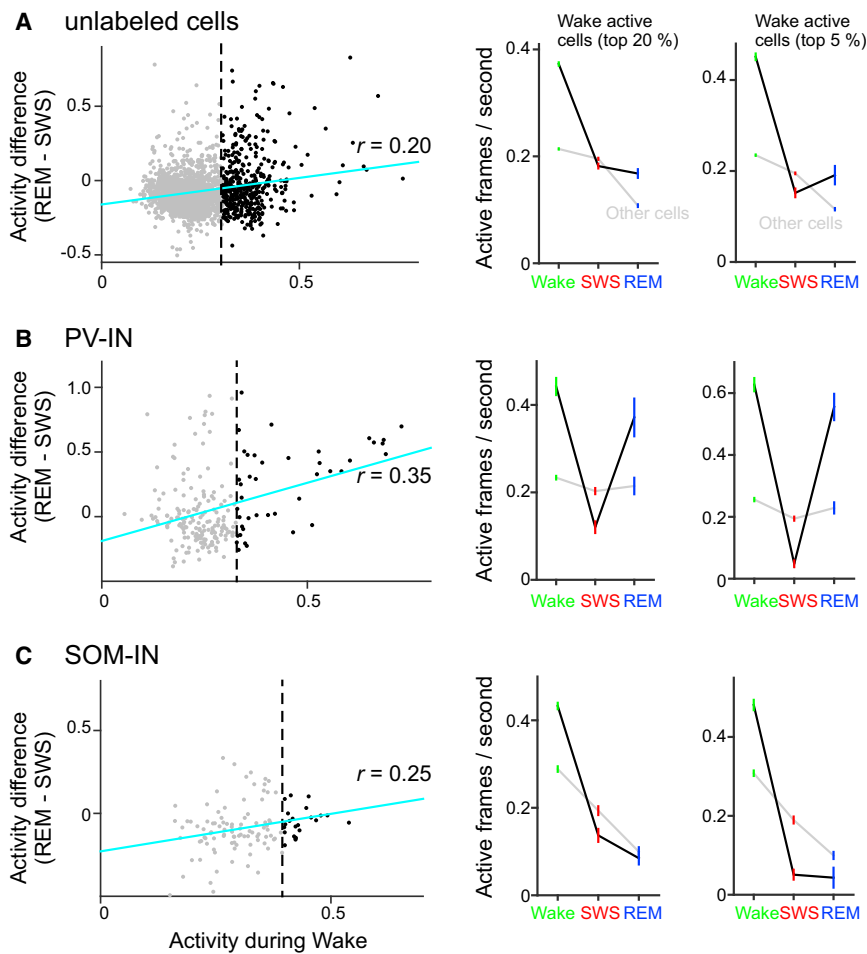
B PV-IN

C SOM-IN

Activity during Wake

Figure 5. Activity Patterns of Neurons with High versus Low Activity during Wake

Left panels: relationship between activity during wake and the difference in activity between REM sleep and SWS (REM − SWS) for unlabeled cells (A), PV-Ins (B), and SOM-INs (C). These values were positively correlated for all three cell types. Light blue lines indicate the regression lines; the dashed lines indicate the border between the top 20% most wake active cells and the rest, as used in the right panels. The cells on the left to this border (with low activity during wake) are shown in light gray. Right panels: mean ± SEM activity during wake, SWS, and REM sleep is shown for a cell subset whose activity during wake was within the top 20% and top 5%, respectively (black), compared with activity of the remaining cells of the respective type (gray). Note that wake active cells display relatively enhanced activity also during REM sleep, which is most apparent for PV-INs. See also Figure S3 and Table S1.

DISCUSSION

It is well-established that wake and sleep states manifest themselves in distinct patterns of cortical activity. However, it is not clear how these states modulate cortical activity, at the global level or at the fine-scale circuitry level, to regulate the network's excitation/inhibition balance and the processing of information in local circuits. In the current study, we addressed this question using wide-field calcium imaging and in vivo two-photon calcium imaging. Wide-field imaging revealed that the global cortical activity decreases from wakefulness to SWS and, surprisingly, further decreased from SWS to REM sleep, with these dynamics being independent of the cortical area. Two-photon imaging indicated that the reduced global cortical activity was accompanied by reduced activity in the majority of the pyramidal cells and increased activity of PV-INs, but not of SOM-INs, pointing to a crucial role of PV-INs in mediating the global reduction of activity during REM sleep. The PV-INs with the highest activity during wakefulness also showed highest activity during REM sleep, and the same relationship was observed for pyramidal cells and SOM-INs, although less pronounced. These modulations of neural activity produce changes in the excitation/inhibition balance in the cortical circuits, with REM sleep hallmarked by a shift toward predominant inhibition in cortical networks. Thus, our findings provide novel insights into the framing conditions of cortical information processing during the different stages of sleep.

The global decrease in cortical activity during SWS well fits with findings from electrophysiological recordings and might originate from the slow oscillation, which hallmarks SWS and which imposes periods of neural silence and disfacilitation (down states) interleaving with periods of wake-like enhanced activity [1]. However, the overall reduced cortical activity during REM sleep was unexpected and stands in contrast with the

SWS (0.52 ± 0.01), and highest during wake (0.53 ± 0.01; p < 0.006 for all pairwise comparison). In a more-fine-grained analysis accounting for the temporal dynamics in activity patterns, we correlated across imaging frames the proportion of active unlabeled cells with that of active PV-INs, or active SOM-INs, separately for the wake, SWS, and REM sleep epochs of each imaging session (Figure 6). During wake periods, whenever a larger portion of PV-INs or SOM-INs was active, this was accompanied also by an enhanced proportion of active unlabeled cells in the same frame, resulting in maximum correlations of activation. This co-activation was slightly diminished in SWS but reached a distinct minimum during REM sleep, where, in a substantial number of frames, inhibitory cell activity occurred in the absence of activity in unlabeled cells. This finding was not a result of the overall lower firing rates during REM sleep because rank correlations coefficients calculated separately for the 20% most-active putative pyramidal cells during REM, which showed the same trend of significantly reduced correlations during SWS compared with wakefulness and even lower correlations during REM. These data indicate that, whereas PV-INs and SOM-INs tend to be co-activated with pyramidal cells during wake, during sleep, and in particular during REM sleep, activity of inhibitory and excitatory cells becomes dissociated.
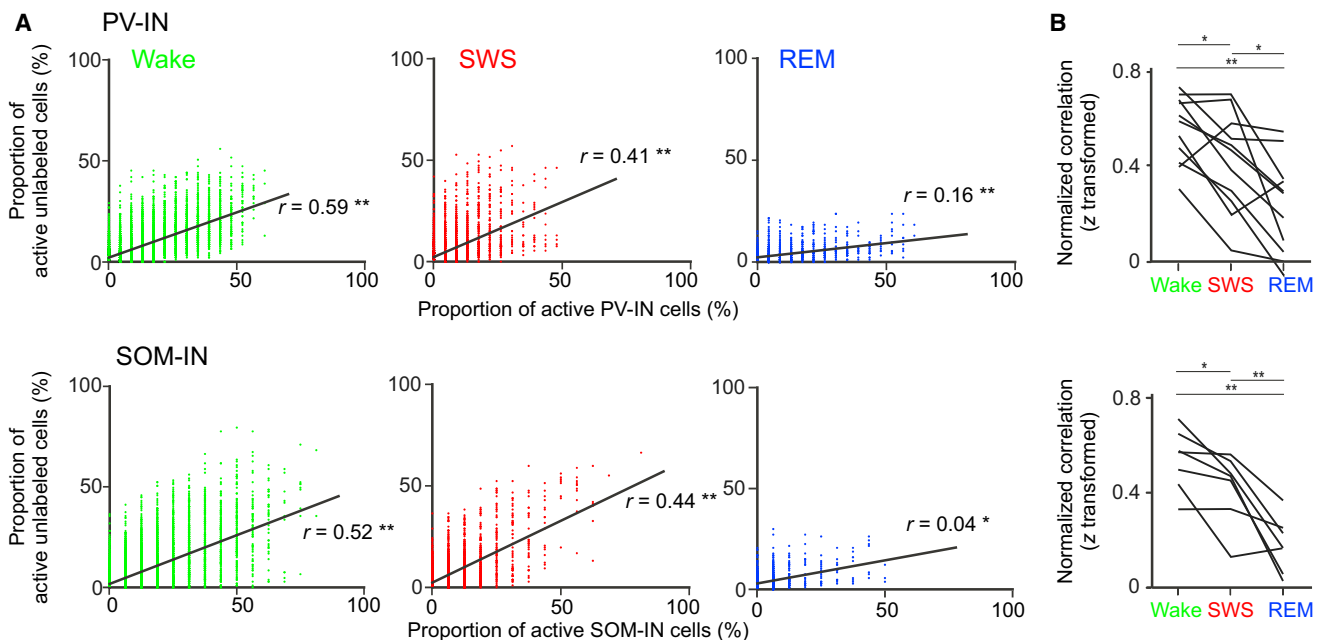
Figure 6. Co-activation Patterns of Unlabeled Cells and Inhibitory Interneurons during Wake, SWS, and REM Sleep

(A) Upper panels: example scatterplots showing the distribution for the proportion (with reference to total number cells) of unlabeled cells and the proportion of PV-INs that are active within the same imaging frame during a session, separately for periods of wake, SWS, and REM sleep. Lower panels: same, for the proportions of unlabeled cells versus SOM-INs active within the same imaging frame. Co-activation between unlabeled cells and PV-INs and SOM-INs, respectively, across the imaging session is also indicated by the Spearman rank correlation coefficient. (Frames showing neither unlabeled cell activity nor activity of the respective interneuron were omitted in these analyses.) **p < 0.01.

(B) Co-activation between unlabeled cells and PV-INs (upper panel) and SOM-INs (lower panel) expressed as correlation (z-transformed) across imaging sessions (n = 12 and n = 7, respectively), separately for periods of wake, SWS, and REM sleep. **p < 0.01; *p < 0.05 for pairwise comparisons between brain states. Distinctly reduced co-activation between unlabeled cells and PV-INs as well as unlabeled cells and SOM-INs during REM sleep is shown. See also Table S1.

general view that REM sleep is an active phase of sleep with intense cortical activity. In the EEG, REM sleep is characterized by low-amplitude, high-frequency activity similar to that during the vigilant states of wakefulness, although the EEG signal primarily reflects synchrony of membrane potential changes rather than levels of neural firing activity. Indeed, early studies of cortical activity using extracellular unit recording also reported higher cortical activity during REM sleep compared to SWS in both monkeys and cats [18, 19]. Intracellular electrophysiological recordings in cats revealed that all cells, including regularly spiking and fast spiking neurons, fire tonically at high rates during REM sleep as high as during wakefulness [1]. More-recent studies in rodents confirmed that cortical activity during REM was equal to or higher, but not lower, than that during SWS [27, 29]. The discrepancy between our findings and these previous studies is difficult to explain. It might partly reflect difference in the species investigated or differences in the cortical regions as they were revealed in human studies using fMRI and positron emission tomography (PET) [30–32]. The latter is, however, unlikely because we observed the suppression of activity during REM sleep uniformly in a large portion of the cortex. Also, layer-specific changes might contribute to this discrepancy, because most electrophysiological recordings of single-unit activity were performed from layer V, whereas the present calcium imaging concentrated on layer II/III cells, although also activity of neurons in deeper layers was assessed, with the same result

(Figure 2). Another factor to be considered here is the low frame rate of calcium imaging that results in under-sampling, in particular of activity of fast-spiking neurons. The slow sampling rate makes this approach less sensitive to changes in the pattern of neuronal activity that might be even more characteristic for the different sleep stages. Nevertheless, calcium imaging, as performed here, allows for the reliable assessment of general levels of activity in different subtypes of neurons (see Figure 3) [24]. Indeed, we confirmed our results using ΔF/F values (see Figure S3) where multiple spiking in one frame expresses itself in an accumulated light signal. Also, such under-sampling cannot explain a generally reduced excitatory activity that is specific to REM sleep. We rather think the discrepancy between our and previous electrophysiological studies might derive from the biased sampling of the extracellular unit recordings against neurons with low activity [33]. By selecting a subset of neurons with high activity during wakefulness, we observed that these neurons, pyramidal cells as well as PV-INs, exhibited larger activity during REM sleep compared to SWS, consistent with the earlier electrophysiological studies. Still, for firm conclusions regarding the discrepancy between the present calcium imaging data and previous data from electrophysiological recordings, approaches combining simultaneous recordings of both types of activity may be necessary. Interestingly, our data concur with recent findings that employed gene expression analysis, which has less sampling bias compared to extracellular unit

recordings, revealing that, during REM sleep, only a small portion of cortical neurons are active [34]. Taken together, our presumably more-representative sampling of cortical cells based on in vivo calcium imaging demonstrates that REM sleep is not associated with intense cortical activity but is a period of prevalent suppression of neural activity where a subset of neurons with high activity during the wake period is reactivated.

The reduced activity of pyramidal neurons during REM sleep was accompanied by an increased activity of PV-INs, but not SOM-INs, which identifies PV-INs as a likely source of cells driving the suppression of cortical activity during REM sleep. This raises the question of the input origin for the increased PV-IN activity. In general, PV-INs receive strong excitatory inputs with high probability from the nearby pyramidal cells [25, 35, 36]. Through these synaptic inputs, PV-INs integrate the activity of surrounding pyramidal neurons [7, 25, 37, 38], which is considered to be critical in balancing excitation and inhibition in the local circuits [10, 39]. Our data are consistent with this scheme during wake, where PV-INs were tightly co-activated with pyramidal cells. However, during sleep and in particular during REM sleep, this coupling was distinctly decreased and the correlation between PV-INs and pyramidal cell activity was lowered, indicating that here PV-INs do not simply follow the excitatory activity in the local circuits. Instead, during REM sleep, PV-INs are likely to be influenced more strongly by long-range inputs. This could be, for example, long-range inputs from sleep-related areas, such as basal forebrain [40, 41]. However, our data (Figures 5E and 5F) also provide evidence that such long-range inhibitory control over cortical networks is conveyed by only a distinct subset of PV-INs that display high activity also during wakefulness. Whether this subset corresponds to basket cells or other inhibitory cells known to be involved in the regulation of REM sleep activity cannot be said [42]. However, the pattern tempts the speculation that networks involved in specific information processing during waking contribute to this suppression by gating the long-range activation of PV-INs in select networks. Although our data strongly suggest that reduced excitatory pyramidal cell activity is a consequence of increased activity of PV-INs, and although it is well established that PV-IN activation mediates a reduction in cortical activity and inhibition of pyramidal neurons (e.g., [43, 44]), we emphasize that firm conclusions about causal relationships can be drawn only on the basis of direct manipulations of a subset of PV-IN. In fact, stimulation of PV-INs can result in signs of increased cortical activity (e.g., increased gamma oscillations) [44, 45], and how subgroups of PV-INs might generally reduce activity in large cortical networks is currently unclear.

Note also activation of SOM-INs and pyramidal cells is more dissociated during REM sleep compared with the other two brain states (Figure 6). However, considering that SOM-INs, unlike PV-INs, exhibit a general decrease rather than increase in activity during REM sleep, we suppose this dissociation to be an immediate consequence of the locally changed balance between PV-INs and pyramidal cells during this sleep stage rather than a response of SOM-INs to long-range inputs.

It can be questioned that the activity of unlabeled cells in our two-photon experiments reflected pyramidal cell activity. Indeed, there are probably other interneurons among these cells, the proportion of which is negligible (<10%) in deeper cortical layers but can be substantial in superficial layers [25, 26]. Still,

the majority of interneurons in cortical layers II/III are PV-IN and SOM-IN cells, which we labeled in these experiments. Importantly, the profound decrease in activity across sleep stages, and particularly during REM sleep, which we observed for unlabeled cells using two-photon imaging, was likewise revealed in our wide-field imaging experiments, where we used mice expressing GCaMP6f in CaMKII-positive cells, which are pyramidal cells. Thus, it appears justified to assume that, also in the two-photon imaging data, the strong REM sleep-associated decrease in activity of unlabeled cells reflected to a substantial degree pyramidal cell activity.

Although our two-photon imaging approach provides novel insights into the unique regulation of the excitation/inhibition balance in cortical circuitry during sleep, the findings are in need of further elaboration. First, although we excluded non-neural activity changes (e.g., in metabolic rate and blood flow) as primary source of the distinct suppression of excitatory activity during REM sleep (Figure S1), the size of such possible confounds needs to be scrutinized. Second, we restricted recordings to the dorsal cortex surface, and network dynamics might be different if deeper cortex areas, such as the anterior cingulate and the retrosplenial cortex or the hippocampus, are considered [34], although electrophysiological recordings of hippocampal activity in rats revealed a pattern (with narrow-spiking interneurons displaying strongly elevated firing in REM sleep) that seems quite consistent with the present results [46]. Third, activity patterns might also depend on the cortical layers. Although lower fluorescence level was observed during REM sleep also for neurons in deep layers, the fluorescence signals in Figures 2E–2H originated mainly from the dendritic tufts. Therefore, although unlikely, the possibility cannot be entirely ruled out that neurons in deep layers might act differently at the level of the somata [47, 48]. Fourth, we did not look at other types of interneurons that also add to the inhibitory control of cortical networks. However, in the neocortex, these cells are clearly outnumbered by PV-INs and SOM-INs, rendering unlikely that they substantially contribute to the global cortical excitation/inhibition balance.

In sum, the present calcium imaging studies revealed that cortical neural activity shows a progressive decrease from wakefulness to SWS to REM sleep, with the decrease during SWS and REM sleep likely mediated by entirely different mechanisms, i.e., states of neural silence and disfacilitation during the slow oscillation of SWS and increased activity of PV-INs in REM sleep, respectively. In fact, the present two-photon study is the first to identify REM sleep as a state of distinctly increased inhibitory activity in neocortical networks, to a level even exceeding inhibitory control during wakefulness. The function of such shift in the excitation/inhibition balance remains to be elucidated. It might generally prime the cortical network for synapse formation [49], thereby supporting the formation of new neural circuits. Alternatively, rather than conveying a general priming influence on synapse formation, it may shape selective processing of distinct memory representations reactivated in these networks [50].

EXPERIMENTAL PROCEDURES

Animals and Surgery
All experimental procedures were approved by the University of Tübingen and the local institutions in charge of animal welfare. CaMKII-Cre mice [51] crossed

with Ai95 (RCL-GCaMP6f; Jax #024105) [52] and C57BL6/J were used for wide-field calcium imaging; PV-Cre mice [53] (Jax #008069) and SOM-Cre mice [54] (Jax #013044) were used for in vivo two-photon calcium imaging. The mice were housed in groups of up to five mice in temperature (22°C ± 2°C)- and humidity (45%–65%)-controlled cages. Experiments were performed during the light period of the 12 hr:12 hr light-dark cycle. Data collection in all mice started 1 hr after light onset of the 12 hr:12 hr light-dark cycle. All mice were male and older than 8 weeks.

The mice were implanted with a headpost for subsequent experimentation. They were anesthetized with 0.1 mg/g ketamine and 0.008 mg/g xylazine with a supplement of isoflurane. Dexamethasone (0.08 mg) was sometimes administered to reduce tissue swelling. Lidocaine was applied to the wound margins for topical anesthesia. A custom-built headpost was glued to the skull and subsequently cemented with dental acrylic (Lang Dental).

The headpost implantation was followed by virus injection and window implantation. First, a craniotomy was made above the sensorimotor cortex (1.1 mm caudal and 1–1.3 mm lateral from the bregma). The size of the craniotomy was 1.2 × 2 mm for all experiments except for those shown in Figures 1 and S1, where the craniotomy was larger (3 × 4 mm or 8 × 9 mm; see Figure S1) and covered the dorsal cortex. In the area of craniotomy, two viruses (AAV2/1-syn-GCaMP6f 2.96 × 10^{12} genomes/mL and AAV2/1-Flex-tdTomato 1.48 × 10^{11} genomes/mL) were injected at multiple sites (10–20 nL/site; 3–5 min/injection). For GFP control experiment (see Figure S5), the procedure was conducted in the same way, but just one virus (AAV2/1-EF1α-GFP) was injected. The depth of the injection was 130–300 μm, except for the experiments shown in Figures 2E–2H (depth; 700–900 μm). After the virus injection, two layers of coverglasses (1 mm × 1.5 mm and 2.0 mm × 2 mm, depending on the area of craniotomy) were implanted as an imaging window. The space between the imaging window and skull was sealed with 1.5%–2% agarose, and the window was cemented with dental acrylic.

The electrodes for the EEG were implanted contralateral to the imaging window. First, the skull was exposed, and then two bone screws (PlasticOne) were implanted on the cortical surface (frontal electrode: anterior +1.5 mm, lateral 1.5 mm; parietal electrode: posterior −2.5 mm, lateral +2.5 mm from bregma). One silver wire (Science Products) was implanted on the brain surface (posterior 1 mm; lateral 0 mm from lambda) and served as reference. Additionally, two stainless steel wires (Science Products) were implanted into the neck muscle for EMG recordings. After surgery, the animals were single housed in their home cages, and calcium imaging was conducted after at least 10 days of recovery.

Head Fixation Procedure
After handling the animals 10 min per day for 1 week, the animal was habituated to the head fixation. Habituation consisted of four sessions with increasing fixation durations (30 s, 3 min, 10 min, and 30 min) interleaved by 10-min resting intervals. Habituation was conducted 24 hr prior to the first imaging session during the early light phase. The procedure was the same for all animals.

EEG and EMG Recordings
Sleep stages were identified based on EEG and EMG recordings during the imaging sessions. EEG and EMG signals were amplified, filtered (EEG: 0.01–300 Hz; EMG: 30–300 Hz), and sampled at a rate of 1,000 Hz (amplifier: model 15A54; Grass Technologies). Based on EEG/EMG signals for succeeding 10-s epochs, the brain state of the mouse was classified into wake, SWS, and REM sleep stages [16]. Sleep stage identification was supported using the software SleepSign for animals (Kissei Comtech).

Wide-Field Imaging
For wide-field calcium imaging, a charge-coupled device (CCD) camera (iXon X3 888; Andor Technology) was focused on the cortical surface using a macroscope (MVX-10; Olympus). The illumination light source was 470 nm light-emitting diodes (Thorlabs). The filter cube contained an excitation bandpass filter of 470/40 nm, a dichroic filter of 495 nm, and an emission bandpass filter of 525/50 nm. The zoom was adjusted to cover the entire window. The imaging frame consisted of 125 × 125 pixels, and the frame rate was 48.86–56.26 Hz (17.8–20.5 ms per frame). The precise timing of individual frames was saved as voltage pulse in the EEG recording system. To account for possible confounding influences on the fluorescence signal resulting from more-gradual changes in metabolic rate and blood flow, all subsequent analyses on wide-field imaging data were additionally performed after high-pass pre-filtering [55] the original data at 0.1 Hz. Here, we present, where relevant (i.e., regarding the effects of REM sleep), results from analyses after pre-filtering in addition to analyses of the original data (see Figures 1 and S5).

Two-Photon Imaging
In vivo imaging was performed using a two-photon microscope based on the MOM system (Sutter) controlled by ScanImage software [56]. The light source was a pulsed Ti:sapphire laser (λ = 980 nm; Chameleon; Coherent). Red and green fluorescence photons were collected with an objective lens (Nikon; 16×; 0.80 numerical aperture [NA]), separated by a 565-nm dichroic mirror (Chroma; 565dcxr) and barrier filters (green: ET525/70 m-2p; red: ET605/70 m-2p), and measured using photomultiplier tubes (Hamamatsu Photonics; H10770PA-40). The imaging frame consisted of 1,024 × 256 pixels, and the frame rate was 5.92 Hz (169 ms per frame). Images were collected in layer II/III at a depth of 150–250 μm. All subsequent analyses were performed on the original data or after high-pass pre-filtering at 0.1 Hz to eliminate slower changes possibly originating from metabolic and blood flow changes. As both analyses yielded essentially the same results, and also because of the lower sensitivity to changes in blood flow of two-photon imaging, this report is restricted to analyses based on unfiltered two-photon imaging data.

Wide-Field Image Analysis
To define regions of interest (ROIs) for the imaging data from CaMKII-GCaMP6 mice, the area within the window was divided into 4 × 4 grids, resulting in 16 ROIs (Figure 1). For the data from virus-injected mice, a circle with ten pixels radius was drawn around each injection site (Figure 2). The precise location of ROIs did not affect the outcome. For each frame, the pixel values within an individual ROI were summed, and then this value was normalized by dividing by the 30th percentile value of all frames within a ±3-min interval (F_{norm}). This normalization affects all frames within a 6-min interval in a constant way (see [57] for a similar procedure). Signals from all sleep stages were normalized in the same way. The mean F_{norm} for wake, SWS, and REM sleep was calculated as the average F_{norm} across all frames within the respective sleep stage. For statistical evaluation, the mean F_{norm} was compared between the different sleep stages using a bootstrap-based algorithm [21], where the distribution of differences in F_{norm} values between sleep stages was established by randomly permuting the frames for a given sleep stage. Ten thousand iterations were performed, and the p value was determined by the proportion of iterations for which the difference was smaller (or larger) than zero.

Two-Photon Image Analysis
Lateral motion was corrected in two steps [58]. A cross-correlation-based image alignment (Turboreg) was performed, followed by a line-by-line correction using an algorithm based on a hidden-Markov model [59]. ROIs containing individual neurons were drawn manually, and the pixel values within each ROI were summed to estimate the fluorescence of this neuron. PV-INs and SOM-INs were manually detected by red fluorescence signal expressed by AAV2/1-Flex-tdTomato. The individual cell traces were calculated as the average pixel intensity within the ROIs for each frame. The cell traces were transformed into the percent signal change (ΔF/F), in which the baseline for each cell was defined as the 20th percentile value of all frames within a ±3-min interval. We confirmed that the neuropil signal did not affect our results by performing neuropil subtraction (Figure S3) [24, 37]. The neuropil signal was estimated for each ROI as the average pixel values within two pixels outside the ROI (excluding adjacent cells). The true signal was estimated as F(t) = F_{inROI} − r × $F_{roundROI}$, where r = 0.7. This procedure yielded essentially the same results (see Figure S3).

The activity of individual neurons was quantified by either mean ΔF/F or the frequency of active frames that showed calcium events, with both approaches yielding essentially the same results. The frequency of active frames for an individual neuron was defined as follows: a neuron was considered active in a given frame if the ΔF/F value was more than two SDs above the mean in a

sliding time window of ±3 min. The number of active frames was divided by the total number of frames in each sleep stage and then multiplied by the frame rate, such that the value represents frames per second. Statistical comparisons between sleep stages were based on the same bootstrap algorithm described above.

The network excitation/inhibition balance was quantified based on the proportion of active pyramidal cells to that of active PV-INs. The distribution of these two values (ranging between 0% and 100%) was calculated separately for wake, SWS, and REM sleep stages for each imaging session. Then, for each imaging session, after excluding the frames with no active cells, the Spearman rank correlation coefficients between the proportion of active pyramidal cells and that of PV-INs was calculated separately for wake, SWS, and REM sleep stages. Distributions of Fisher z-transformed correlation coefficients were compared between sleep stages using t test.

Generally, statistical analyses relied on bootstrapping for comparisons of repeated measures to test directed hypotheses. Only comparisons of inhibitory/excitatory balance and z-transformed correlations were done using t tests. No corrections for multiple comparisons were applied.

Immunohistochemistry

Immunostaining was performed using standard procedures (n = 2 mice). Following the experiments, the mice were deeply anesthetized (0.3 mg/g ketamine and 0.024 mg/g xylazine, intraperitoneally [i.p.]) and intracardially perfused with 4% paraformaldehyde in 0.1 M PBS (4% paraformaldehyde [PFA]). The brains were removed from the skull, post-fixed in 4% PFA at 4°C overnight, rinsed with 0.1 M PBS, and transferred to 30% sucrose/PBS overnight. Coronal slices (thickness 20 μm) were cut using a cryostat and blocked in carrier solution (5% normal goat serum; Jackson ImmunoResearch Laboratories) and 0.3% Triton X-100 (Sigma-Aldrich) in 0.1 M PBS) for 1 hr at room temperature on a shaker. Slices were then incubated with anti-PV rabbit primary antibody (1:500 in carrier solution; #24428; Immunostar) or anti-SOM rabbit primary antibody (1:500 in carrier solution; #20089; Immunostar) at 4°C overnight. After three rinses with 0.1 M PBS for 30 min, sections were incubated in donkey anti-rabbit immunoglobulin G (IgG) antibody conjugated with Alexa Fluor 647 (Thermo Fisher Scientific; 1:500 in carrier solution) for 1 hr at room temperature on the shaker. After a few additional rinses for 30 min in 0.1 M PBS, slices were cleared in a sequence of sucrose solutions (15%, 30%, 45%, and 60% sucrose in 0.1 M PBS/2% Triton X-100; with a 4-hr period per sucrose concentration) and then mounted on slide glasses for imaging.

SUPPLEMENTAL INFORMATION

Supplemental Information includes five figures, one table, and two movies and can be found with this article online at http://dx.doi.org/10.1016/j.cub.2016.08.035.

REFERENCES

1. Steriade, M., Timofeev, I., and Grenier, F. (2001). Natural waking and sleep states: a view from inside neocortical neurons. J. Neurophysiol. 85, 1969–1985.

2. Brown, R.E., Basheer, R., McKenna, J.T., Strecker, R.E., and McCarley, R.W. (2012). Control of sleep and wakefulness. Physiol. Rev. 92, 1087–1187.

3. Nir, Y., and Tononi, G. (2010). Dreaming and the brain: from phenomenology to neurophysiology. Trends Cogn. Sci. 14, 88–100.

4. Aronoff, R., Matyas, F., Mateo, C., Ciron, C., Schneider, B., and Petersen, C.C. (2010). Long-range connectivity of mouse primary somatosensory barrel cortex. Eur. J. Neurosci. 31, 2221–2233.

5. Rasch, B., and Born, J. (2013). About sleep's role in memory. Physiol. Rev. 93, 681–766.

6. Kawaguchi, Y., and Kubota, Y. (1997). GABAergic cell subtypes and their synaptic connections in rat frontal cortex. Cereb. Cortex 7, 476–486.

7. Petersen, C.Ch. (2014). Cell-type specific function of GABAergic neurons in layers 2 and 3 of mouse barrel cortex. Curr. Opin. Neurobiol. 26, 1–6.

8. Stryker, M.P. (2014). A neural circuit that controls cortical state, plasticity, and the gain of sensory responses in mouse. Cold Spring Harb. Symp. Quant. Biol. 79, 1–9.

9. Alitto, H.J., and Dan, Y. (2010). Function of inhibition in visual cortical processing. Curr. Opin. Neurobiol. 20, 340–346.

10. Gentet, L.J., Avermann, M., Matyas, F., Staiger, J.F., and Petersen, C.C. (2010). Membrane potential dynamics of GABAergic neurons in the barrel cortex of behaving mice. Neuron 65, 422–435.

11. Gentet, L.J., Kremer, Y., Taniguchi, H., Huang, Z.J., Staiger, J.F., and Petersen, C.C. (2012). Unique functional properties of somatostatin-expressing GABAergic neurons in mouse barrel cortex. Nat. Neurosci. 15, 607–612.

12. Fu, Y., Tucciarone, J.M., Espinosa, J.S., Sheng, N., Darcy, D.P., Nicoll, R.A., Huang, Z.J., and Stryker, M.P. (2014). A cortical circuit for gain control by behavioral state. Cell 156, 1139–1152.

13. Lee, S., Kruglikov, I., Huang, Z.J., Fishell, G., and Rudy, B. (2013). A disinhibitory circuit mediates motor integration in the somatosensory cortex. Nat. Neurosci. 16, 1662–1670.

14. Vanni, M.P., and Murphy, T.H. (2014). Mesoscale transcranial spontaneous activity mapping in GCaMP3 transgenic mice reveals extensive reciprocal connections between areas of somatomotor cortex. J. Neurosci. 34, 15931–15946.

15. Andermann, M.L., Kerlin, A.M., Roumis, D.K., Glickfeld, L.L., and Reid, R.C. (2011). Functional specialization of mouse higher visual cortical areas. Neuron 72, 1025–1039.

16. Neckelmann, D., Olsen, O.E., Fagerland, S., and Ursin, R. (1994). The reliability and functional validity of visual and semiautomatic sleep/wake scoring in the Møll-Wistar rat. Sleep 17, 120–131.

17. Oyanedel, C.N., Kelemen, E., Scheller, J., Born, J., and Rose-John, S. (2015). Peripheral and central blockade of interleukin-6 trans-signaling differentially affects sleep architecture. Brain Behav. Immun. 50, 178–185.

18. Evarts, E.V. (1964). Temporal patterns of discharge of pyramidal tract neurons during sleep and waking in the monkey. J. Neurophysiol. 27, 152–171.

19. Hobson, J.A., and McCarley, R.W. (1971). Cortical unit activity in sleep and waking. Electroencephalogr. Clin. Neurophysiol. 30, 97–112.

20. Feldmeyer, D., Lübke, J., and Sakmann, B. (2006). Efficacy and connectivity of intracolumnar pairs of layer 2/3 pyramidal cells in the barrel cortex of juvenile rats. J. Physiol. 575, 583–602.

21. Sato, T.R., Gray, N.W., Mainen, Z.F., and Svoboda, K. (2007). The functional microarchitecture of the mouse barrel cortex. PLoS Biol. 5, e189.

22. Sato, T.R., and Svoboda, K. (2010). The functional properties of barrel cortex neurons projecting to the primary motor cortex. J. Neurosci. 30, 4256–4260.

23. Stosiek, C., Garaschuk, O., Holthoff, K., and Konnerth, A. (2003). In vivo two-photon calcium imaging of neuronal networks. Proc. Natl. Acad. Sci. USA 100, 7319–7324.

24. Chen, T.W., Wardill, T.J., Sun, Y., Pulver, S.R., Renninger, S.L., Baohan, A., Schreiter, E.R., Kerr, R.A., Orger, M.B., Jayaraman, V., et al. (2013). Ultrasensitive fluorescent proteins for imaging neuronal activity. Nature 499, 295–300.

25. Hofer, S.B., Ko, H., Pichler, B., Vogelstein, J., Ros, H., Zeng, H., Lein, E., Lesica, N.A., and Mrsic-Flogel, T.D. (2011). Differential connectivity and response dynamics of excitatory and inhibitory neurons in visual cortex. Nat. Neurosci. 14, 1045–1052.

26. Meyer, H.S., Schwarz, D., Wimmer, V.C., Schmitt, A.C., Kerr, J.N., Sakmann, B., and Helmstaedter, M. (2011). Inhibitory interneurons in a cortical column form hot zones of inhibition in layers 2 and 5A. Proc. Natl. Acad. Sci. USA 108, 16807–16812.

27. Vyazovskiy, V.V., Olcese, U., Lazimy, Y.M., Faraguna, U., Esser, S.K., Williams, J.C., Cirelli, C., and Tononi, G. (2009). Cortical firing and sleep homeostasis. Neuron 63, 865–878.

28. Nir, Y., Staba, R.J., Andrillon, T., Vyazovskiy, V.V., Cirelli, C., Fried, I., and Tononi, G. (2011). Regional slow waves and spindles in human sleep. Neuron 70, 153–169.

29. Nir, Y., Vyazovskiy, V.V., Cirelli, C., Banks, M.I., and Tononi, G. (2015). Auditory responses and stimulus-specific adaptation in rat auditory cortex are preserved across NREM and REM sleep. Cereb. Cortex 25, 1362–1378.

30. Braun, A.R., Balkin, T.J., Wesensten, N.J., Gwadry, F., Carson, R.E., Varga, M., Baldwin, P., Belenky, G., and Herscovitch, P. (1998). Dissociated pattern of activity in visual cortices and their projections during human rapid eye movement sleep. Science 279, 91–95.

31. Braun, A.R., Balkin, T.J., Wesenten, N.J., Carson, R.E., Varga, M., Baldwin, P., Selbie, S., Belenky, G., and Herscovitch, P. (1997). Regional cerebral blood flow throughout the sleep-wake cycle. An H2(15)O PET study. Brain 120, 1173–1197.

32. Maquet, P., Péters, J., Aerts, J., Delfiore, G., Degueldre, C., Luxen, A., and Franck, G. (1996). Functional neuroanatomy of human rapid-eye-movement sleep and dreaming. Nature 383, 163–166.

33. Brecht, M., Roth, A., and Sakmann, B. (2003). Dynamic receptive fields of reconstructed pyramidal cells in layers 3 and 2 of rat somatosensory barrel cortex. J. Physiol. 553, 243–265.

34. Renouard, L., Billwiller, F., Ogawa, K., Clément, O., Camargo, N., Abdelkarim, M., Gay, N., Scoté-Blachon, C., Touré, R., Libourel, P.A., et al. (2015). The supramammillary nucleus and the claustrum activate the cortex during REM sleep. Sci. Adv. 1, e1400177.

35. Bock, D.D., Lee, W.C., Kerlin, A.M., Andermann, M.L., Hood, G., Wetzel, A.W., Yurgenson, S., Soucy, E.R., Kim, H.S., and Reid, R.C. (2011). Network anatomy and in vivo physiology of visual cortical neurons. Nature 471, 177–182.

36. Avermann, M., Tomm, C., Mateo, C., Gerstner, W., and Petersen, C.C. (2012). Microcircuits of excitatory and inhibitory neurons in layer 2/3 of mouse barrel cortex. J. Neurophysiol. 107, 3116–3134.

37. Kerlin, A.M., Andermann, M.L., Berezovskii, V.K., and Reid, R.C. (2010). Broadly tuned response properties of diverse inhibitory neuron subtypes in mouse visual cortex. Neuron 67, 858–871.

38. Scholl, B., Pattadkal, J.J., Dilly, G.A., Priebe, N.J., and Zemelman, B.V. (2015). Local integration accounts for weak selectivity of mouse neocortical parvalbumin interneurons. Neuron 87, 424–436.

39. Haider, B., Duque, A., Hasenstaub, A.R., and McCormick, D.A. (2006). Neocortical network activity in vivo is generated through a dynamic balance of excitation and inhibition. J. Neurosci. 26, 4535–4545.

40. Freund, T.F., and Meskenaite, V. (1992). Gamma-aminobutyric acid-containing basal forebrain neurons innervate inhibitory interneurons in the neocortex. Proc. Natl. Acad. Sci. USA 89, 738–742.

41. Xu, M., Chung, S., Zhang, S., Zhong, P., Ma, C., Chang, W.C., Weissbourd, B., Sakai, N., Luo, L., Nishino, S., and Dan, Y. (2015). Basal forebrain circuit for sleep-wake control. Nat. Neurosci. 18, 1641–1647.

42. Klausberger, T., Magill, P.J., Marton, L.F., Roberts, J.D., Cobden, P.M., Buzsaki, G., and Somogyi, P. (2003). Brain-state- and cell-type-specific firing of hippocampal interneurons in vivo. Nature 421, 844–848.

43. Lee, S.H., Kwan, A.C., Zhang, S., Phoumthipphavong, V., Flannery, J.G., Masmanidis, S.C., Taniguchi, H., Huang, Z.J., Zhang, F., Boyden, E.S., et al. (2012). Activation of specific interneurons improves V1 feature selectivity and visual perception. Nature 488, 379–383.

44. Cardin, J.A., Carlén, M., Meletis, K., Knoblich, U., Zhang, F., Deisseroth, K., Tsai, L.H., and Moore, C.I. (2009). Driving fast-spiking cells induces gamma rhythm and controls sensory responses. Nature 459, 663–667.

45. Sohal, V.S., Zhang, F., Yizhar, O., and Deisseroth, K. (2009). Parvalbumin neurons and gamma rhythms enhance cortical circuit performance. Nature 459, 698–702.

46. Grosmark, A.D., Mizuseki, K., Pastalkova, E., Diba, K., and Buzsáki, G. (2012). REM sleep reorganizes hippocampal excitability. Neuron 75, 1001–1007.

47. Häusser, M., Spruston, N., and Stuart, G.J. (2000). Diversity and dynamics of dendritic signaling. Science 290, 739–744.

48. Helmchen, F., Svoboda, K., Denk, W., and Tank, D.W. (1999). In vivo dendritic calcium dynamics in deep-layer cortical pyramidal neurons. Nat. Neurosci. 2, 989–996.

49. Akerman, C.J., and Cline, H.T. (2007). Refining the roles of GABAergic signaling during neural circuit formation. Trends Neurosci. 30, 382–389.

50. Duarte, R.C., and Morrison, A. (2014). Dynamic stability of sequential stimulus representations in adapting neuronal networks. Front. Comput. Neurosci. 8, 124.

51. Casanova, E., Fehsenfeld, S., Mantamadiotis, T., Lemberger, T., Greiner, E., Stewart, A.F., and Schütz, G. (2001). A CamKIIalpha iCre BAC allows brain-specific gene inactivation. Genesis 31, 37–42.

52. Madisen, L., Garner, A.R., Shimaoka, D., Chuong, A.S., Klapoetke, N.C., Li, L., van der Bourg, A., Niino, Y., Egolf, L., Monetti, C., et al. (2015). Transgenic mice for intersectional targeting of neural sensors and effectors with high specificity and performance. Neuron 85, 942–958.

53. Hippenmeyer, S., Vrieseling, E., Sigrist, M., Portmann, T., Laengle, C., Ladle, D.R., and Arber, S. (2005). A developmental switch in the response of DRG neurons to ETS transcription factor signaling. PLoS Biol. 3, e159.

54. Taniguchi, H., He, M., Wu, P., Kim, S., Paik, R., Sugino, K., Kvitsiani, D., Fu, Y., Lu, J., Lin, Y., et al. (2011). A resource of Cre driver lines for genetic targeting of GABAergic neurons in cerebral cortex. Neuron 71, 995–1013.

55. Roth, M.M., Dahmen, J.C., Muir, D.R., Imhof, F., Martini, F.J., and Hofer, S.B. (2016). Thalamic nuclei convey diverse contextual information to layer 1 of visual cortex. Nat. Neurosci. 19, 299–307.

56. Pologruto, T.A., Sabatini, B.L., and Svoboda, K. (2003). ScanImage: flexible software for operating laser scanning microscopes. Biomed. Eng. Online 2, 13.

57. Tian, L., Hires, S.A., Mao, T., Huber, D., Chiappe, M.E., Chalasani, S.H., Petreanu, L., Akerboom, J., McKinney, S.A., Schreiter, E.R., et al. (2009). Imaging neural activity in worms, flies and mice with improved GCaMP calcium indicators. Nat Methods 6, 875–881.

58. Komiyama, T., Sato, T.R., O'Connor, D.H., Zhang, Y.X., Huber, D., Hooks, B.M., Gabitto, M., and Svoboda, K. (2010). Learning-related fine-scale specificity imaged in motor cortex circuits of behaving mice. Nature 464, 1182–1186.

59. Dombeck, D.A., Khabbaz, A.N., Collman, F., Adelman, T.L., and Tank, D.W. (2007). Imaging large-scale neural activity with cellular resolution in awake, mobile mice. Neuron 56, 43–57.

Supplemental Information

Sleep-Stage-Specific Regulation

of Cortical Excitation and Inhibition

Niels Niethard, Masashi Hasegawa, Takahide Itokazu, Carlos N. Oyanedel, Jan Born, and Takashi R. Sato

Figure S1
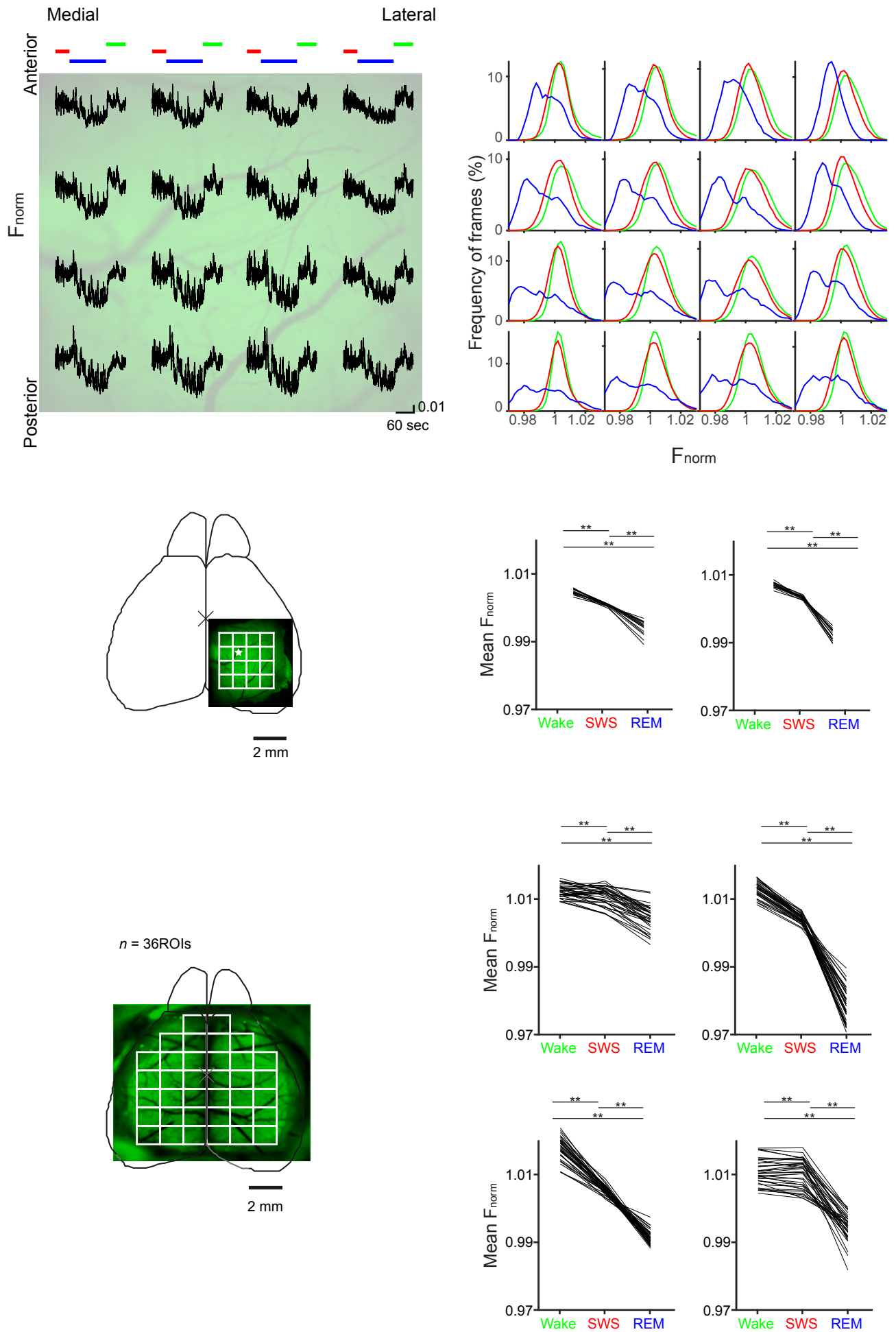
Figure S1. **Wide-field imaging during Wake, SWS and REM sleep. Related to Figure 1.**

Top, example recording of F_{norm} and concurrent epochs of Wake (green bars), SWS (red) and

REM sleep (blue) for the 16 ROIs imaged simultaneously for one example mouse. Conventions

as in Figure 1C in the main text. Bottom, the distribution of the F_{norm} signal during Wake, SWS

and REM sleep for the 16 ROIs in each mouse. Conventions as Figure 1D of the main text.

Bottom, Mean F_{norm} activity during Wake, SWS and REM sleep for 16 ROIs for two mice and for

36 ROIs for 4 mice. In all ROIs, the F_{norm} signal is highest during Wake, intermediate during

SWS, and lowest during REM sleep ($p < 0.001$).

Figure S2

Mouse 3

Mouse 4
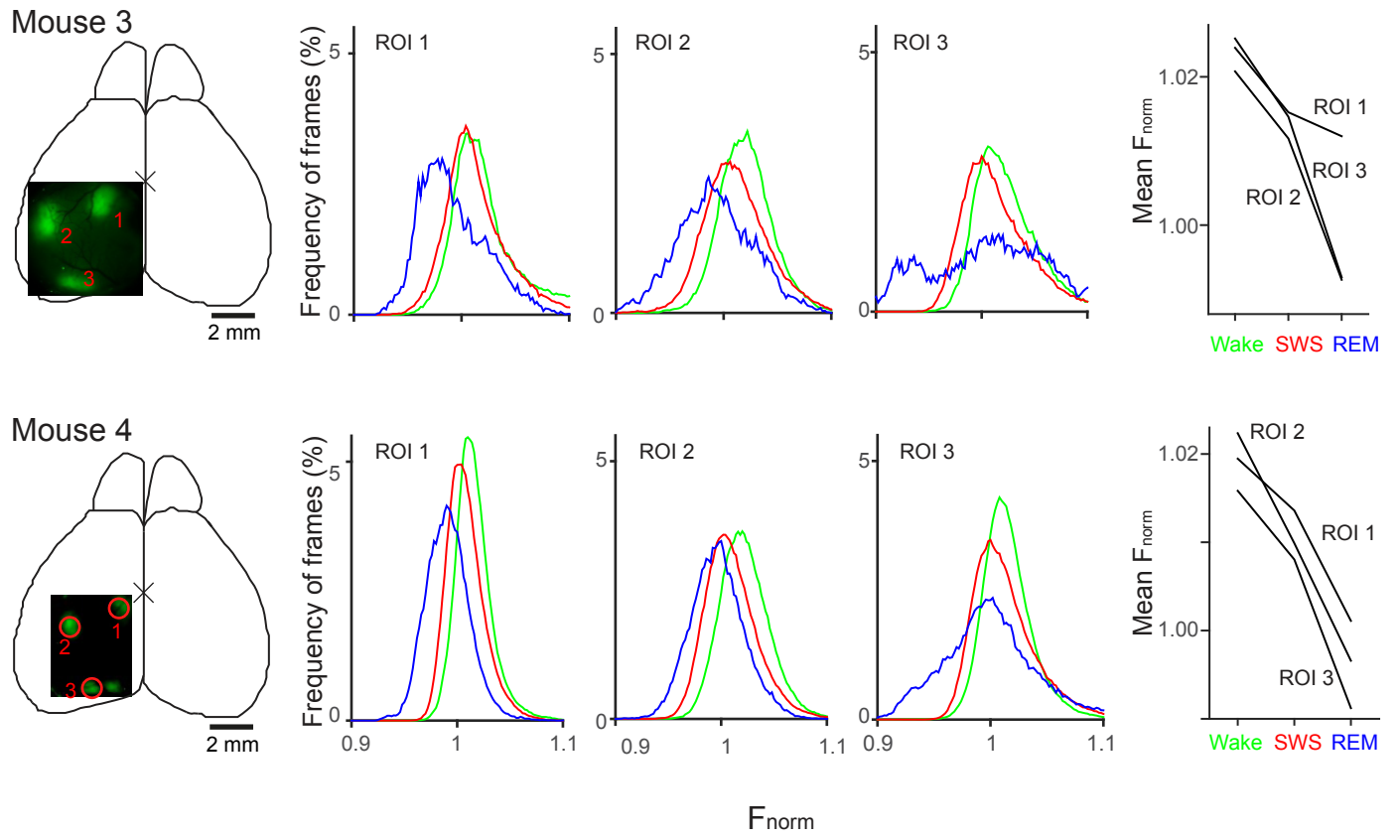
Figure S2. **Reduced fluorescence signal of virally expressed GCaMP6f during REM sleep. Related to Figure 1.** Left, a virus expressing GCaMP6f (AAV-syn-GCaMP6f) was injected into sensorimotor (1), barrel (2) and visual (3) cortex ($n = 2$ mice). Red circles indicate ROIs in each cortical area. Middle, the distribution of F_{norm} signal during Wake (green), SWS (red) and REM sleep (blue) for each of the ROIs. Right, in all three ROIs, the mean fluorescence signal was highest during Wake, intermediate during SWS and at a distinct minimum during REM sleep ($p < 0.01$, for all pairwise comparisons).

Figure S3

A unlabeled cells (*n* = 2042)
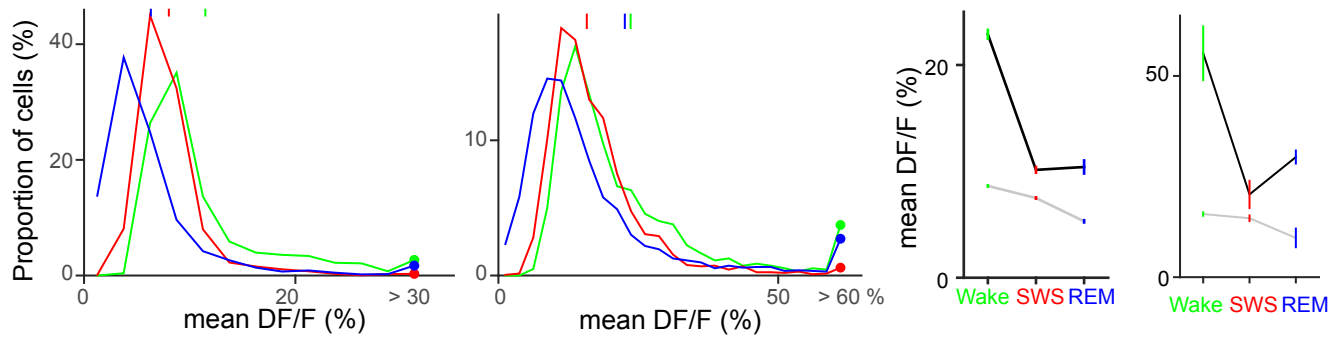
B PV-IN (*n* = 211)
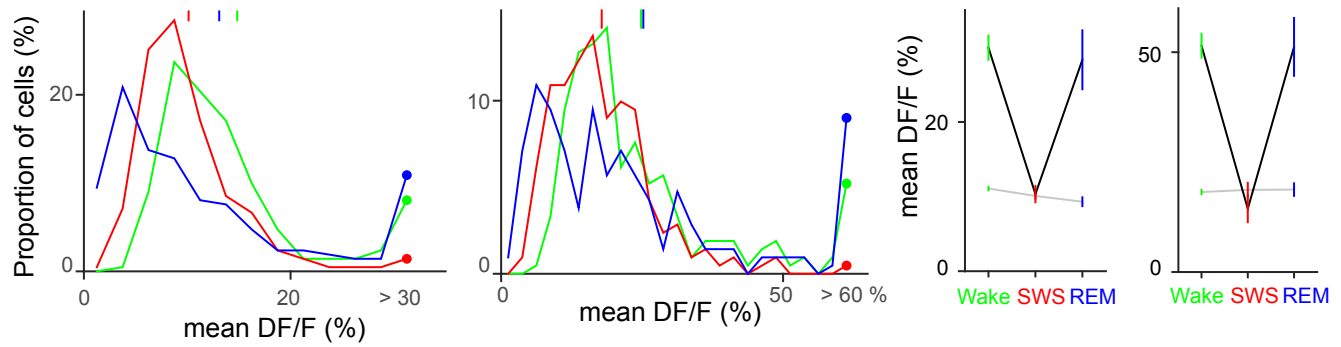
C SOM-IN (*n* = 117)
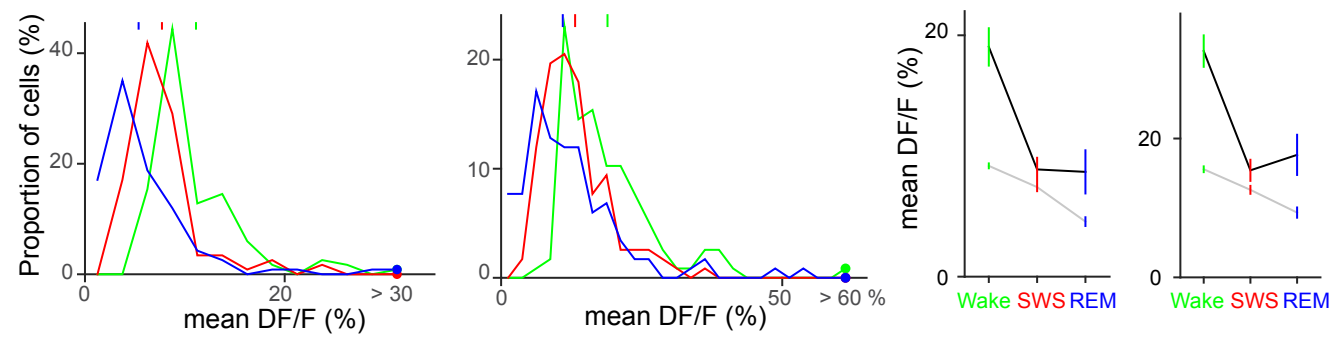
Figure S3. **Cell-type specific changes in neural activity during Wake, SWS, and REM sleep - analysis based on mean $\Delta F/F$ before and following neuropil correction. Related to Figure 4 and Figure 5.** Instead of the frequency of active frames (as in Figure 4 of the main text), here mean $\Delta F/F$ was used to quantify neural activity during Wake, SWS and REM, yielding essentially the same results. Left two panels, the distributions of activity for the three cell-types of interest before and after neuropil correction. Conventions as in Figure 4 of the main text. Right two panels, activity patterns of neurons showing high (top 20%) and low activity (remaining 80 %) during Wake, before and after neuropil correction. Conventions as in Figure 5 of the main text.

Figure S4
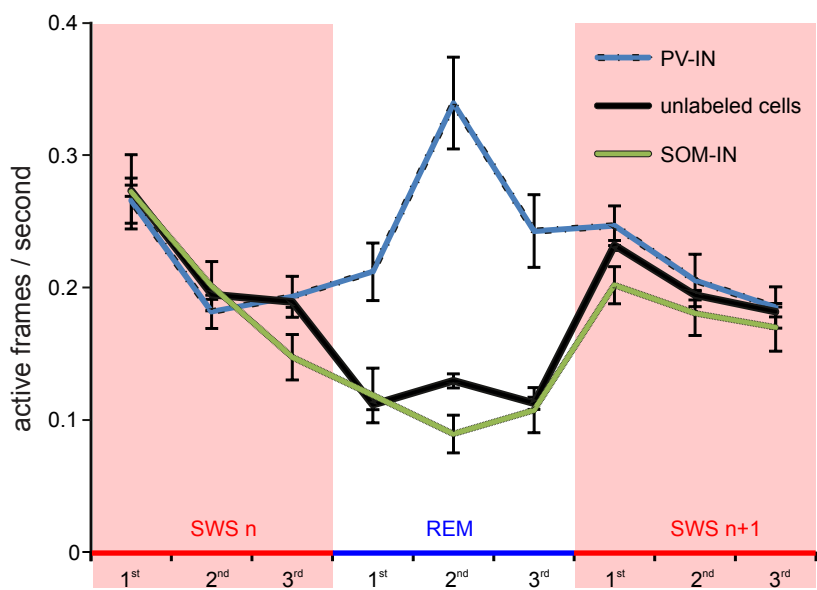
Figure S4. Time course of neural activity during SWS-REM-SWS epochs. Related to Figure 4.

Time course of activity (active frames per second) for PV-INs (blue), SOM-INs (green) and unlabeled cells (red) across triplets of SWS-REM sleep-SWS epochs. Data represent mean ± s.e.m. from 128 triplets recorded in 10 mice. Sleep stage periods were normalized to a common duration and divided into thirds (1st, 2nd, 3rd). Note differential dynamics of PV-IN which show peak activity during the middle part of a REM sleep epoch, and SOM-IN cells and unlabeled cells showing minimum activity at this time.

Figure S5

A

GCaMP6f

Wake
SWS
REM

raw F$_{norm}$

filtered F$_{norm}$

0.01

30 sec

GFP control

Wake
SWS
REM

raw F$_{norm}$

filtered F$_{norm}$

0.01

30 sec

B

GFP control   GCaMP6f

difference median F$_{norm}$

0

-0.06

-0.12

**

*
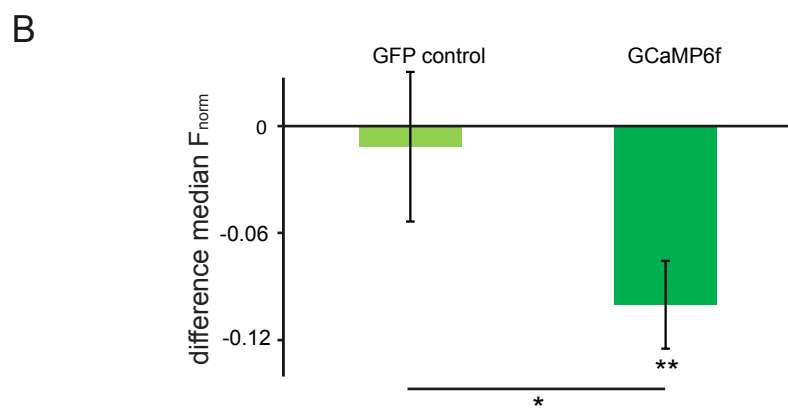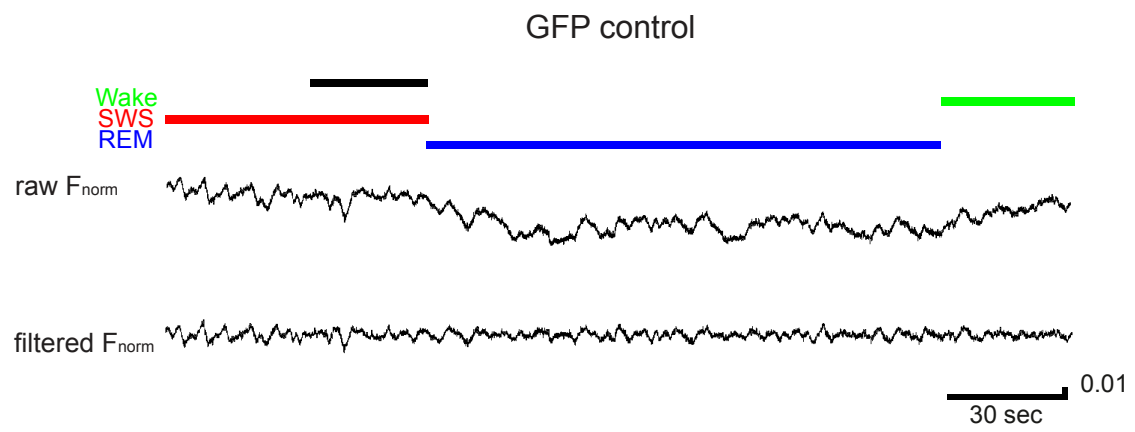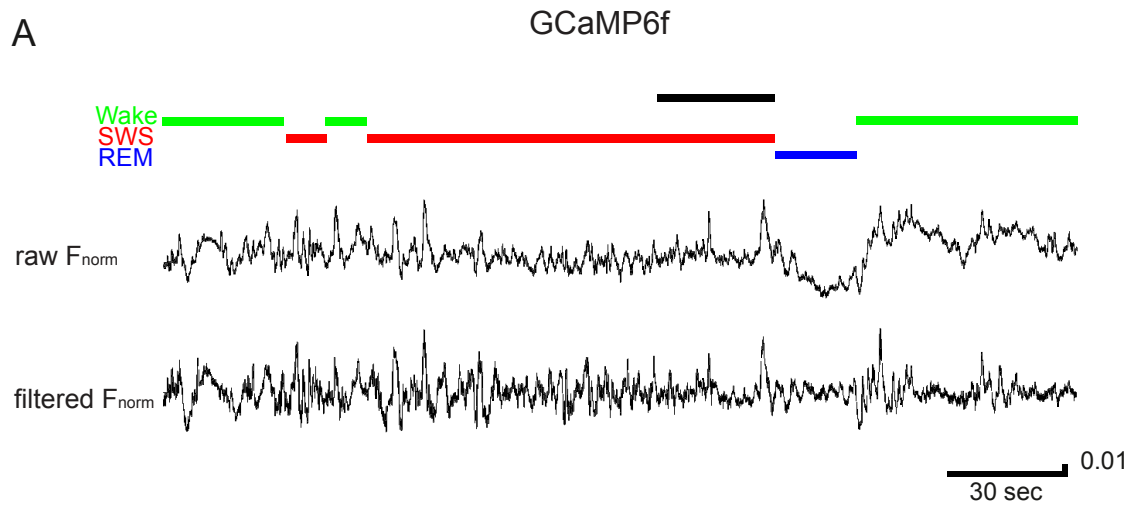
Figure S5. Control experiments with GFP. Related to Experimental Procedures, Figure 1 and Figure 2.

To estimate possible confounding effects on the calcium fluorescence signal during wide field imaging (e.g., coming from blood flow or temperature changes) 3 additional control animals expressing a calcium independent green fluorescence protein (gfp control animals, AAV2/1-EF1α-GFP) were recorded during sleep. (A) Analyses of unfiltered data showed a drop in fluorescence signal during REM sleep. However, when data were high-pass pre-filtering (at 0.1 Hz) before analyses, to remove gradual drifts in the signal possibly reflecting changes in temperature or blood flow or temperature, this drop completely disappeared. (B) Comparing pre-filtered data from 3 gfp mice (n=42 REM episodes) and 6 GCaMP6f-mice (n = 47 REM episodes) revealed that only GCaMP6f mice showed a strong drop in activity during REM sleep which was almost 10 times stronger than in the gfp control mice ($p < 0.05$). This data (1) suggest the presence of slow changes in non-neural activity confounding calcium-dependent neural activity, and (2) indicate that such possible confounding influences can be effectively eliminated by high-pass pre-filtering the signal. Means ± SEM of the difference in median F_{norm} activity during REM sleep and a 40-s pre-REM sleep baseline are indicated. ** $p < 0.001$, * $p < 0.05$.

Table S1

PV-cre animals	Imaging sessions	Total number of cells	PV-IN
1	2	353	38
2	2	154	28
3	3	447	46
4	3	354	66
5	1	127	17
6	1	121	16
SOM-cre animals	Imaging sessions	Total number of cells	SOM-IN
1	3	342	45
2	2	229	38
3	1	123	16
4	1	120	18

Table S1. Number of animals, imaging sessions and cells per animal. Related to Figures 4 – 6.

2.3 Study II: Cortical circuit activity underlying sleep slow oscillations and spindles

Published as:

Niethard, N., Ngo, H.-V. V, Ehrlich, I., and Born, J. (2018). Cortical circuit activity underlying sleep slow oscillations and spindles. Proceedings of the National Academy of Science U. S. A. 115, E9220–E9229

Author contributions study II

Author	Author position	Scientific ideas %	Data generation %	Analysis & interpretation %	Paper writing %
Niels Niethard	1st Corresponding.	50	99	33.3	50
Hong-Viet V. Ngo	2nd	0	0	33.3	0
Ingrid Ehrlich	3rd	0	1	0	0
Jan Born	Last Corresponding.	50	0	33.3	50
Title of paper:		Cortical circuit activity underlying sleep slow oscillations and spindles.			
Status in publication process		Published in: Proceedings of the National Academy of Science U. S. A. 115, E9220–E9229			

Cortical circuit activity underlying sleep slow oscillations and spindles

Niels Niethard[a,1], Hong-Viet V. Ngo[a,b], Ingrid Ehrlich[c,d,2], and Jan Born[a,c,1]

[a]Institute of Medical Psychology and Behavioral Neurobiology, University of Tübingen, 72076 Tübingen, Germany; [b]School of Psychology, University of Birmingham, B15 2TT Birmingham, United Kingdom; [c]Center for Integrative Neuroscience, University of Tübingen, 72076 Tübingen, Germany; and [d]Hertie Institute for Clinical Brain Research, University of Tübingen, 72076 Tübingen, Germany

Slow oscillations and sleep spindles are hallmarks of the EEG during slow-wave sleep (SWS). Both oscillatory events, especially when co-occurring in the constellation of spindles nesting in the slow oscillation upstate, are considered to support memory formation and underlying synaptic plasticity. The regulatory mechanisms of this function at the circuit level are poorly understood. Here, using two-photon imaging in mice, we relate EEG-recorded slow oscillations and spindles to calcium signals recorded from the soma of cortical putative pyramidal-like (Pyr) cells and neighboring parvalbumin-positive interneurons (PV-Ins) or somatostatin-positive interneurons (SOM-Ins). Pyr calcium activity was increased more than threefold when spindles co-occurred with slow oscillation upstates compared with slow oscillations or spindles occurring in isolation. Independent of whether or not a spindle was nested in the slow oscillation upstate, the slow oscillation downstate was preceded by enhanced calcium signal in SOM-Ins that vanished during the upstate, whereas spindles were associated with strongly increased PV-In calcium activity. Additional wide-field calcium imaging of Pyr cells confirmed the enhanced calcium activity and its widespread topography associated with spindles nested in slow oscillation upstates. In conclusion, when spindles are nested in slow oscillation upstates, maximum Pyr activity appears to concur with strong perisomatic inhibition of Pyr cells via PV-Ins and low dendritic inhibition via SOM-Ins (i.e., conditions that might optimize synaptic plasticity within local cortical circuits).

sleep | calcium imaging | slow oscillation | spindle | inhibition

Mammalian slow-wave sleep (SWS) is characterized by two major EEG oscillatory events (the slow oscillation and the sleep spindle). The slow oscillation, also considered a neurophysiological substrate of EEG slow-wave activity, is characterized by widespread synchronized changes in the membrane potential of cortical neurons between hyperpolarization during the slow oscillation downstate and depolarization during the slow oscillation upstate, occurring at frequencies between 0.1 and 4 Hz (1, 2). Neural silence characterizing the slow oscillation downstate pertains to excitatory neurons as well as inhibitory interneurons (3, 4). The slow oscillation is primarily generated within cortical networks, where it can occur in the absence of thalamocortical input, with major participation of layer 5 neurons (5–7). Nevertheless, in natural conditions, thalamic inputs substantially contribute to the occurrence of cortical slow oscillation upstates (8). Slow oscillations often show propagation patterns as waves traveling from anterior to posterior cortical areas (9–11).

Sleep spindles are characterized by waxing and waning oscillatory field potentials in a frequency range between 7 and 15 Hz and with a duration of 0.5–3 s (1). Within this frequency band in the human EEG, fast and slow spindles can be discriminated, which differ in topography and possibly also in their function (12, 13). Sleep spindles are generated in intrathalamic circuits comprising GABAergic neurons within the nucleus reticularis thalami and in collaterals of glutamatergic thalamocortical projection neurons, with these projections also mediating their propagation to widespread neocortical regions (14–16), where they reach both excitatory and inhibitory

cells. The initiation and termination of spindles critically depend on corticothalamic feedback (17, 18). The generation of spindles is driven by the depolarizing upstate of the neocortical slow oscillation such that they tend to nest in the beginning phase of the cortical slow oscillation upstate (2).

There is convergent evidence that slow oscillations, as well as spindles, contribute to the consolidation of memory during sleep and underlying cortical synaptic plasticity mediating this memory effect (19–23). The slow oscillation is thought to convey primarily global processes of synaptic downscaling and renormalization (24), although it might concurrently contribute to long-term potentiation and upscaling of synapses in local cortical circuits (25). Spindles and associated neural firing patterns have been shown to promote cortical synaptic long-term potentiation (23, 26, 27). The consolidation of memory during sleep likely originates from the repeated reactivation of respective neural ensemble activity in hippocampal as well as neocortical networks (28–30). Such reactivations occur preferentially during the upstate of the cortical slow oscillation. In fact, the depolarizing upstate of the slow oscillation appears to drive neural memory reactivations and thalamocortical spindles in parallel (31–33). In this framework, slow oscillations co-occurring with spindles have been proposed to be particularly effective in forming long-term memory and in regulating underlying synaptic plasticity (34–36).

Significance

Slow oscillations and spindles are hallmarks of the EEG during slow-wave sleep. They are thought to support memory consolidation, particularly in instances where the faster spindle nests into the "upstate" of a slow oscillation. Using two-photon and wide-field imaging, we recorded calcium transients from distinct populations of cortical excitatory and inhibitory neurons during sleep in mice. Compared with spindles or slow oscillations occurring in isolation, events where spindles nested in a slow oscillation upstate were indeed accompanied by a unique pattern of calcium activity where high pyramidal cell activity appears to concur with high perisomatic inhibition through parvalbumin-positive interneurons and with low dendritic inhibition through somatostatin-positive interneurons. These conditions might foster dendritic plasticity.

Here, we aimed to directly link calcium activity, also as a factor that has been considered to eventually enable the neural plasticity underlying memory formation during SWS (37) in the mouse cortex, to EEG measures of slow oscillations and spindles, reflecting synchronized membrane potential oscillations in cortical networks. Two-photon imaging was used to assess calcium activity before, during, and after solitary slow oscillations and spindles, and spindles co-occurring with slow oscillation upstates, in pyramidal-like (Pyr) cells and neighboring parvalbumin-positive interneurons (PV-Ins) and somatostatin-positive interneurons (SOM-Ins) representing the major populations of excitatory and inhibitory neurons, respectively, in cortical circuits. We find that solitary slow oscillation upstates and spindles are accompanied by increased Pyr calcium activity. Inhibitory regulation during the slow oscillation appears to be conveyed mainly by SOM-Ins, which show strongly increased calcium activity in the beginning of the slow oscillation downstate and also a transient increase in the beginning of the slow oscillation upstate, whereas inhibitory PV-In activity is dominant during spindles. Notably, spindles nesting in the slow oscillation upstate are accompanied by maximal increases in Pyr activity, while inhibitory PV-In activity is maintained at the same high level as during solitary spindles and SOM-In activity is low.

Results

We investigated the activity of layer 2/3 PV-Ins and SOM-Ins and of neighboring putative Pyr cells during slow oscillations and spindles occurring in isolation and during co-occurring slow oscillation-spindle events during SWS (Fig. 1 *A*, *C*, and *D*). For this purpose, we identified PV-Ins and SOM-Ins in PV-Cre and SOM-Cre transgenic mice by Cre-dependent expression of tdTomato and assessed the calcium signal as a proxy for cellular activity by panneuronal expression of GCaMP6f (cf. ref. 38) (Fig. 1 *B* and *D*). Calcium activity of all three cell types was compared during a 5-s time window lasting from 2 s before to 3 s after the negative slow oscillation half-wave peak and the spindle onset, respectively. Activity between −3 and −2 s before the negative slow oscillation half-wave peak and spindle onset, respectively, was used as a baseline. Average calcium activity during this baseline interval did not differ between solitary slow oscillations, solitary spindles, and spindles co-occurring with slow oscillations ($P > 0.23$). Three different frequency bands were used to analyze spindles: slow spindles (7–10 Hz), fast spindles (11–15 Hz), and broad-band spindles (7–15 Hz). As no major differences were found, we focused on broad-band 7–15-Hz spindles as characterized in previous reports (3, 15, 17).

SI Appendix, Table S1 summarizes basic features of the analyzed slow oscillations and spindles. With our criteria for slow oscillation and spindle detection (*Materials and Methods*), we detected a total of 18,931 solitary slow oscillations in seven animals (PV-Cre animals: 8,062, SOM-Cre animals: 10,869), 1,311 solitary spindles (PV-Cre animals: 557, SOM-Cre animals: 754) and 1,092 spindles co-occurring with slow oscillation upstates (PV-Cre: 451, SOM-Cre: 641). Across imaging sessions and animals, mean slow oscillation duration (0.61 ± 0.008 s vs. 0.61 ± 0.01 s) and amplitude (0.26 ± 0.01 mV vs. 0.27 ± 0.01 mV) were closely comparable between slow oscillations and slow oscillations co-occurring with spindles. Whereas the duration of solitary spindles was slightly shorter than for spindles co-occurring with slow oscillations (0.71 ± 0.01 s vs. 0.77 ± 0.01 s; $P < 0.001$), interevent intervals (3.26 ± 0.2 s vs. 3.63 ± 0.1 s) and peak frequencies (12.14 ± 0.04 Hz vs. 12.09 ± 0.04 Hz) did not differ between the spindle types ($P > 0.1$; Fig. 1*E*).

Activity of Pyr Cells, PV-Ins, and SOM-Ins During Slow Oscillations and Spindles. All three cell types of interest showed distinct modulations of their activity during solitary slow oscillations and spindles, and during slow oscillation-spindle events (Fig. 2 *A* and

B). To assess the temporal dynamics of cell activity during the slow oscillation, the slow oscillation cycle was divided into four phases (Fig. 2*C*, *Top*): (*i*) a positive-to-negative "transition" phase (0.32 to −0.00 s before a negative half-wave peak), (*ii*) the "down" phase (−0.00 to +0.16 s), the "up" phase (+0.32 to +0.48 s), and an "after" phase (+0.54–3 s). In solitary slow oscillations, the transition phase was hallmarked by a distinct increase in SOM-In activity paralleled by a significant decrease in PV-In activity (both $P < 0.01$ with reference to baseline activity; Fig. 2 *B* and *C*). Increases in Pyr cell activity during the transition phase were not significant. During the subsequent down phase, we observed significantly reduced activity, on average, across all three cell types [in percent signal change value ($\Delta F/F$) $\times 10^{-3}$: −6.3 ± 0.5, −7.1 ± 0.7, and −6.1 ± 0.6 for Pyr cells, PV-Ins, and SOM-Ins, respectively; all $P < 0.001$]. In the up phase, putative Pyr cells and SOM-Ins displayed significant increases in activity ($P < 0.01$), averaging +2.8 ± 0.5 and +1.7 ± 0.7 (in $\Delta F/F \times 10^{-3}$), respectively. For SOM-Ins, this increase was restricted to the initial part of the up phase (Fig. 2*B*). By contrast, PV-In activity during the up phase did not differ from baseline. In the after phase, all cell types displayed significantly reduced activity (all $P < 0.01$). Exploratory principal component analyses (PCAs) confirmed a predominant inhibitory control via SOM-Ins rather than PV-Ins during the slow oscillation. This analysis identified one component starting with the transition phase and extending over the whole slow oscillation, with component scores in the opposite direction for SOM-Ins and PV-Ins (*SI Appendix*, Fig. S1).

During solitary spindles [+0.00 to +1.00 s with reference to spindle onset ("during")], PV-Ins showed distinctly increased activity (on average, by +10.1 ± 3.0 $\Delta F/F \times 10^{-3}$; $P < 0.001$). For putative Pyr cells, a similar increase did not reach significance (Fig. 2*B*). By contrast, SOM-In activity did not differ from baseline (Fig. 2*C*). After solitary spindles [+1.00 to +3.00 s with reference to spindle onset (after)], activity of SOM-Ins was decreased, compared with baseline levels ($P < 0.05$). PCA confirmed an opposing modulation of PV-In and SOM-In cells, reflecting high PV-In activity and low SOM-In activity, for the major component covering the whole spindle range (*SI Appendix*, Fig. S1).

To examine how the temporal dynamics in cell activity during a slow oscillation were modified by a spindle nesting in its up phase, we compared patterns during solitary slow oscillations and slow oscillation-spindle events (Fig. 2*C*). For all three cell types, activity did not significantly differ between solitary slow oscillations and slow oscillation-spindle events before (transition phase) and during the slow oscillation down phase. During the subsequent up phase, co-occurring spindles consistently enhanced Pyr cell activity more than threefold ($P < 0.01$) and PV-In activity more than 20-fold ($P < 0.01$), but did not change SOM-In activity (Fig. 2*C*). Additional analyses revealed that for both Pyr cells and PV-Ins, the duration of calcium transients, as assessed per cell, during the up phase was longer for slow oscillation-spindle events compared with calcium transients observed during solitary slow oscillations ($P < 0.01$). In the after phase of slow oscillations, when spindles co-occurred with slow oscillations, we observed a reduction in activity for putative Pyr cells and PV-Ins ($P < 0.01$) compared with solitary slow oscillations, but not for SOM-Ins. ANOVA across all slow oscillation phases confirmed significant co-occurring/solitary × phase interactions for all three cell types (Pyr: $F = 8.2$, $P < 0.001$; PV-In: $F = 10.7$, $P < 0.001$; SOM-In: $F = 4.1$, $P < 0.01$).

After comparing solitary slow oscillations and slow oscillations co-occurring with spindles, we likewise assessed whether the presence of a slow oscillation upstate changed the dynamics of cell activity seen during solitary spindles (Fig. 2*C*, *Right*). This analysis confirmed that the activity of putative Pyr cells was more than threefold higher during a spindle that nested in a slow oscillation upstate than during a solitary spindle ($P < 0.05$),
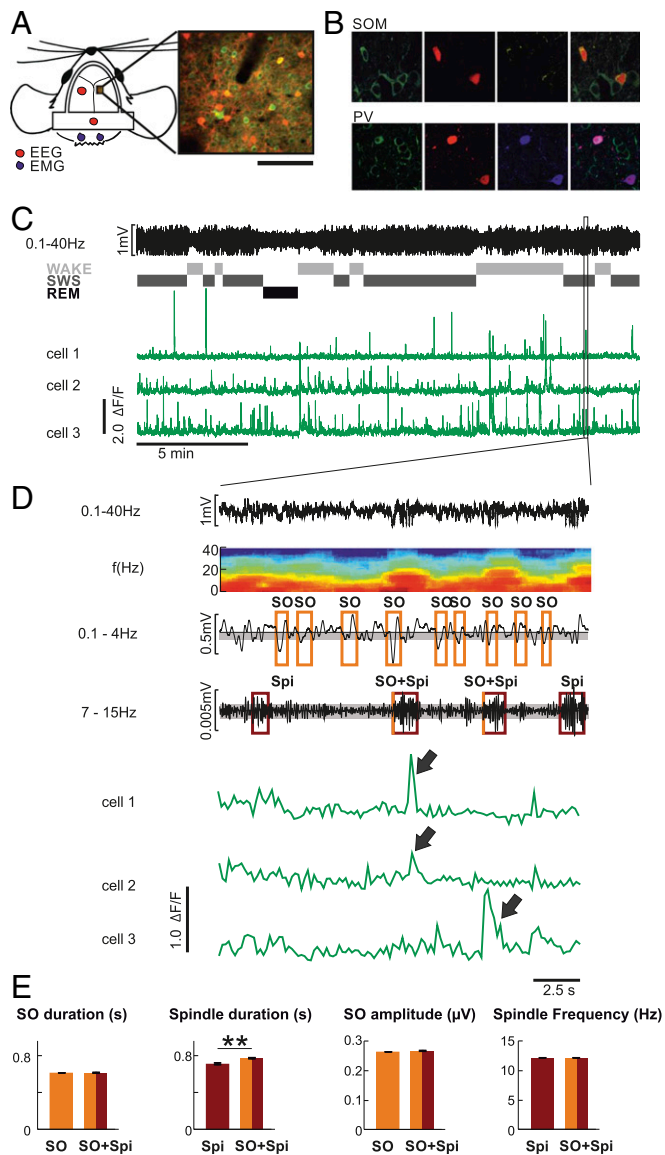
Fig. 1. Simultaneous EEG recording and two-photon calcium imaging. (*A*, *Left*) Illustration of EEG and electromyography (EMG) electrode positions and of the imaging window for the two-photon experiments. (*A*, *Right*) Example frame from one SOM-Cre animal. (Scale bar: 100 μm.) (*B*) Fluorescence image of GCaMP6f (green) and td-tomato–positive interneurons (red; *Top*, SOM-Cre; *Bottom*, PV-Cre) and immunohistochemical staining (yellow, SOM; blue, PV). (*C*) Example EEG trace (from a parietal electrode) and, underneath, corresponding classification of sleep stages [wake, SWS, rapid eye movement (REM) sleep] and example calcium activity traces from three individual putative Pyr cells. The frame marks the interval magnified in *D*. (*D*, *Top*) Zoomed-in EEG trace (from a parietal electrode) and, underneath, the corresponding time-frequency plot. For detection of slow oscillation(s) (SO), the EEG signal was filtered between 0.1 and 4.0 Hz. An SO was identified in the EEG when (*i*) the distance between consecutive positive-to-negative zero crossings was between 0.4 and 2 s, (*ii*) the amplitude of the negative half-wave peak in this interval exceeded 0.66 SD (gray-shaded range) from the mean of all identified intervals in a recording session, and (*iii*) the difference in amplitude between the negative and succeeding positive peak was greater than 2/3 of the average negative-to-positive peak amplitude for all identified intervals in a recording session. Spindle(s) (Spi) were detected when the amplitude of the filtered EEG signal (7–15 Hz) was greater than 1.5 SDs from the mean (gray-shaded range) amplitude during a recording session for at least 0.5 s. (*D*, *Bottom*) Example fluorescence traces (ΔF/F) from three individual putative Pyr cells during the same time interval. Note the synchronous activity of cells 1 and 2 during the first Spi co-occurring with an SO and of cell 3 during the second Spi co-occurring with an SO (arrows). (*E*) Summary of SO and Spi properties (mean duration, mean SO amplitude, mean Spi frequency across all animals and all recorded events), separately for isolated SO and Spi and for SO co-occurring with Spi (SO + Spi). **$P <$ 0.01, for pairwise comparison (corresponding results for each animal are shown in *SI Appendix*, Table S1).

whereas activity of PV-Ins during these two types of spindles was at a high but comparable level during solitary and nested spindles. Also, the after phase of spindles was characterized by enhanced Pyr cell activity when the spindle had occurred during a slow oscillation compared with solitary spindles [$F = 5.1$, $P < 0.05$ for co-occurring/solitary main effect in an ANOVA across both phases (i.e., during and after the spindle)].

To examine to what extent scattered fluorescence from the neuropil contaminated the fluorescence signal from the cell soma, we repeated the analyses using ΔF/F values that were neuropil-corrected. In this approach, calcium events were detected whenever the signal within a frame exceeded 2 SDs of the median neuropil-corrected fluorescence signal of the cell (*Materials and Methods*). This analysis revealed temporal dynamics of calcium event rates during solitary spindles, slow oscillations, and slow oscillation-spindle events, which are summarized in *SI Appendix*, Fig. S2. These control analyses rule out the possibility that the results concerning uncorrected ΔF/F signal from the three neuron subpopulations of interest reported above are substantially contaminated by scattering dendritic fluorescence.

Overall, these findings indicate the existence of specific mechanisms of circuit regulation for slow oscillations and spindles. On one side, slow oscillations are characterized by enhanced SOM-In activity, which precedes the initial negative slow oscillation half-wave peak and seems to also counterregulate the distinct increase in Pyr cell activity during the slow oscillation upstate. On the other side, during spindles, increased PV-In activity appears to counterregulate the increase in Pyr cell activity. The co-occurrence of a slow oscillation upstate with a spindle produces a maximum increase in Pyr cell activity in the presence of high levels of PV-In activity and low levels of SOM-In activity.

Wake-Active Versus Wake-Inactive Neurons. Previous studies have revealed that cell activity dynamics differ depending on the cell's activity during wakefulness (38–40). To investigate whether the wake activity level affected cell-specific calcium activity during slow oscillations and spindles, we compared, separately for each of the three cell types of interest, fluorescence signals between the 20% of cells (fifth quintile) that were most active during wakefulness and the 20% of cells (first quintile) that were least active during wake phases (*SI Appendix*, Fig. S3).

This comparison revealed that wake-inactive SOM-In cells displayed a stronger modulation of calcium activity by slow oscillations and spindles than the wake-active SOM-In cells (*SI Appendix*, Fig. S3). For putative Pyr and PV-In cells, the direct comparisons between wake-active and wake-inactive cells did not reach significance, which might partly reflect the enhanced signal variability in these subsamples.

Fluorescence Signal Correlates with EEG Signal During Slow Oscillations and Spindles. To clarify the relationship between fluorescence intensity and EEG signal amplitude during slow oscillations and spindles, we calculated Pearson's correlation coefficients between respective measures. Only a few survived Bonferroni corrections for multiple testing. For slow oscillations, correlations were stronger for the negative-to-positive peak amplitude measure than for the other amplitude measures (negative half-wave and positive half-wave peak amplitudes) and slightly higher for slow oscillations co-occurring with spindles than for solitary slow oscillations. Correlations between $r = 0.12$ and $r = 0.09$ ($P < 0.01$) were found between the slow oscillation negative-to-positive amplitude and
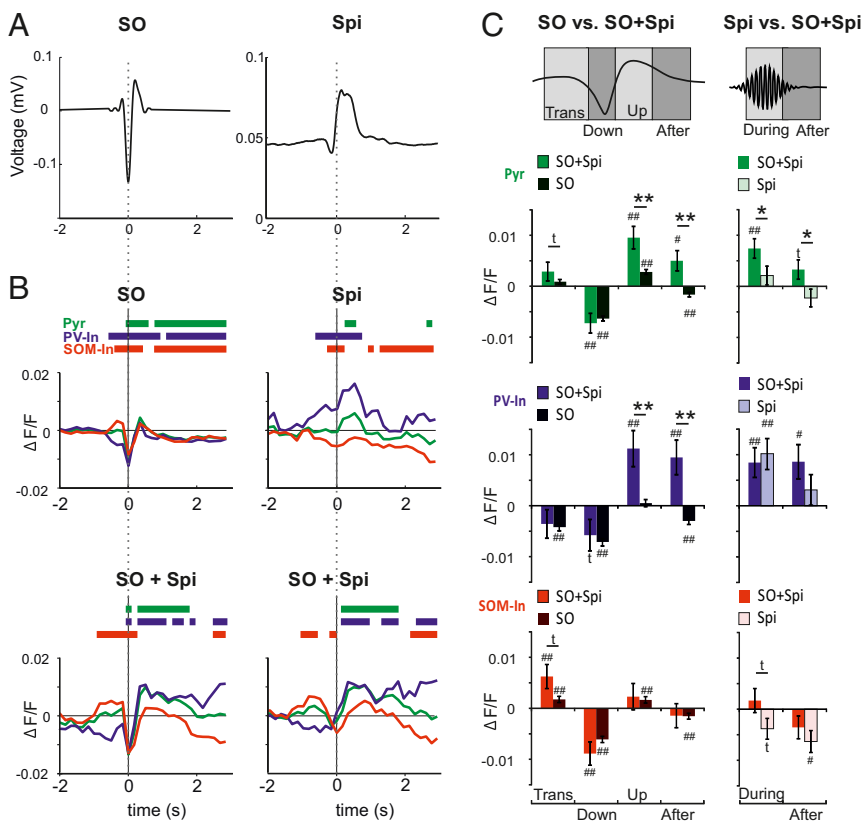
Fig. 2. Distinct modulation of calcium activity during slow oscillation and spindle. (*A, Left*) Grand average (across all events from all animals) of the EEG signal (filtered between 0.1 and 4 Hz) during slow oscillation(s) (SO) time-locked to the negative SO half-wave peak (0 s). (*A, Right*) Grand average of the rms of EEG spindle (Spi) signal (7–15 Hz) time-locked to Spi onset (0 s). (*B*) Mean ΔF/F signals for putative Pyr cells (green), PV-Ins (blue), and SOM-Ins (red) during solitary SO (*Top Left*) and solitary Spi (*Top Right*) and during SO co-occurring with Spi (SO + Spi), time-locked to a negative SO half-wave peak (*Bottom Left*) and to Spi onset (*Bottom Right*). Bars on top indicate significance ($P < 0.05$) with reference to a baseline (-3 to -2 s) set to zero. Average traces across all events from all animals are indicated. (*C, Left*) Comparison of mean ($\pm$SEM) ΔF/F signals between solitary SO and SO + Spi events for the positive-to-negative transition phase (Trans; -0.32 to -0.00 s, with reference to the SO negative half-wave peak = 0 s), the down phase (-0.00 to 0.16 s), the up phase (0.32–0.48 s), and the following after phase (0.54–3 s). (*C, Right*) Comparisons between mean ($\pm$SEM) ΔF/F signals between solitary Spi and SO + Spi events for the phase during the acute Spi (0–1 s with reference to Spi onset set to 0 s) and the after phase (1–3 s). $**P < 0.01$, $*P < 0.05$, and $^tP < 0.1$ for pairwise comparisons between solitary events and SO + Spi events respectively. $^{\#\#}P < 0.01$, $^{\#}P < 0.05$, and $^tP < 0.1$ for difference from baseline activity (-3 to -2 s).

the ΔF/F signal of Pyr cells and SOM-Ins, respectively, during the transition, down, and up phases of slow oscillations co-occurring with spindles, with overall highest coefficients for correlations with the signal during the up phase.

Analyses of spindles revealed somewhat higher correlations (Fig. 3). The ΔF/F signal of putative Pyr cells showed significant positive correlations with spindle power, with this correlation being more robust for spindles co-occurring with slow oscillations ($r = 0.19$, $P < 0.001$) than for solitary spindles ($r = 0.12$, $P < 0.001$). Moreover, for spindles co-occurring with slow oscillations, this correlation was significantly ($P < 0.001$) stronger for wake-active Pyr cells (fifth quintile; $r = 0.27$, $P < 0.001$) than for wake-inactive cells (first quintile; $r = 0.12$, $P < 0.001$). On the other side, wake-inactive SOM-Ins (first quintile) showed stronger correlations between ΔF/F signals and spindle power than wake-active SOM-Ins during spindles co-occurring with slow oscillations ($r = 0.18$, $P < 0.001$ vs. $r = 0.04$ $P = 0.27$; $P < 0.001$ for difference between coefficients).

We also calculated pairwise correlations of ΔF/F signals within the populations of putative Pyr cells, PV-In cells, and SOM-In cells, as well as between Pyr cells and the two inhibitory cell populations (*SI Appendix*, Fig. S4). Generally, these correlations were small ($r < 0.15$), and their distribution did not provide evidence for the presence of highly correlated subgroups of cells accompanying the occurrence of slow oscillations or spindles.

Cortical Topography of Calcium Activity During Slow Oscillations and Spindles. To characterize the cortical topography of slow oscillation and spindle-related changes in calcium activity, we used wide-field imaging of the dorsal surface of the cortex in mice (Fig. 4 *A* and *B*). This technique provides calcium signals with high temporal resolution (50–60 frames per second) and, additionally, broader fields of view covering cortical areas in ranges of square centimeters (38, 41). The cortical surface of transgenic animals expressing a genetically encoded calcium indicator

(GCaMP6f) in almost all cortical Pyr cells (CaMKII-positive cells) was monitored. To investigate the topographical distribution of calcium activity during sleep spindles and slow oscillations, we compared grand averages (across all events from all animals) of f_{norm} signals in 36 regions of interest (ROIs) during solitary slow oscillations, solitary spindles, and slow oscillations co-occurring with spindles, with the EEG events detected in recordings from either the left frontal cortex or the left occipital cortex. To characterize anterior and posterior cortical activities, and for the respective statistical comparisons, activity was averaged across four frontal and four occipital target ROIs (Fig. 4*A*).

During solitary slow oscillations, calcium signal showed a widespread and significant reduction during the down phase regardless of whether the slow oscillation was identified in the frontal or occipital EEG channel ($P < 0.05$ for analysis of target ROIs, with reference to baseline levels -3 to -2 s before the negative half-wave peak; Fig. 4*C* and *SI Appendix*, Fig. S5). This decrease was followed by a transient increase in calcium signal in the beginning of the slow oscillation up phase, which did not significantly differ from baseline, however. Solitary spindles detected in the frontal EEG channel were associated with significantly increased calcium signal in the anterior target ROIs, which was succeeded by a widespread reduction in calcium signal persisting for more than 3 s after the spindle had ceased ($P < 0.01$). This reduction in signal was likewise significant for solitary spindles identified in the occipital EEG ($P < 0.01$ for posterior target ROIs; *SI Appendix*, Fig. S5). Slow oscillations that co-occurred with a spindle were marked by a clear increase in calcium signal during the up phase, most pronounced over the anterior ROIs ($P < 0.01$). However, the mean f_{norm} signal amplitude during a 1-s interval starting with spindle onset did not significantly differ between solitary spindles and spindles that occurred during a slow oscillation upstate ($P > 0.1$). Like solitary slow oscillations, these slow oscillation-spindle events were associated with a widespread decrease in activity during the prior

down phase, and, like solitary spindles, they were followed by a widespread persisting suppression of activity ($P < 0.05$ across all target ROIs; *SI Appendix*, Figs. S5 and S6 show corresponding data for events detected in the occipital EEG channel).

Calcium activity associated with the slow oscillation revealed a systematic traveling from frontal to occipital cortical regions, such that reductions in activity during the negative half-wave peaked slightly earlier over frontal cortical areas than over posterior areas (Fig. 5 and Movie S1). This traveling was significant for both solitary slow oscillations and slow oscillation-spindle events (mean ± SEM delay between frontal ROIs 25–36 and occipital ROIs 1–12: 10.5 ± 1.7 ms; $P < 0.001$). No significant delay between hemispheres was found, and there were also no hints at a systematic traveling of spindle-associated changes in calcium activity.

We wanted to exclude the possibility that changes in fluorescence observed with GCaMP6f imaging are not reflecting calcium activity but are confounded by metabolic and/or blood flow changes, which can affect the intensity of the detected fluorescence signal. To this end, we measured fluorescence change in control animals expressing GFP within cortical layer 2/3, which is
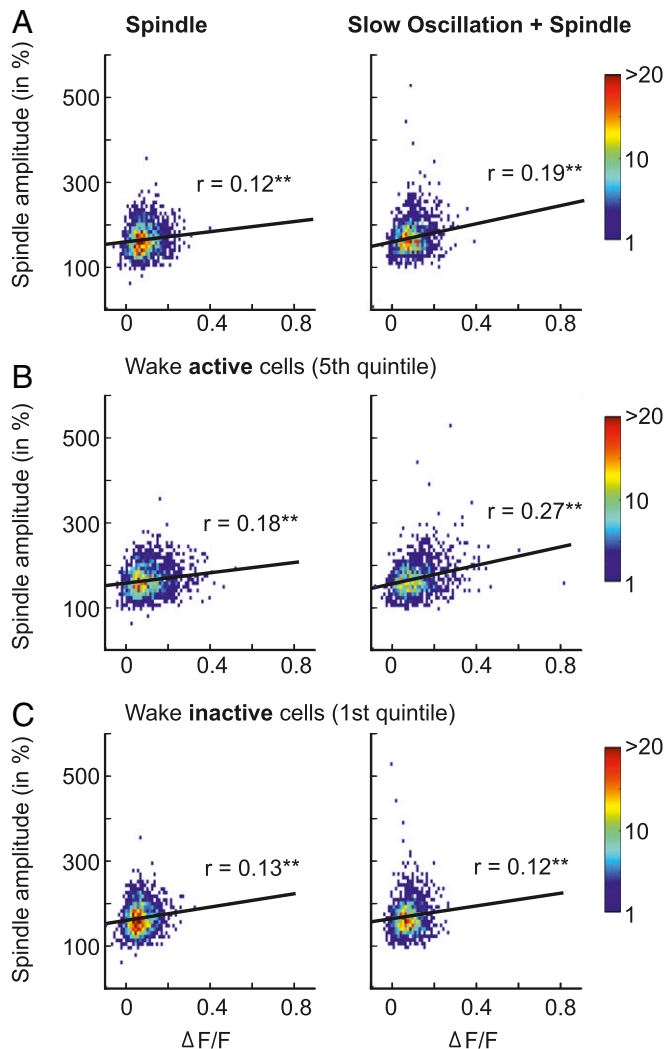
Fig. 3. Calcium activity of putative Pyr cells correlates with spindle amplitude. Density plots showing the correlation between activity of putative Pyr cells (mean ΔF/F across all cells for each event) and EEGs with 7–15-Hz spindle amplitude (normalized rms) for solitary spindles (*Left*) and spindles co-occurring with slow oscillations (*Right*). Results are shown separately for all Pyr cells (*A*), wake-active Pyr cells (*B*), and wake-inactive Pyr cells (*C*). **$P < 0.001$.
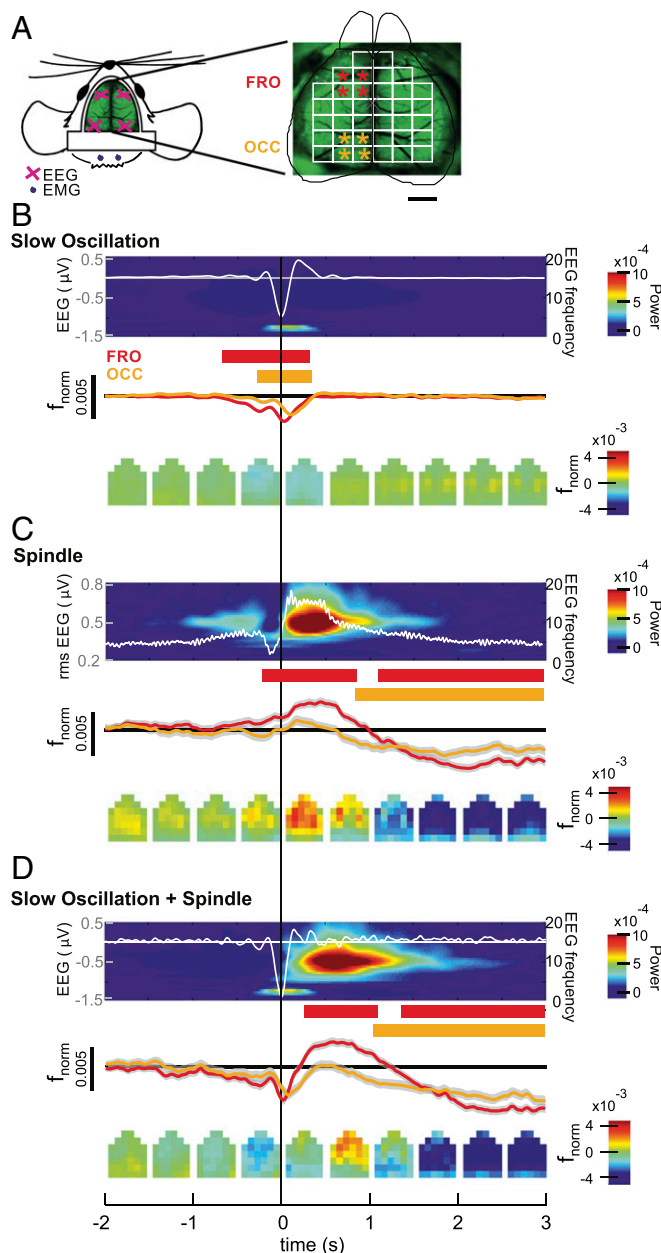
Fig. 4. Cortical topography of calcium activity during slow oscillation and spindle. (*A*) Schematic drawing of the wide field used for calcium imaging, positioning of electrodes for EEG (pink crosses), and electromyography (EMG) recordings (blue dots). (*Right*) Imaging window was divided into 36 ROIs. Asterisks mark ROIs used for statistical comparison of activity between anterior (red) and posterior (orange) regions. (Scale bar: 2 mm.) (*B*) Average EEG signal for solitary slow oscillations (*Top*; from left frontal cortical recordings, white line overlaying average time-frequency plot with color-coded power) together with average (±SEM) calcium activity (f_{norm}) across the four designated anterior (red) and posterior (orange) cortical regions (*Middle*). Averages are time-locked to the negative half-wave peak of the slow oscillation (0 s). Intervals with significant changes in calcium activity ($P < 0.01$, relative to the baseline interval from −3 to −2 s) are indicated in red [for anterior ROIs (FRO)] and orange bars [for posterior ROIs (OCC)]. (*Bottom*) Topographic changes of calcium activity in all 36 ROIs (f_{norm}, color-coded) for subsequent 500-ms time windows. (*C* and *D*) Corresponding data for solitary spindles (Spindle) and slow oscillations co-occurring with spindles (Slow oscillation + Spindle). Note that for solitary spindles, the average EEG signal (overlaying the corresponding EEG time-frequency plot) shows the rms amplitude and averaging is time-locked to the spindle onset. Average traces are shown across events from four animals (total: $n = 9,472$, $n = 706$, and $n = 770$, for solitary slow oscillations, solitary spindles, and slow oscillations co-occurring with spindles, respectively; corresponding results for EEG events identified in occipital recordings are shown in *SI Appendix*, Fig. S5).

not a calcium-dependent fluorescent protein (*Materials and Methods*). As expected, these animals showed neither the acute decrease and increase in calcium signal accompanying the slow oscillation downstate and upstate nor an acute increase in calcium signal during spindles ($P < 0.001$ for all relevant comparisons with the experimental GCaMP6f animals).

Discussion

Using calcium imaging in the naturally sleeping brain, our study provides evidence that the slow oscillations and spindles of SWS

Fig. 5. Slow oscillation-associated calcium signal travels from anterior to posterior cortex. (*A*) Illustration of the 36 cortical ROIs used for wide-field imaging experiments. The red-shaded area indicates anterior ROIs (25–36), and the blue-shaded area indicates posterior ROIs (1–12). (*B*) Histogram showing the distribution of the temporal delays of slow oscillation negative (neg.) half-wave peaks defined in the f_{norm} signal between frontal ROIs and occipital ROIs. Only slow oscillation events were included in this analysis, where the minimum of the f_{norm} signal was associated with the slow oscillation half-wave peak exceeding a critical threshold for both anterior and posterior regions (with the threshold defined by 0.66 SD from the mean activity of the filtered 0.1–4-Hz signal). (*C*) Calcium activity for 36 cortical ROIs using wide-field imaging during solitary slow oscillations (*Left*), solitary spindles (*Center*), and slow oscillations co-occurring with spindles (*Right*, Slow Oscillation + Spindle). The red-shaded area indicates anterior ROIs, and the blue-shaded area indicates posterior ROIs. The numbering of ROIs is indicated in *A*. Average traces across four animals (total: $n = 9472$, $n = 706$, and $n = 770$ for solitary slow oscillations, solitary spindles, and slow oscillations co-occurring with spindles, respectively) are indicated. Averaging is time-locked (0 s) to the negative half-wave peak of slow oscillation and spindle onset, respectively. EEG events were detected in the frontal EEG channel (corresponding results for EEG events detected in occipital recordings are shown in *SI Appendix*, Fig. S6). The red-marked calcium signal indicates intervals of significantly ($P < 0.05$) enhanced or reduced activity (with reference to activity during the baseline interval from −3 to −2 s).

are characterized by a specific balance between the activity of excitatory and specific inhibitory neurons within cortical circuits. We find that the slow oscillation upstates and, to a far lesser extent, spindles are accompanied by an increase in calcium activity of putative Pyr cells. The excitatory drive during the slow oscillation appears to be mainly countered by inhibitory activity of SOM-Ins showing distinct increases in the beginning of the downstate and also transiently in the beginning of the upstate. By contrast, inhibitory activity during spindles is primarily conveyed by increased activity of PV-Ins. Importantly, when spindles co-occur with the slow oscillation upstate, Pyr calcium activity reaches a maximum in the presence of high levels of PV-In activity and low levels of SOM-In activity.

Our results, revealing an increase in SOM-In calcium activity at the transition into the slow oscillation downstate as well as at the transition into the upstate, shed light on the regulation underlying the emergence of the cortical slow oscillation. The slow oscillation downstate is considered a disfacilitatory state (1, 42), which is confirmed by the present findings indicating a general decrease in the activity of excitatory Pyr cells as well as inhibitory PV-Ins or SOM-Ins during the downstate. However, what triggers the downstate, and what explains its high synchrony across cortical columns, has been unclear for a long time. Based on studies of slice preparations of the rodent entorhinal cortex, an involvement of slow GABA(B) receptors as well as D1-like dopaminergic receptors has been suggested (43, 44). Comparisons of local field potentials in mice lacking glutamate decarboxylase 67 in either SOM-Ins or PV-Ins provided the first hints that these cells might specifically contribute to the regulation of slow oscillation downstates and upstates (45). Strong electrophysiological evidence for the induction of the slow oscillation by distinct inhibitory activities has only recently been provided by Timofeev and coworkers (46). They found in natural sleeping cats that the slow oscillation downstate was preceded by a longer (100–300 ms) chloride-mediated inhibitory barrage that was likely mediated by long-range afferent inputs to inhibitory interneurons. The rather similar time course observed here for the increase in SOM-In activity preceding the slow oscillation downstate, together with findings that optogenetic stimulation of SOM-Ins can induce slow oscillations (47), speaks for a contribution of SOM-Ins in initialization of the slow oscillation downstate. This view is further supported by our observation that PV-In activity gradually decreased in the same time interval (i.e., before the downstate), as SOM-Ins are known to directly inhibit PV-Ins and a number of other cortical interneurons (48). The majority (~70%) of cortical SOM-In cells are Martinotti cells (49). They mainly target the apical dendrites of Pyr cells, where they regulate dendritic spike generation and synaptic integration in local networks of Pyr cells (50, 51). These properties make them a strong candidate for active induction of the slow oscillation downstate, as well as for regulating inhibitory control during the downstate-to-upstate transition, when their activity transiently increased.

Our finding that spindles are accompanied by a strong increase in PV-In calcium activity concurs with findings from electrophysiological studies. Not only do PV-In–like fast spiking cells show increased firing rates during spindles but firing is also in synchrony with the spindle oscillation (52, 53). On the other hand, Pyr cells do not show consistent increases in firing during spindles, even though they receive highly synchronized excitatory input. This picture of a predominant inhibitory regulation of spindles via feedforward or intracortical feedback inputs to PV-Ins agrees well with the present data of a distinct increase in PV-In activity accompanied by only a slight (but significant) increase in Pyr activity (54). Interestingly, at the same time, SOM-In activity was low, possibly reflecting inhibition of SOM-In via PV-In, thereby shifting Pyr inhibition from SOM-In–driven dendritic inhibition to PV-In–driven
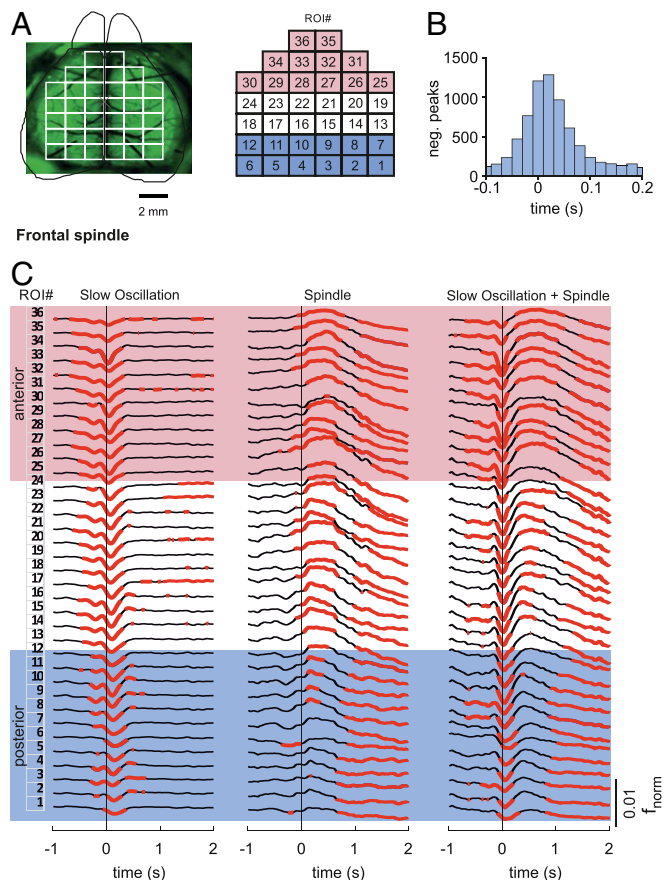
perisomatic inhibition, which might favor dendritic synaptic plasticity (48, 55, 56).

Mainly based on computational models, it has been proposed that a massive intracellular increase in calcium in Pyr cells during spindles mediates persisting synaptic plastic changes underlying memory consolidation during sleep (37). This study provides evidence that calcium activity in cortical layer 2/3 Pyr is only slightly enhanced when spindles occur in isolation but becomes profoundly enhanced when the spindle occurs during a slow oscillation upstate, rendering such slow oscillation-spindle events a condition particularly fostering the consolidation of cortically represented memories (19, 36, 57).

Our data also uncover some of the underlying circuit conditions of the strong increase in Pyr activity during slow oscillation-spindle events, as it concurred with PV-In activity at levels as high as during solitary spindles, as well as with rather low SOM-In activity. The shift toward perisomatic inhibition by PV-Ins in the presence of low dendritic inhibition through SOM-Ins during slow oscillation-spindle events and solitary spindles probably enables local increases in calcium levels within dendrites by excitatory inputs. Such inputs might originate from reactivated memory representations in cortical and extracortical regions such as the hippocampus. As they are synchronized to the depolarizing slow oscillation upstate with a co-occurring spindle, they reach cortical Pyr cells in a time window of dendritic disinhibition, allowing for effective local calcium responses (31, 32, 35, 58). Indeed, in awake rats, dendritic encoding of sensory stimuli and associated increases in dendritic calcium levels were facilitated by increased perisomatic inhibition and simultaneously decreased inhibition through Martinotti cells (50). According to this scenario, low SOM-In activity during spindles nesting in slow oscillation upstates would play a permissive role for dendritic calcium activity, facilitating the induction of persisting plasticity at dendritic synapses in Pyr cells. Although this view is tentative, as we did not directly assess dendritic calcium activity, it concurs well with findings in awake mice showing that low SOM-In activity, in the presence of strong perisomatic inhibition of Pyr cells, facilitates dendritic synaptic plasticity upon encoding of motor memories in these cells (47, 55, 59). Moreover, during SWS, after motor memory encoding dendritic plasticity was shown to occur, as a consequence of reactivated representations, on select apical branches of Pyr cells (60) and dendritic calcium activity was found to be distinctly increased during spindles (54). Collectively, those and the present findings tempt one to propose that the constellation of low SOM-In–mediated dendritic inhibition, together with strong perisomatic inhibition of Pyr cells, is a general feature facilitating dendritic plasticity in postencoding wake conditions as well as during SWS, when newly encoded representations are reactivated in the presence of slow oscillation-spindle events (29, 31, 61).

Recent studies suggest that synaptic plastic changes during sleep depend on the prior activity of the involved neurons during wakefulness (62, 63). In the present study, differences between the most and least active cells during wakefulness were moderate overall and mainly found for inhibitory cells, but not for putative Pyr cells. The described dynamics in calcium activity, especially during spindles, appeared to be more pronounced in SOM-Ins and PV-Ins with the lowest wake activity than in those with highest wake activity, although direct comparisons between the cell clusters often failed to reach significance. This observation might be linked to electrophysiological findings indicating that cells with low firing activity are more likely involved in encoding specific memories (39). However, the greater dynamics in wake-inactive interneurons were observed independent of whether activity levels were determined based on only the wake periods preceding the experimental sleep period or on wake periods preceding and following sleep, suggesting that the enhanced dynamics in wake-inactive cells are unrelated to the encoding of information during the prior wake phase.

Wide-field imaging confirmed the more widespread topography of slow oscillations in comparison to spindles, as well as the anterior-to-posterior traveling of slow oscillation-related activity, a feature also reported in other studies using calcium imaging (7) and electrophysiological recordings (e.g., refs. 10, 12, 64, 65). Whether the traveling of the slow oscillation reflects spreading via long-range intracortical excitatory connections, consequently depending on the excitatory–inhibitory balance within cortical columns, or critically involves thalamic regulation is not clear (7, 66, 67). Notably, our wide-field imaging did not show the pronounced increase in Pyr calcium activity during spindles that nested in slow oscillation upstates, compared with solitary spindles, which we revealed with two-photon imaging of the Pyr soma. This discrepancy might be related to the fact that, for the most part, wide-field imaging covered calcium activity of apical dendrites, whose dynamics are expected to differ from those of the soma [e.g., as to the reflection of action potentials (54)].

Although our calcium imaging data mirrored topography and its temporal dynamics for spindles and slow oscillations quite well, correlations between calcium activity of the cells and our electrophysiological amplitude measures, although significant, remained rather modest. This is owing to the fact that calcium signal and EEG amplitude reflect different aspects of activity: on the one hand, calcium level in the contributing neurons and, on the other hand, the synchronized changes in membrane potential mainly of Pyr cells, as the parallel orientation of these neurons and their dendrites enables the summation of extracellular field potentials. It is thus not unexpected that the observed correlations were highest for Pyr activity. The calcium activity in Pyr cells was most robustly associated with the amplitude of slow oscillation that co-occurred with a spindle, underscoring that the up-regulation of calcium activity in these cells is particularly strong when spindles nest in the slow oscillation upstate.

Not only was the size of correlation coefficients between measures of EEG oscillations and calcium activity modest but statistical effect sizes (partial eta-squared) for the observed main effects were also consistently <0.3 despite their high significance ($P < 0.01$). In fact, the overall moderate magnitude of effects agrees well with electrophysiological studies demonstrating that spontaneous firing rates of cortical neurons are log-normally distributed, with the majority of neurons showing very low firing rates [<0.2 Hz (68)] and, importantly, that only a small fraction of these neurons is recruited for the slow oscillation and spindle events of interest here (69–71). Even during events of highly synchronized activity like the upstate of the slow oscillation, no more than 3% of all cells are synchronously active. Concurring with those findings, our calcium imaging approach unselectively covering all cells revealed that changes in calcium activity accompanying slow oscillations and spindles were always conveyed by only a subsample of neurons covered. Thus, our calcium imaging approach corroborates the notion that slow oscillations and spindles are not associated with a global recruitment of neural firing activity but only with activity in distinct neuronal subpopulations, which are possibly those involved in encoding of information during prior wakefulness (72–74).

In the current study, we aimed at linking changes in calcium activity in distinct subsets of cortical neurons to EEG field potential oscillations known to be involved in memory formation during sleep. The basic question arises of to what extent the assessed calcium signal changes relate to action potential activity. Although the fluorescent calcium indicator we used (GCaMP6f) enables the reliable detection of single action potentials (75), it is likely that not all calcium transients detected in our study represent action potentials. However, additional analysis on neuropil-corrected signals excluded the contamination of our measurements with scattered fluorescence from dendrites. Moreover, such

contamination should bias calcium signal levels in the different cell types toward the same direction, which contrasts with our findings of partly opposed changes. Overall, these analyses ensured that the pattern of calcium signal changes coinciding with the EEG oscillations of interest, for the most part, reflect soma-specific events, although this does not exclude the presence of calcium events without spiking. Nevertheless, it seems justified to assume that our measures of soma-specific calcium activity are substantially correlated to cell activity in terms of action potentials (75, 76). However, to precisely characterize this relationship, further experiments are required combining recordings of calcium and electrical activity in single units.

Despite the insights this study provides into the regulation of microcircuits during slow oscillations and sleep spindles, three principle limitations need to be considered. First, compared with electrophysiological detection of firing activity, the temporal resolution of the applied two-photon calcium imaging is rather low, mainly owing to the rather slow decay times of the calcium indicator (in this case, GCaMP6f). Nevertheless, the decay times, together with the 6-Hz frame rate we used in our experiments, are sufficient to cover the EEG oscillatory phenomena of interest [slow oscillation and spindle events (the latter basically defined by their power envelope)], which comprise frequencies <3 Hz. However, our frame rate for two-photon imaging was not sufficient to dissociate changes in calcium activity for subtypes of spindles with faster and slower oscillatory frequency (77) and, importantly, precludes a reliable discrimination of activity changes occurring in synchrony with a specific phase of these oscillations (52, 53). This limitation possibly relates to the seemingly paradoxical observation that during slow oscillation-spindle events, Pyr cell somata show distinct increases in calcium activity in the presence of perisomatic inhibition and presumed hyperpolarization by PV-Ins, which, itself, is expected to decrease calcium activity (78). The increase in calcium activity in Pyr cells during slow oscillation-spindle events likely reflects excitatory inputs (e.g., from thalamocortical projections) occurring during the excitable troughs of the spindle cycle. PV-In activity, on the other hand, with a slight delay, closes the excitatory phase of the spindle cycle to induce perisomatic hyperpolarization of Pyr cells. However, to scrutinize this scenario, further experimentation is required combining recording of calcium and electrical activity in single units.

A second limitation derives from the fact that we focused on the two major types of cortical interneurons, PV-Ins and SOM-Ins. We revealed a unique constellation of activity between these interneurons that characterizes circuit activity during slow oscillation-spindle events, which raises the question of the factors driving this constellation. Here, long-range connections from subcortical (e.g., thalamic) structures, as well as several other types of intracortical interneurons, might play a role (79–81). Vasoactive intestinal polypeptide (VIP)-positive interneurons are a likely candidate to be considered in future studies. Cortical VIP-positive interneurons have been shown to exert disinhibitory control in cortical circuits via action on SOM-In cells and also appear to be involved in the regulation of EEG oscillations (82–84).

A third limitation relates to our focus on activity in layer 2/3, which might differ from activity in other cortical layers. Slow oscillations propagate from layer 5 to more superficial layers (67), and, in this context, a recent study by Seibt et al. (54) complements the present findings by focusing on layer 5 rather than layer 2/3 neurons. Only concentrating on spindles, the study found spindles to be accompanied by increased calcium activity in the apical dendrites of the cells, but not in the cells' soma throughout the cortical column. Against this backdrop, it is conceivable that the increase in calcium signal observed here in the soma of layer 2/3 Pyr cells specifically during spindle nesting in slow oscillation upstates is even more profound in analyses focusing on apical dendrites of layer 5 neurons (54). While our calcium imaging study

reveals a distinct pattern of activity in cortical circuits associated with slow oscillations and spindles, it did not include any intervention. Thus, the central question of causality (i.e., to what extent the observed changes in calcium activity characterizing slow oscillation and spindles indeed play a causal role in the regulation of these EEG events) remains to be resolved (47).

Nevertheless, the limitations of our study in no way challenge its main finding (summarized in Fig. 6) that spindles nesting in slow oscillation upstates are marked by a maximal increase in calcium activity of excitatory Pyr cells, which occurs in the presence of strong perisomatic inhibition by PV-Ins and low dendritic inhibition by SOM-Ins. This might optimize local synaptic plasticity underlying the formation of long-term memory in these circuits.

Materials and Methods

Experimental procedures were approved by the local institutions in charge of animal welfare (Regierungspraesidium Tübingen, State of Baden-Wuerttemberg, Germany). Procedures of surgery and recordings followed, in large part, protocols described previously (38). All used resources are summarized in *SI Appendix*, Table S2.

Animals and Surgery. PV-Cre mice [RRID:IMSR_JAX:008069 (85)] and SOM-Cre mice [RRID:IMSR_JAX:013044 (86)] were used for in vivo two-photon calcium imaging. CaMKII-Cre mice [RRID:IMSR_EM:01153 (87)] crossed with Ai95RCL-GCaMP6f mice [RRID:IMSR_JAX:024105 (88)] and C57BL6/J mice were used for wide-field calcium imaging. The mice were housed in groups of up to five mice in temperature-controlled (22 ± 2 °C) and humidity-controlled (45–65%) cages. Experiments were performed during the light (i.e., rest) period of the l2-h/12-h light/dark cycle. Data collection in all mice started 1 h after light onset. All mice were male and older than 8 wk of age. Detailed information about the surgical implantation procedures is provided in *SI Appendix*.

Two-Photon Image Analysis. Lateral motion was corrected in two steps (89). A cross-correlation–based image alignment (Turboreg) was performed, followed by a line-by-line correction using an algorithm based on a hidden Markov model (90). ROIs containing individual neurons were drawn manually, and the pixel values within each ROI were summed to estimate the fluorescence of this neuron. PV-Ins and SOM-Ins were manually detected by

A Solitary Slow Oscillation **B** Solitary Spindle **C** Slow Oscillation + Spindle
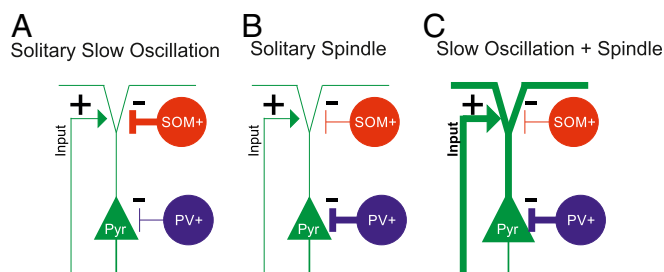
Fig. 6. Schematic illustration of the main findings. Our findings indicate distinct constellations of the excitation/inhibition balance in cortical circuits during slow oscillations and spindles depending on whether these events occur in isolation (Solitary Slow Oscillation, Solitary Spindle) or together, with the spindle nesting in the slow oscillation upstate (Slow Oscillation + Spindle). (*A*) Solitary slow oscillations are hallmarked by increased SOM-In (SOM$^+$) activity mediating dendritic inhibition of putative Pyr cells at the transition to the downstate and in the initial upstate of the slow oscillation. (*B*) Solitary spindles are hallmarked by increased PV-In (PV$^+$) activity mediating distinct perisomatic inhibition of Pyr cells in the presence of weak dendritic inhibition by SOM-In cells. (*C*) Spindles nesting in the slow oscillation upstate are hallmarked by a more than threefold increase in Pyr cell activity (compared with respective solitary events), which is possibly driven by specific excitatory inputs to these cells. Simultaneously, Pyr cells receive strong perisomatic inhibition through PV-Ins, while their dendritic inhibition via SOM-Ins is reduced. We speculate that this constellation of excitatory and inhibitory inputs during slow oscillation-spindle events facilitates dendritic synaptic plasticity in Pyr cells underlying memory formation during sleep. The "+" and "−" symbols indicate excitatory–inhibitory inputs, and the thick vs. thin lines indicate the strength of inputs to Pyr cells.

red fluorescence signal expressed by AAV2/1-Flex-tdtomato. Surrounding neurons not expressing tdTomato were considered putative Pyr cells [these cells likely include other types of interneurons, although the proportion of them is negligible (<10%) (80, 91)]. The analyses aimed at globally assessing calcium transients in the cells of interest during solitary EEG slow oscillations, spindles, and slow oscillation-spindle events. For this purpose, the raw fluorescence signal for an individual cell was calculated by averaging the pixel intensity within the respective ROIs for each frame. Subsequently, these values were transformed into ΔF/F values, in which the baseline for each frame and each cell was defined by the corresponding 20th percentile value within a sliding ±3-min window. This procedure simultaneously normalizes and high-pass-filters the signal. The values were then used for statistical testing in all analyses, except if based on neuropil-corrected values. To examine to what extent nonspecific neuropil signal contributed to our results, we performed additional analyses in which the neuropil signal was subtracted from the ΔF/F signal of each individual cell (75, 76) (*SI Appendix*, Fig. S2). The neuropil signal was estimated for each ROI as the average pixel values within a donut-shaped neuropil area, which was defined as a circle (three-pixel radius) around each cell's ROI omitting soma from other cells and the pixels directly adjoining to the cell's soma. The corrected signal was estimated as $\Delta F/F_{cell\_corrected(t)} = \Delta F/F_{cell\_measured} - r \times \Delta F/F_{neuropil}$, where $r = 0.7$ (76).

Wide-Field Image Analysis. To define ROIs for the imaging data from CaMKII-GCaMP6 mice, the area within the window was divided into 36 ROIs (Fig. 4). For each frame, the pixel values within an individual ROI were summed, and this value was then normalized by dividing by the 30th percentile value of all frames of this ROI within a ±3-min interval (f_{norm}). This normalization affects all frames within a 6-min interval in an analogous way [a similar procedure is reported by Tian et al. (92)].

Statistical Analyses. To link calcium signal recordings to the EEG oscillatory phenomena of interest, data from all recordings were baseline-corrected to a common baseline interval, which was the interval 3 to 2 s before the onset of the respective EEG events of interest (i.e., slow oscillations, spindles, slow oscillation-spindle events). For two-photon experiments, calcium signals were baseline-corrected separately for each detected cell. Then, the mean ΔF/F signal was calculated for each frame across all cells. For neuropil-corrected calcium events, event rates (per second) for each cell were likewise first calculated for the baseline interval 3 to 2 s before event onset. Then, mean rates across all cells were calculated. ANOVAs comprising a co-occurring/solitary factor and a phase factor were used to test for significant differences between (co-occurring) slow oscillation-spindle events and solitary slow oscillations and spindles, respectively, and their phases (i.e., transition, up, down, and after phases for comparisons of the slow oscillations and during and after phases for spindle comparisons). Post hoc *t* tests were applied to specify significant main and interaction effects. For the analyses of differences from baseline levels of activity during solitary slow oscillations and spindles and during slow oscillation-spindle events, we used nonparametric permutation tests, as these tests are known to overcome the multiple comparisons problem (93).

Pearson correlations were calculated to assess the relationship between calcium activity and slow oscillation amplitude and spindle power, respectively. Correlations were calculated between the mean ΔF/F signal of all Pyr cells, PV-Ins, and SOM-Ins during the transition, down, up, and after phases and the different slow oscillation amplitude measures (i.e., negative-to-positive peak amplitude, negative half-wave peak amplitude, positive half-wave peak amplitude), separately for solitary slow oscillations and slow oscillation-spindle events. Corresponding correlations were calculated between the mean ΔF/F signal and spindle amplitude. As the amplitude measure during an acute spindle, we used the rms of EEG power (in the 7–15-Hz band) during a spindle, which was normalized for each animal to the average rms signal during all SWS intervals not containing any slow oscillation or spindle (set to 100%). For wide-field imaging experiments, differences from the baseline interval were assessed using nonparametric permutation tests.

1. Steriade M (2003) The corticothalamic system in sleep. *Front Biosci* 8:d878–d899.
2. Steriade M (1993) Cholinergic blockage of network- and intrinsically generated slow oscillations promotes waking and REM sleep activity patterns in thalamic and cortical neurons. *Prog Brain Res* 98:345–355.
3. Steriade M, Timofeev I, Grenier F (2001) Natural waking and sleep states: A view from inside neocortical neurons. *J Neurophysiol* 85:1969–1985.
4. Volgushev M, Chauvette S, Mukovski M, Timofeev I (2006) Precise long-range synchronization of activity and silence in neocortical neurons during slow-wave oscillations [corrected]. *J Neurosci* 26:5665–5672.
5. Fiáth R, et al. (2016) Laminar analysis of the slow wave activity in the somatosensory cortex of anesthetized rats. *Eur J Neurosci* 44:1935–1951.
6. Steriade M, Nuñez A, Amzica F (1993) Intracellular analysis of relations between the slow (< 1 Hz) neocortical oscillation and other sleep rhythms of the electroencephalogram. *J Neurosci* 13:3266–3283.
7. Stroh A, et al. (2013) Making waves: Initiation and propagation of corticothalamic Ca2+ waves in vivo. *Neuron* 77:1136–1150.
8. Lemieux M, Chen J-Y, Lonjers P, Bazhenov M, Timofeev I (2014) The impact of cortical deafferentation on the neocortical slow oscillation. *J Neurosci* 34:5689–5703.
9. Luczak A, Barthó P, Marguet SL, Buzsáki G, Harris KD (2007) Sequential structure of neocortical spontaneous activity in vivo. *Proc Natl Acad Sci USA* 104:347–352.
10. Massimini M, Huber R, Ferrarelli F, Hill S, Tononi G (2004) The sleep slow oscillation as a traveling wave. *J Neurosci* 24:6862–6870.
11. Olcese U, Esser SK, Tononi G (2010) Sleep and synaptic renormalization: A computational study. *J Neurophysiol* 104:3476–3493.
12. Klinzing JG, et al. (2016) Spindle activity phase-locked to sleep slow oscillations. *Neuroimage* 134:607–616.
13. Mölle M, Born J (2011) Slow oscillations orchestrating fast oscillations and memory consolidation. *Prog Brain Res* 193:93–110.
14. Contreras D, Steriade M (1997) Synchronization of low-frequency rhythms in corticothalamic networks. *Neuroscience* 76:11–24.
15. Timofeev I, Steriade M (1996) Low-frequency rhythms in the thalamus of intact-cortex and decorticated cats. *J Neurophysiol* 76:4152–4168.
16. Lüthi A (2014) Sleep spindles: Where they come from, what they do. *Neuroscientist* 20:243–256.
17. Bonjean M, et al. (2011) Corticothalamic feedback controls sleep spindle duration in vivo. *J Neurosci* 31:9124–9134.
18. De Gennaro L, Ferrara M (2003) Sleep spindles: An overview. *Sleep Med Rev* 7:423–440.
19. Diekelmann S, Born J (2010) The memory function of sleep. *Nat Rev Neurosci* 11:114–126.
20. Neske GT (2016) The slow oscillation in cortical and thalamic networks: Mechanisms and functions. *Front Neural Circuits* 9:88.
21. Rasch B, Born J (2013) About sleep's role in memory. *Physiol Rev* 93:681–766.
22. Steriade M, Timofeev I (2003) Neuronal plasticity in thalamocortical networks during sleep and waking oscillations. *Neuron* 37:563–576.
23. Ulrich D (2016) Sleep spindles as facilitators of memory formation and learning. *Neural Plast* 2016:1796715.
24. Tononi G, Cirelli C (2014) Sleep and the price of plasticity: From synaptic and cellular homeostasis to memory consolidation and integration. *Neuron* 81:12–34.
25. Chauvette S, Seigneur J, Timofeev I (2012) Sleep oscillations in the thalamocortical system induce long-term neuronal plasticity. *Neuron* 75:1105–1113.
26. Rosanova M, Ulrich D (2005) Pattern-specific associative long-term potentiation induced by a sleep spindle-related spike train. *J Neurosci* 25:9398–9405.
27. Timofeev I, et al. (2002) Short- and medium-term plasticity associated with augmenting responses in cortical slabs and spindles in intact cortex of cats in vivo. *J Physiol* 542:583–598.
28. Ji D, Wilson MA (2007) Coordinated memory replay in the visual cortex and hippocampus during sleep. *Nat Neurosci* 10:100–107.
29. Ramanathan DS, Gulati T, Ganguly K (2015) Sleep-dependent reactivation of ensembles in motor cortex promotes skill consolidation. *PLoS Biol* 13:e1002263.
30. Rasch B, Büchel C, Gais S, Born J (2007) Odor cues during slow-wave sleep prompt declarative memory consolidation. *Science* 315:1426–1429.
31. Bergmann TO, Mölle M, Diedrichs J, Born J, Siebner HR (2012) Sleep spindle-related reactivation of category-specific cortical regions after learning face-scene associations. *Neuroimage* 59:2733–2742.
32. Clemens Z, et al. (2007) Temporal coupling of parahippocampal ripples, sleep spindles and slow oscillations in humans. *Brain* 130:2868–2878.
33. Staresina BP, et al. (2015) Hierarchical nesting of slow oscillations, spindles and ripples in the human hippocampus during sleep. *Nat Neurosci* 18:1679–1686.
34. Dudai Y, Karni A, Born J (2015) The consolidation and transformation of memory. *Neuron* 88:20–32.
35. Inostroza M, Born J (2013) Sleep for preserving and transforming episodic memory. *Annu Rev Neurosci* 36:79–102.
36. Latchoumane CV, Ngo H-VV, Born J, Shin H-S (2017) Thalamic spindles promote memory formation during sleep through triple phase-locking of cortical, thalamic, and hippocampal rhythms. *Neuron* 95:424–435.e6.
37. Sejnowski TJ, Destexhe A (2000) Why do we sleep? *Brain Res* 886:208–223.
38. Niethard N, et al. (2016) Sleep-stage-specific regulation of cortical excitation and inhibition. *Curr Biol* 26:2739–2749.
39. Grosmark AD, Buzsáki G (2016) Diversity in neural firing dynamics supports both rigid and learned hippocampal sequences. *Science* 351:1440–1443.
40. Watson BO, Levenstein D, Greene JP, Gelinas JN, Buzsáki G (2016) Network homeostasis and state dynamics of neocortical sleep. *Neuron* 90:839–852.

41. Vanni MP, Murphy TH (2014) Mesoscale transcranial spontaneous activity mapping in GCaMP3 transgenic mice reveals extensive reciprocal connections between areas of somatomotor cortex. *J Neurosci* 34:15931–15946.

42. Steriade M (2000) Corticothalamic resonance, states of vigilance and mentation. *Neuroscience* 101:243–276.

43. Mann EO, Kohl MM, Paulsen O (2009) Distinct roles of GABA(A) and GABA(B) receptors in balancing and terminating persistent cortical activity. *J Neurosci* 29:7513–7518.

44. Mayne EW, Craig MT, McBain CJ, Paulsen O (2013) Dopamine suppresses persistent network activity via D(1) -like dopamine receptors in rat medial entorhinal cortex. *Eur J Neurosci* 37:1242–1247.

45. Kuki T, et al. (2015) Contribution of parvalbumin and somatostatin-expressing GABAergic neurons to slow oscillations and the balance in beta-gamma oscillations across cortical layers. *Front Neural Circuits* 9:6.

46. Lemieux M, Chauvette S, Timofeev I (2015) Neocortical inhibitory activities and long-range afferents contribute to the synchronous onset of silent states of the neocortical slow oscillation. *J Neurophysiol* 113:768–779.

47. Funk CM, et al. (2017) Role of somatostatin-positive cortical interneurons in the generation of sleep slow waves. *J Neurosci* 37:9132–9148.

48. Pfeffer CK, Xue M, He M, Huang ZJ, Scanziani M (2013) Inhibition of inhibition in visual cortex: The logic of connections between molecularly distinct interneurons. *Nat Neurosci* 16:1068–1076.

49. Jiang X, et al. (2015) Principles of connectivity among morphologically defined cell types in adult neocortex. *Science* 350:aac9462.

50. Murayama M, et al. (2009) Dendritic encoding of sensory stimuli controlled by deep cortical interneurons. *Nature* 457:1137–1141.

51. Palmer L, Murayama M, Larkum M (2012) Inhibitory regulation of dendritic activity *in vivo*. *Front Neural Circuits* 6:26.

52. Peyrache A, Battaglia FP, Destexhe A (2011) Inhibition recruitment in prefrontal cortex during sleep spindles and gating of hippocampal inputs. *Proc Natl Acad Sci USA* 108:17207–17212.

53. Puig MV, Ushimaru M, Kawaguchi Y (2008) Two distinct activity patterns of fast-spiking interneurons during neocortical UP states. *Proc Natl Acad Sci USA* 105:8428–8433.

54. Seibt J, et al. (2017) Cortical dendritic activity correlates with spindle-rich oscillations during sleep in rodents. *Nat Commun* 8:684.

55. Chen SX, Kim AN, Peters AJ, Komiyama T (2015) Subtype-specific plasticity of inhibitory circuits in motor cortex during motor learning. *Nat Neurosci* 18:1109–1115.

56. Wolff SBE, et al. (2014) Amygdala interneuron subtypes control fear learning through disinhibition. *Nature* 509:453–458.

57. Ruch S, et al. (2012) Sleep stage II contributes to the consolidation of declarative memories. *Neuropsychologia* 50:2389–2396.

58. Rothschild G, Eban E, Frank LM (2017) A cortical-hippocampal-cortical loop of information processing during memory consolidation. *Nat Neurosci* 20:251–259.

59. Cichon J, Gan W-B (2015) Branch-specific dendritic Ca$^{(2+)}$ spikes cause persistent synaptic plasticity. *Nature* 520:180–185.

60. Yang G, et al. (2014) Sleep promotes branch-specific formation of dendritic spines after learning. *Science* 344:1173–1178.

61. Niethard N, Burgalossi A, Born J (2017) Plasticity during sleep is linked to specific regulation of cortical circuit activity. *Front Neural Circuits* 11:65.

62. Diering GH, et al. (2017) Homer1a drives homeostatic scaling-down of excitatory synapses during sleep. *Science* 355:511–515.

63. de Vivo L, et al. (2017) Ultrastructural evidence for synaptic scaling across the wake/sleep cycle. *Science* 355:507–510.

64. Cox R, Korjoukov I, de Boer M, Talamini LM (2014) Sound asleep: Processing and retention of slow oscillation phase-targeted stimuli. *PLoS One* 9:e101567.

65. Kim D, Hwang E, Lee M, Sung H, Choi JH (2015) Characterization of topographically specific sleep spindles in mice. *Sleep (Basel)* 38:85–96.

66. Crunelli V, Hughes SW (2010) The slow (<1 Hz) rhythm of non-REM sleep: A dialogue between three cardinal oscillators. *Nat Neurosci* 13:9–17.

67. Sanchez-Vives MV, McCormick DA (2000) Cellular and network mechanisms of rhythmic recurrent activity in neocortex. *Nat Neurosci* 3:1027–1034.

68. Buzsáki G, Mizuseki K (2014) The log-dynamic brain: How skewed distributions affect network operations. *Nat Rev Neurosci* 15:264–278.

69. Cossart R, Aronov D, Yuste R (2003) Attractor dynamics of network UP states in the neocortex. *Nature* 423:283–288.

70. Gardner RJ, Hughes SW, Jones MW (2013) Differential spike timing and phase dynamics of reticular thalamic and prefrontal cortical neuronal populations during sleep spindles. *J Neurosci* 33:18469–18480.

71. Nir Y, et al. (2011) Regional slow waves and spindles in human sleep. *Neuron* 70:153–169.

72. Chen Z, Wilson MA (2017) Deciphering neural codes of memory during sleep. *Trends Neurosci* 40:260–275.

73. Hanlon EC, Faraguna U, Vyazovskiy VV, Tononi G, Cirelli C (2009) Effects of skilled training on sleep slow wave activity and cortical gene expression in the rat. *Sleep* 32:719–729.

74. Vyazovskiy VV, Cirelli C, Pfister-Genskow M, Faraguna U, Tononi G (2008) Molecular and electrophysiological evidence for net synaptic potentiation in wake and depression in sleep. *Nat Neurosci* 11:200–208.

75. Chen T-W, et al. (2013) Ultrasensitive fluorescent proteins for imaging neuronal activity. *Nature* 499:295–300.

76. Peron S, Chen TW, Svoboda K (2015) Comprehensive imaging of cortical networks. *Curr Opin Neurobiol* 32:115–123.

77. Ayoub A, et al. (2013) Differential effects on fast and slow spindle activity, and the sleep slow oscillation in humans with carbamazepine and flunarizine to antagonize voltage-dependent Na$^+$ and Ca^{2+} channel activity. *Sleep (Basel)* 36:905–911.

78. Magee JC, Avery RB, Christie BR, Johnston D (1996) Dihydropyridine-sensitive, voltage-gated Ca2+ channels contribute to the resting intracellular Ca2+ concentration of hippocampal CA1 pyramidal neurons. *J Neurophysiol* 76:3460–3470.

79. Piantoni G, Halgren E, Cash SS (2016) The contribution of thalamocortical core and matrix pathways to sleep spindles. *Neural Plast* 2016:3024342.

80. Meyer HS, et al. (2011) Inhibitory interneurons in a cortical column form hot zones of inhibition in layers 2 and 5A. *Proc Natl Acad Sci USA* 108:16807–16812.

81. Freund TF, Meskenaite V (1992) gamma-Aminobutyric acid-containing basal forebrain neurons innervate inhibitory interneurons in the neocortex. *Proc Natl Acad Sci USA* 89:738–742.

82. Neske GT, Connors BW (2016) Distinct roles of SOM and VIP interneurons during cortical up states. *Front Neural Circuits* 10:52.

83. Pi H-J, et al. (2013) Cortical interneurons that specialize in disinhibitory control. *Nature* 503:521–524.

84. Walker F, et al. (2016) Parvalbumin- and vasoactive intestinal polypeptide-expressing neocortical interneurons impose differential inhibition on Martinotti cells. *Nat Commun* 7:13664.

85. Hippenmeyer S, et al. (2005) A developmental switch in the response of DRG neurons to ETS transcription factor signaling. *PLoS Biol* 3:e159.

86. Taniguchi H, et al. (2011) A resource of Cre driver lines for genetic targeting of GABAergic neurons in cerebral cortex. *Neuron* 71:995–1013, and erratum (2011) 72:1091.

87. Casanova E, et al. (2001) A CamKIIalpha iCre BAC allows brain-specific gene inactivation. *Genesis* 31:37–42.

88. Madisen L, et al. (2015) Transgenic mice for intersectional targeting of neural sensors and effectors with high specificity and performance. *Neuron* 85:942–958.

89. Komiyama T, et al. (2010) Learning-related fine-scale specificity imaged in motor cortex circuits of behaving mice. *Nature* 464:1182–1186.

90. Dombeck DA, Khabbaz AN, Collman F, Adelman TL, Tank DW (2007) Imaging large-scale neural activity with cellular resolution in awake, mobile mice. *Neuron* 56:43–57.

91. Hofer SB, et al. (2011) Differential connectivity and response dynamics of excitatory and inhibitory neurons in visual cortex. *Nat Neurosci* 14:1045–1052.

92. Tian L, et al. (2009) Imaging neural activity in worms, flies and mice with improved GCaMP calcium indicators. *Nat Methods* 6:875–881.

93. Maris E, Oostenveld R (2007) Nonparametric statistical testing of EEG- and MEG-data. *J Neurosci Methods* 164:177–190.

NEUROSCIENCE

Supplementary Information for

Cortical circuit activity underlying sleep slow oscillations and spindles

Niels Niethard[1*], Hong-Viet V. Ngo[1,2], Ingrid Ehrlich[3,4], Jan Born[1,3*]

[1] Institute of Medical Psychology and Behavioral Neurobiology, University of Tübingen, 72076 Tübingen, Germany.
[2] School of Psychology, University of Birmingham, Birmingham, United Kingdom.
[3] Center for Integrative Neuroscience, University of Tübingen, 72076 Tübingen, Germany.
[4] Hertie Institute for Clinical Brain Research, University of Tübingen, 72076, Germany

Email: jan.born@uni-tuebingen.de or niels.niethard@uni-tuebingen.de

This PDF file includes:
> Supplementary text
> Figs. S1 to S4
> Tables S1 to S2
> Captions for movies S1
> References for SI reference citations

Supplementary Information Text

Surgery. The mice were implanted with a headpost for subsequent experimentation. They were anesthetized with 0.1 mg/g ketamine and 0.008 mg/g xylazine with a supplement of isoflurane. Dexamethasone (0.08 mg) was sometimes administered to reduce tissue swelling. Lidocaine was applied to the wound margins for topical anesthesia. A custom-built headpost was glued to the skull and subsequently cemented with dental acrylic (Lang Dental, U.S.A.).

The headpost implantation was followed by virus injection and window implantation. For two-photon experiments, a craniotomy of 1.2 x 2.0 mm was made above the sensorimotor cortex (1.1 mm caudal and 1.0-1.3 mm lateral from the bregma). In the area of the craniotomy, two viruses were injected (AAV2/1-syn-GCaMP6f and AAV2/1-flex-tdTomato) at a depth of 130-300 μm below the dura. Control animals were injected with one virus only (AAV1.CB7.CI.eGFP.WPRE.rBG) to express calcium-independent green fluorescent protein (GFP). For wide-field imaging experiments, the craniotomy was larger (8 mm x 9 mm) and covered the whole dorsal cortex (Fig. 4). Two layers of coverglasses (size depending on the area of craniotomy) were implanted as an imaging window. The space between the imaging window and the skull was sealed with 1.5 - 2 % agarose, and the window was cemented with dental acrylic.

Electrodes for electroencephalographic (EEG) recordings in the two-photon experiments were implanted contralateral to the imaging window. The skull was exposed and two bone screws (PlasticOne, U.S.A.) were implanted (frontal electrode: anterior +1.5 mm, lateral 1.5 mm; parietal electrode: posterior -1.5 mm, lateral 2.5 mm from bregma). A silver wire (Science Products, Germany) implanted on the brain surface (posterior 1 mm, lateral 0 mm from lambda) served as reference. For wide-field imaging experiments, four silver wires (Science Products, Germany) were implanted between the dura mater and the imaging window (Fig. 4), two in the anterior region of the imaging window (anterior +1.5 mm, lateral 1.5 mm; from bregma) and two in occipital regions (anterior -3 mm, lateral 1.5 mm; from bregma). For electromyographic (EMG) recordings, in all experiments two stainless steel wires (Science Products, Germany) were implanted into the neck muscle. After surgery the animals were single-housed in their home cages and calcium imaging was conducted after at least 10 days of recovery.

Head fixation procedure. After handling for 10 min per day for one week, the animals were habituated to the head-fixation. Habituation consisted of 4 sessions per day for one week with increasing fixation durations (30 s, 3 min, 10 min, 30 min) interleaved by 10-min resting intervals. Habituation was conducted until the day prior to the first imaging session during the early light phase.

EEG and EMG recordings. Sleep stages were identified based on EEG and EMG recordings during the imaging sessions. EEG and EMG signals were amplified, filtered (EEG: 0.01 – 300 Hz; EMG: 30 – 300 Hz) and sampled at a rate of 1000 Hz (amplifier: Model 15A54, Grass Technologies, U.S.A.). Based on EEG/EMG signals for succeeding 10-s epochs, the brain state of the mouse was classified into Wake, Slow wave sleep (SWS), and Rapid Eye Movement (REM) sleep stages (1,2). Sleep stage identification was supported using the software SleepSign for animals (Kissei Comtech, Japan).

Offline detection of sleep slow oscillations and spindles. To detect discrete slow oscillation events during SWS, offline algorithms were adopted from previously described procedures (3-5). In brief, the EEG was bandpass filtered between 0.2 - 4.5 Hz and then, all positive-to-negative zero crossings of the signal as well as the local minimum and maximum between each two successive crossings were marked. Intervals between two succeeding positive-to-negative zero-crossings were identified as a slow oscillation event when the length of this interval was between 0.4 - 2 s and when the minimum amplitude and minimum-to-maximum amplitude was greater than 66.6 % of the average of the respective amplitude values across the whole recording. For these remaining events the enclosing zero-crossings represent the onset and end of the corresponding slow oscillation cycle.

For analyses, identified SO events were averaged time locked to the negative-half wave peak (0 s). The analyses of concurrent calcium activity concentrated on a window from -2 to +3 s around the negative SO halfwave peak. This window was wide enough to also cover SO events with upstates of longer duration and has been similarly used in previous studies (5 - 7). Averaging was time-locked to the negative half-wave peak of the SO (reflecting the downstate maximum) because it represents the temporally most distinct event during the SO and, thus, allows for optimally estimating the beginning and end of processes of interest, associated with the SO up- and down states, respectively. Previous studies comparing SO averaging time-locked the negative versus positive half-wave peaks of the SO revealed that time-locking to the positive half-wave peak (i.e., upstate) does not only result in a more smeared average SO waveform (with lower amplitude). Also, the increase in spindle activity occurring phase-locked to the SO upstate was distinctly reduced with phase-locking of the signal to the positive half-wave peak (8), which reflects that the positive half-wave peak provides only an imprecise time reference for averaging SO-related signals.

Detection of discrete spindles was performed following an algorithm described by (9). The EEG signal was band pass filtered between 7 - 15 Hz, rectified and, subsequently, all maxima were interpolated to yield the envelope for this frequency band. A spindle event was identified whenever the envelope exceeded an individual threshold for a duration of 0.5 to 3.0 s, whereby the threshold was defined by the standard deviation of the filtered signal during all SWS epochs of an individual mouse multiplied by a factor of 1.5. Thus, the positive and subsequent negative threshold crossing represented the onset and end of a spindle event. Detected spindle events were then characterized by their onset. For analyses, the root mean square signal (RMS) during identified spindle events was averaged time-locked to the spindle onset. The analyses of accompanying calcium signal centered – as for SO events – on an interval -2 to +3 s around the spindle event.

The same procedure was applied to separately identify slow and fast spindles, after pre-filtering the EEG signal in the respective 7 - 11 Hz and 11 - 15 Hz bands.

In subsequent analyses the calcium signal was analyzed for three different EEG events: (i) solitary slow oscillations that occurred in the absence of a spindle during the slow oscillation-cycle and in a 250-ms interval before and after the cycle, (ii) solitary spindles that occurred without any overlap with an identified slow oscillation-event, and (iii) slow oscillation-spindle events defined by slow oscillation-events where a spindle nested in the slow oscillation-upstate. Specifically, spindle onset occurred in the interval between slow oscillation-onset and the positive slow oscillation half-wave peak + 250 ms. Also, there were no spindles in the 250-ms interval preceding the slow oscillation-spindle event.

Immunohistochemistry. Immunostaining was performed using standard procedures. Following experiments, mice were deeply anesthetized (0.3 mg/g ketamine and 0.024 mg/g xylazine, i.p.) and intracardially perfused with 4 % paraformaldehyde in 0.1 M phosphate buffered saline (4 % PFA). The brains were removed from the skull, post-fixed in 4 % PFA at 4 °C overnight, and rinsed 3 x with 0.1 M phosphate buffered saline (PBS). Coronal slices (thickness 65 μm) were cut using a vibratome and blocked in 10 % normal goat serum (NGS, Jackson ImmnunoResearch, West Grove, U.S.A) and 0.3 % Triton X-100 (Sigma-Aldrich, Buchs, Switzerland) in 0.1 M PBS for 1.5 h at room temperature. Slices were incubated with anti-PV rabbit primary antibody (1:1000; #24428, Immunostar, U.S.A., RRID: AB_572259) or anti-SOM rabbit primary antibody (1:1000; #T-4547, Peninsula Laboratories, U.S.A., RRID AB_518618) in carrier solution (2% NGS and 0.3% Triton in PBS) for 48 h at 4 °C. After 4 x 10 min rinses with 0.1 M PBS sections were incubated in goat anti-Rabbit IgG antibodies conjugated either with Alexa 405 (for PV staining, AB_221605) or Alexa 633 (for SOM staining, AB2535732) (both from Thermo Fisher Scientific, 1:1000) in carrier solution for 3 h at room temperature on the shaker. After washing in 0.1 M PBS, slices were mounted on slides for imaging. Images were acquired on a confocal microscope (LSM 710, Carl Zeiss, Germany) with a 40x 1.3 NA oil-immersion objective. The frame size was 1024 x 1024 pixels and the z-resolution was set to one airy unit. The following laser lines were used: 488 nm (GCaMP6f) 561 nm (tdTomato), and 405 or 633 nm (for detection of PV or SOM secondary antibodies). To ensure co-labeling of PV-In and SOM-In with tdtomato and GCamp6f each imaging area was manually chosen before the actual recording session started, thus maximizing the number of cells expressing both tdtomato and GCamp6f. Overall, the fraction of cells only expressing tdtomato but not GCamp6f for PV-In and SOM-In was below 2%.

Two-photon imaging. *In vivo* imaging was performed as described previously (10): A two-photon microscope was used based on the MOM system (Sutter, U.S.A) controlled by ScanImage software (11). The light source was a pulsed Ti:sapphire laser ($\lambda = 980$ nm; Chameleon, Coherent, U.S.A.). Red and green fluorescence photons were collected with an objective lens (Nikon, 16x, 0.80 NA, Japan), separated by a 565 nm dichroic mirror (Chroma, 565dcxr, U.S.A.) and barrier filters (green: ET525/70m-2p, red: ET605/70m-2p), and measured using photomultiplier tubes (Hamamatsu Photonics,

H10770PA-40, Japan). The imaging frame consisted of 1024 x 256 pixels, and the frame rate was 5.92 Hz (169 ms per frame). Images were collected from neurons in layer 2/3 at a depth of 150-250 μm.

Wide-field imaging. For wide-field calcium imaging, a CCD camera (iXon X3 888, Andor Technology, U.S.A.) was focused on the cortical surface using a macroscope (MVX-10, Olympus, Japan). The illumination light sources were 470 nm light emitting diodes (Thorlabs, U.S.A.). The filter cube contained an excitation bandpass filter of 470/40 nm, a dichroic filter of 495 nm, and an emission bandpass filter of 525/50 nm. The zoom was adjusted to cover the entire window. The imaging frame consisted of 125 x 125 pixels, and the frame rate was 48.86 – 56.26 Hz (17.8 – 20.5 ms per frame). The precise timing of individual frames was saved as voltage pulse in the EEG recording system.

Principal component analysis (PCA). PCA was used to further explore the temporal dynamics in calcium activity for the three different cell types during solitary slow oscillations and solitary spindles. Analyses were run in Matlab (functions: "pca" and "rotatefactors"). We performed two separate PCAs on the ΔF/F signals during the 2s to +3 s windows around the EEG slow oscillations (0 s referring to the negative half-wave peak of the individual events) and spindles (0 s referring to the individual spindle onset). PCAs revealed three main components, which explained 63.05 % (solitary slow oscillations) and 63.3 % (solitary spindles) of the total variance. We, then, compared the varimax rotated component scores only for the component showing highest (positive or negative) factor loadings during the oscillatory event of interest between the three different cell types using ANOVA with subsequent *t*-tests.
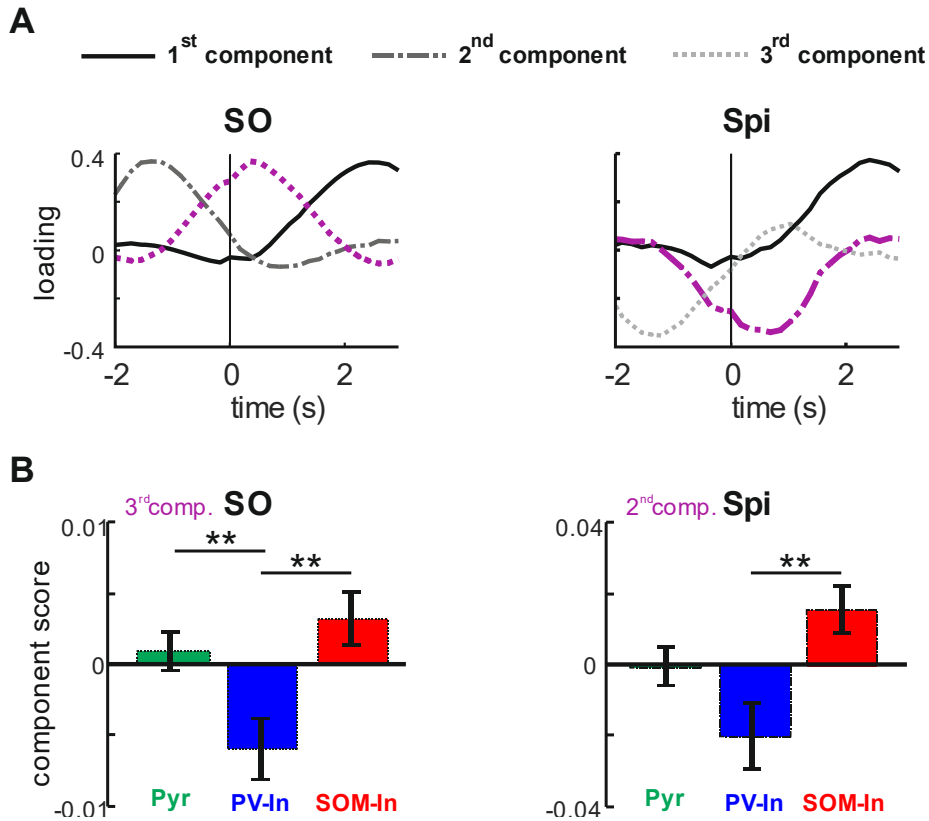
Fig. S1. Principal components of calcium activity during slow oscillations and spindles discriminate PV-In and SOM-In activity. (*A*) Component loadings for the first three varimax rotated components of calcium activity during solitary slow oscillations (SO), time-locked to the negative half-wave peak (0 s) and during solitary spindles (Spi), time-locked to the spindle onset. Components used for analysis shown in B are in violet. For SOs, this is the 3nd extracted component showing high positive loadings in a window covering both the downstate and upstate of the SO. For spindles, this is the 2nd component with high negative loadings reaching maximum values around the spindle maximum. (*B*) Mean (± SEM) component scores for the components showing highest (absolute) loadings around the reference time point (0 s) for solitary SOs (left) and solitary spindles (right) for putative Pyr (green), PV-In (blue) and SOM-In (red) cells. ** $p <$ 0.01 for pairwise comparisons between cell types. Note: PV-In and SOM-In show opposing scores during slow oscillations and spindles, reflecting predominant activity of SOM-In over PV-in the course of SOs but - because of the negative loadings of the respective component during this time - predominant PV-In over SOM-In activity in the course of spindles.
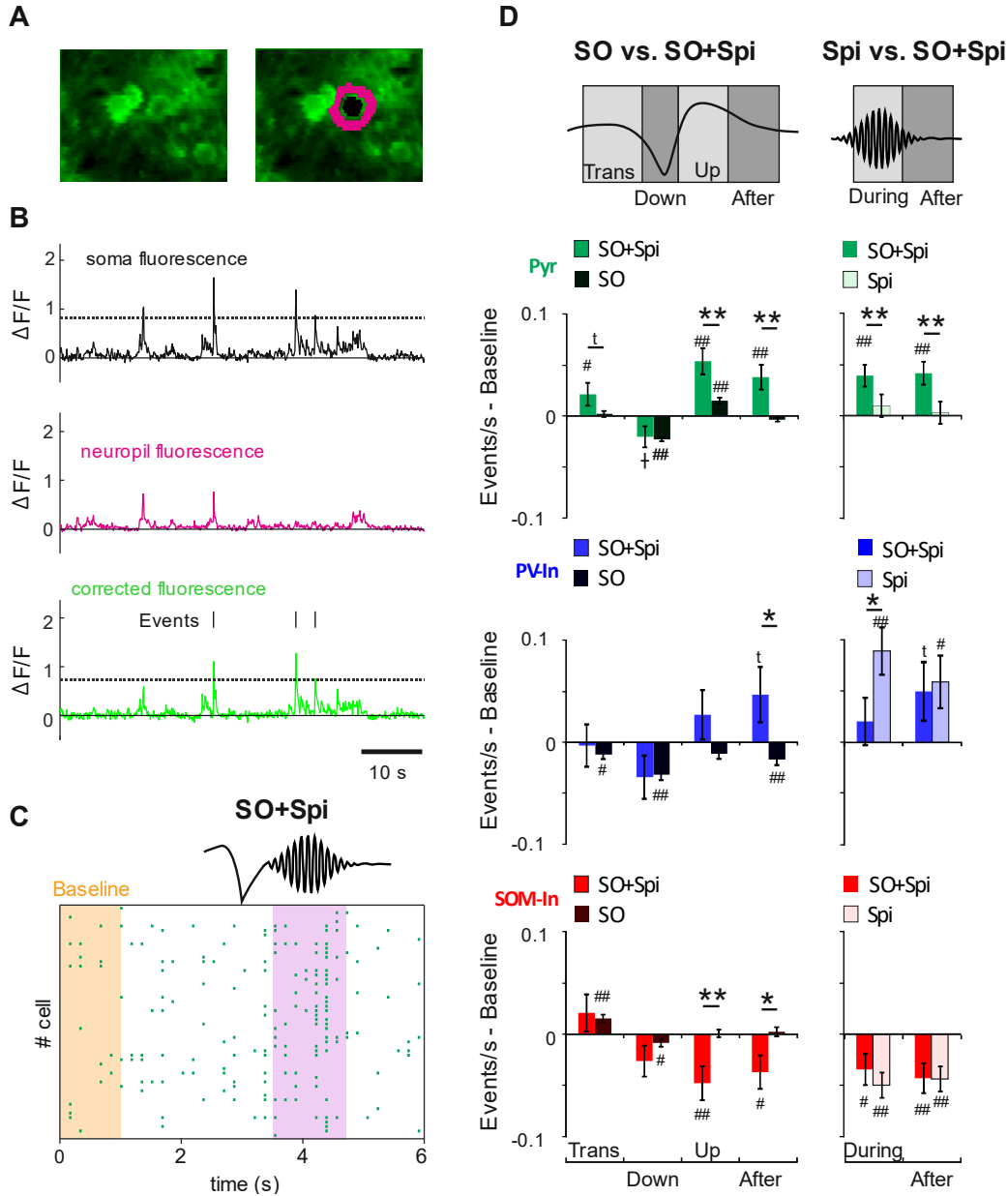
Fig. S2. Neuropil correction of ΔF/F signal. (*A*) Illustration of the area defined for neuropil fluorescence correction. The donut-shaped neuropil area (pink) was defined as a circle (three pixel radius) around each cell's ROI (black) omitting soma from other cells and the pixels directly adjoining the cell's soma. (*B*) Example ΔF/F signal traces from the cell shown in *A*, (top) from the soma, (middle) from the neuropil area, and (bottom), the corrected ΔF/F signal after subtracting 0.7 x neuropil ΔF/F. The dotted horizontal line represents the threshold (two standard deviations above the median of the corrected signal) used for event detection. (*C*) Example raster plot showing activity from putative pyramidal cells (Pyr) being active during a six second

example interval including a slow oscillation-spindle event (SO + Spi). Yellow shaded area indicates the interval used to measure baseline activity; right violet shaded area indicates Up interval of the slow oscillation covering the spindle (with high event rates). (*D*) Left: Comparison of mean (± SEM) event rates (per second) between solitary SO and SO + Spi events for the positive-to-negative Transition phase (Trans, -0.32 to -0.00 s, with reference to SO negative half-wave peak = 0 s), the Down phase (-0.00 to 0.16 s), the Up phase (0.32 to 0.48 s) and the following After phase (0.54 to 3 s). Right: Comparisons between mean (± SEM) event rates between solitary spindles and SO + Spi events for the phase During the acute spindle (0 to 1 s with reference to spindle onset set to 0 s) and the After phase (1 to 3 s). ** $p < 0.01$, * $p < 0.05$, $p < 0.1$ for pairwise comparisons between solitary events and SO + Spi events respectively. ## $p < 0.01$, # $p < 0.05$, t $p < 0.1$, for difference from baseline activity (-3 to -2 s).

A

SO Spindle SO + Spindle

Wake active cells (5th quintile)

Pyr
PV-In
SOM-In

ΔF/F

Wake inactive cells (1st quintile)

ΔF/F

time (s) time (s) time (s)

B SOM-In ■ Wake active (5th quintile)
        ■ Wake inactive (1st quintile)

SO Spindle SO + Spindle

ΔF/F

Trans Down Up After

During After

Trans Down Up After

C

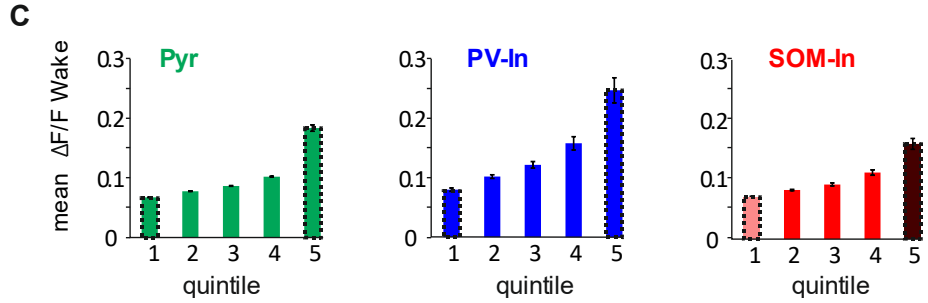mean ΔF/F Wake

Pyr PV-In SOM-In

quintile quintile quintile

Fig. S3. (*A*) Mean ± SEM ΔF/F signal for cell clusters of putative Pyr (green), PV-In (blue) and SOM-In (red) during slow oscillations (SO), solitary spindles (Spindle) and slow oscillations co-occurring with spindles (SO + Spindle). Signals are time locked (0 s) to the negative peak of slow oscillations (SO and SO + Spindle) or the spindle onset (Spindle). Bars on top indicate significance ($p < 0.05$) for each cell type with reference to baseline (-3 to -2 s) set to zero. Top: average traces for the 20 % cells most active during wakefulness (5th quintile) for each cell type. Bottom: average traces of the 20 % cells least active during wakefulness for each cell type (1st quintile). Average traces across all events from all animals are indicated. (*B*) Left: Comparison of mean (± SEM) ΔF/F signals between SOM-In cell cluster during solitary SO events for the positive-to-negative Transition phase (Trans, -0.32 to -0.00 s, with reference to slow oscillation negative half-wave peak = 0 s), the Down phase (-0.00 to 0.16 s), the Up phase (0.32 to 0.48 s) and the following After phase (0.54 to 3 s). Middle: Comparisons between mean (± SEM) ΔF/F signals between SOM-In cell cluster during solitary spindle events for the phase During the acute spindle (0 to 1 s with reference to spindle onset set to 0 s) and the After phase (1 to 3 s). Right: Comparison of mean (± SEM) ΔF/F signals between SOM-In cell cluster during SO + Spi events for the positive-to-negative Transition phase (Trans, -0.32 to -0.00 s, with reference to slow oscillation negative half-wave peak = 0 s), the Down phase (-0.00 to 0.16 s), the Up phase (0.32 to 0.48 s) and the following After phase (0.54 to 3 s). ** $p < 0.01$, * $p < 0.05$, t $p < 0.1$ for pairwise comparisons between solitary events and SO + Spi events respective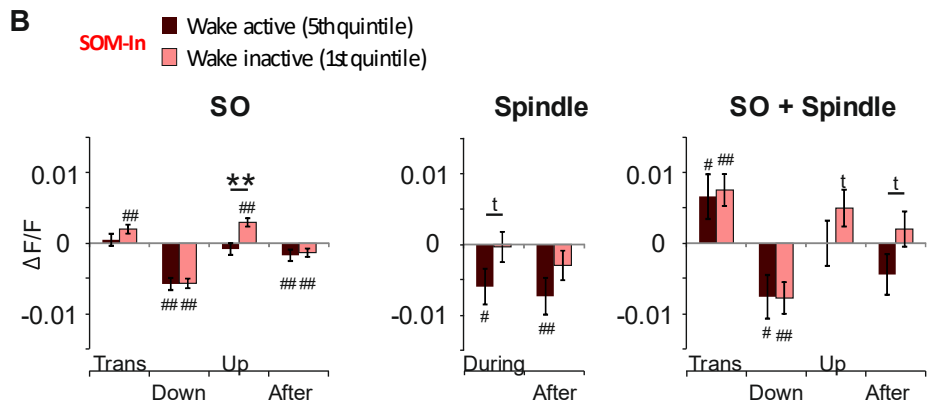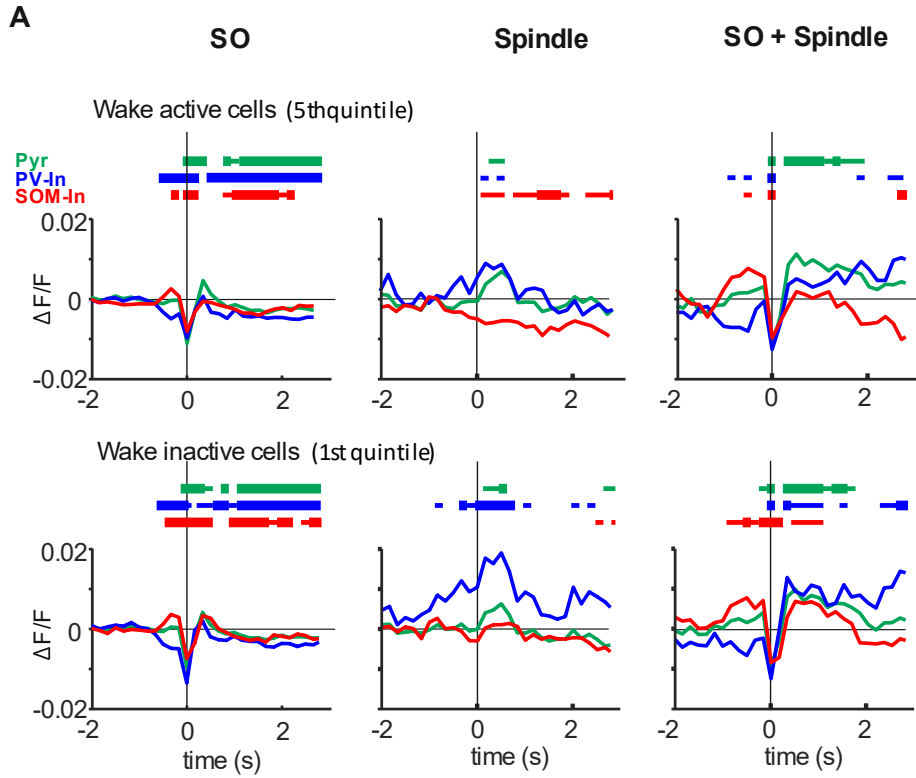ly. ## $p < 0.01$, # $p < 0.05$, t $p < 0.1$(*C*) Mean ΔF/F ± SEM during wakefulness for quintiles of each cell type. Note highest levels for 5th quintile of PV-In.
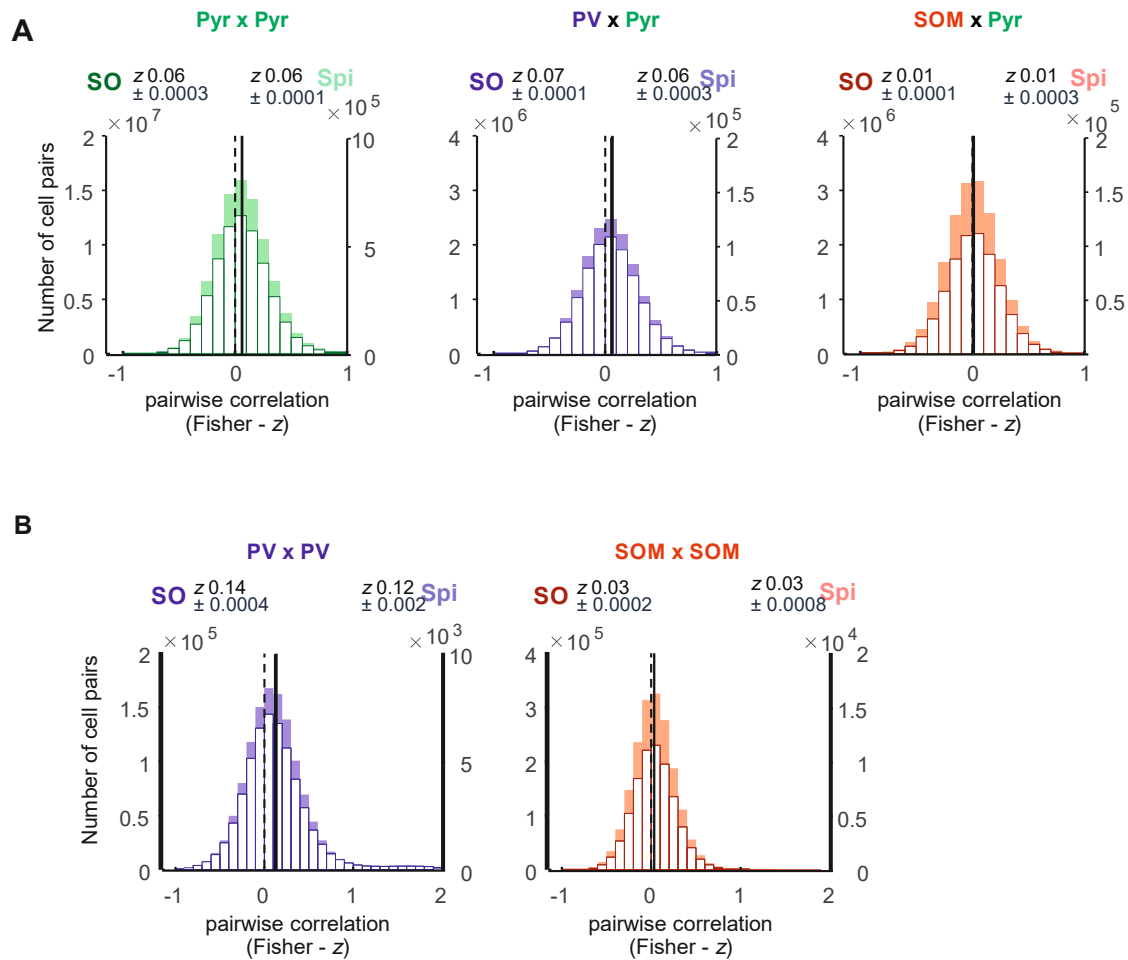
Fig. S4. Distributions of pairwise correlations in calcium activity within putative Pyr cells, PV-In, and SOM-In cells during solitary slow oscillations and spindles. Pairwise Pearson correlation of the ΔF/F signal between all cell pairs within one cell type and between all putative Pyr cells and each interneuron population were calculated during all detected solitary EEG slow oscillations and spindles (in a -2 s to +3 s-window around the slow oscillation negative half-wave peak and spindle onset). Fisher z-transformed coefficients are shown. (A) Distribution of correlation coefficients within the populations of putative Pyr cells (green) and between putative Pyr cells and PV-In (blue) and SOM-In (red) during solitary slow oscillations and (white) solitary spindles (colored). Distribution of correlations within PV-In (blue) and SOM-In (red) during solitary slow oscillations (white) and solitary spindles (colored). For each distribution the mean (± SEM) is indicated. Note, distributions did not reveal distinct subgroups of highly correlated cells and none of the distributions differed significantly from normal distribution (Chi^2 –tests: all $p > 0.1$). Mean correlations, i.e., synchrony in activity for PV x Pyr and PV x PV correlations during slow oscillations was higher than during spindles. However, though significant ($p < 0.01$), effects sizes were very small (Cohen's $d < 0.1$). Note also that correlations were generally rather small, possibly reflecting that the proportion of cells actually engaging in slow oscillation and spindle events is relatively small.

A

Slow Oscillation

B

Spindle

C

Slow Oscillation + Spindle
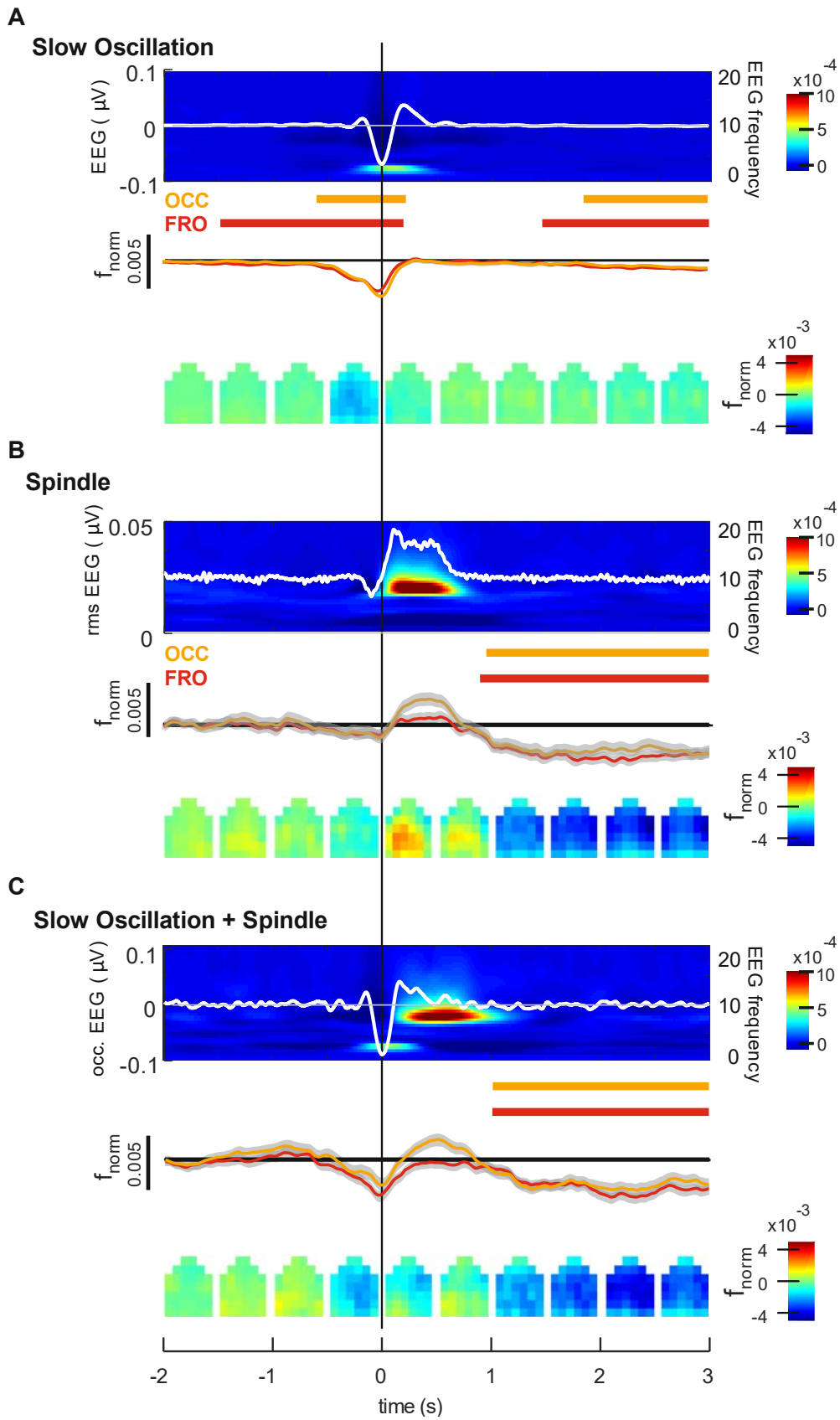
Fig. S5. (*A*) From top to bottom: Average EEG signal (across all events from all animals) for solitary slow oscillations (from left occipital cortical recordings, white line overlaying average time-frequency plot with color-coded power) together with (middle panel) average (±SEM) calcium activity (f_{norm}) across the 4 designated anterior (red) and posterior (orange) cortical regions. Averages are time-locked to the negative half-wave peak of the slow oscillation (0 s). Intervals with significant changes in calcium activity ($p < 0.01$, relative to the baseline interval from -3 to -2 s) are indicated by red (for anterior ROIs - FRO) and orange bars (for anterior ROIs - FRO, see Figure 4 of main text for location of target ROIs). The bottom panel shows topographic changes of calcium activity in all 36 ROIs (in f_{norm}, color coded) for subsequent 500-ms time windows. Panels (*B*) and (*C*) show corresponding data for solitary spindles (Spindle) and slow oscillations co-occurring with spindles (Slow oscillation + Spindle). Note, for solitary spindles the average EEG signal (overlaying the corresponding EEG time frequency plot) shows the root mean square (RMS) amplitude, and averaging is time-locked to the spindle onset. Average traces are shown across events from 4 animals (total n = 9864, 766, 762, for solitary slow oscillations, solitary spindles, and slow oscillations co-occurring with spindles).
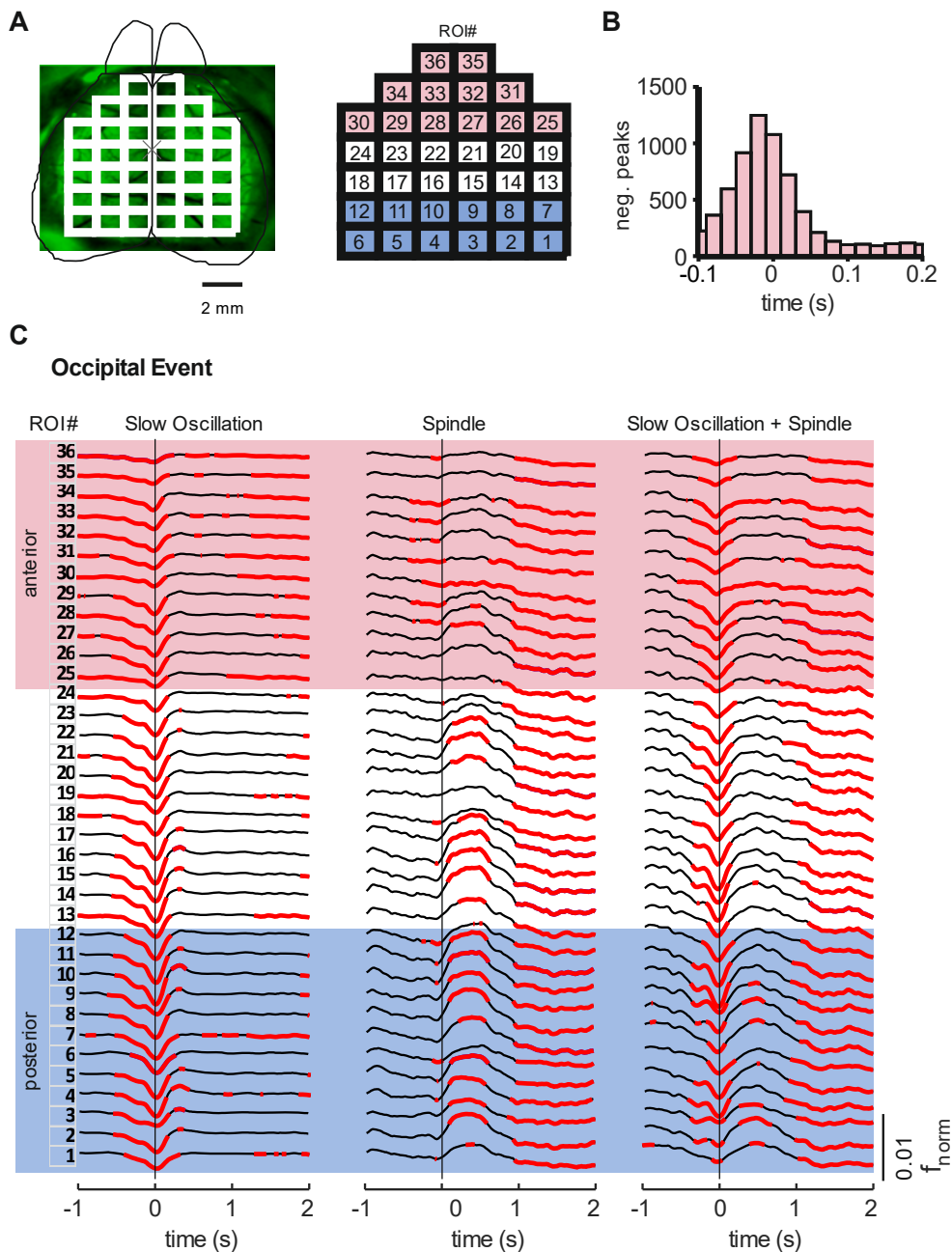
Fig. S6 (*A*) Illustration of the 36 cortical ROIs used for wide-field imaging experiments. Red-shaded area indicates anterior ROIs (#25 - #36), blue-shaded area posterior ROIs (#1 - #12). (*B*) Histogram showing the distribution of the temporal delays of slow oscillation negative half-wave peaks defined in the f_{norm} signal between frontal ROIs and occipital ROIs. Only slow oscillation events were included in this analysis, where the minimum of the f_{norm} signal was associated with the slow oscillation half-wave peak exceeding a critical threshold for both anterior and posterior regions (with the threshold defined by 0.66 standard deviations from the mean activity of the filtered 0.1 - 4 Hz signal). (*C*) Calcium activity for 36 cortical ROIs using wide-field imaging during solitary slow oscillations (left), solitary spindles (middle) and slow oscillations co-occurring with spindles (Slow oscillation + Spindle, right). Red-shaded area indicates anterior ROIs, blue-shaded area posterior ROIs. Numbering of ROIs is indicated in A. Average traces

across all events from 4 animals (total n = 9864, 766, 762, for solitary slow oscillations, solitary spindles, and slow oscillations co-occurring with spindles, respectively) are indicated. Averaging is time locked (0 s) to the negative half-wave peak of the slow oscillation and spindle onset, respectively. EEG events were identified in occipital EEG channel. Red marked calcium signal indicates intervals of significantly ($p < 0.05$) enhanced or reduced activity (with reference to activity during the baseline interval from -3 to -2 s).

Subject characteristics

animal #	genotype	imaging sessions	recorded Pyr	interneurons	SOs	Spindles	SOs+Spindles
1	PV-cre	1	126	17	3135	160	166
2	PV-cre	3	329	43	1272	129	52
3	PV-cre	2	241	28	3655	268	233
4	SOM-cre	3	342	45	4198	240	181
5	SOM-cre	1	123	16	596	47	32
6	SOM-cre	2	229	38	3239	215	228
7	SOM-cre	1	120	18	2836	252	200
Total:		13	1510	205	18931	1311	1092

Characteristics of EEG events

animal #	genotype	SO Duration	SO Amplitude	Spi Duration	Spi Amplitude	SO+Spi SO Duration	SOSpi SO Amplitude	SOSpi Spi
1	PV-cre	0.60 ±0.003	0.26 ±0.001	0.67 ±0.016	0.17 ±0.002	0.61 ±0.013	0.26 ±0.006	0.68
2	PV-cre	0.59 ±0.005	0.20 ±0.001	0.67 ±0.015	0.11 ±0.002	0.62 ±0.028	0.18 ±0.007	0.70
3	PV-cre	0.60 ±0.003	0.21 ±0.001	0.65 ±0.011	0.15 ±0.002	0.57 ±0.010	0.20 ±0.004	0.67
4	SOM-cre	0.64 ±0.003	0.32 ±0.001	0.67 ±0.012	0.19 ±0.002	0.64 ±0.017	0.31 ±0.007	0.72
5	SOM-cre	0.61 ±0.009	0.18 ±0.002	0.93 ±0.065	0.15 ±0.005	0.66 ±0.051	0.19 ±0.011	1.04
6	SOM-cre	0.64 ±0.004	0.25 ±0.001	0.72 ±0.015	0.15 ±0.003	0.62 ±0.013	0.25 ±0.005	0.83
7	SOM-cre	0.60 ±0.003	0.34 ±0.001	0.81 ±0.021	0.21 ±0.003	0.61 ±0.013	0.35 ±0.009	0.92

Table S1. Top - Subject characteristics: Mice and number of imaging sessions and cells imaged per animal. Bottom - Characteristics of EEG events: Mean (± SEM) duration and amplitude of slow oscillation and spindles for solitary slow oscillation (SO) and (7 - 15 Hz) spindle events and for slow oscillations co-occurring with spindles (SO + Spi).

REAGENT or RESOURCE	SOURCE	IDENTIFIER
Antibodies		
anti-PV rabbit primary antibody	Immunostar, U.S.A.,	RRID: AB_572259
anti-SOM rabbit primary antibody	Peninsula Laboratories, U.S.A.,	RRID: AB_518618
goat anti-Rabbit IgG antibody for PV conjugated with Alexa 405	Thermo Fisher Scientific	RRID: AB_221605
goat anti-Rabbit IgG antibody for SOM conjugated with Alexa 633	Thermo Fisher Scientific	RRID: AB2535732
Bacterial and Virus Strains		
AAV2/1-syn-GCaMP6f	University of Pennsylvania	Cat# CS0201
AAV2/1-flex-tdTomato	University of Pennsylvania	Cat# CS0647
AAV2/1-EF1aGFP	University of Pennsylvania	Cat# AV-1-PV1963
Experimental Models: Organisms/Strains		
Pvalb$^{tm1(cre)Arbr}$/J (PV-Cre)	Jackson	RRID: Jax: 008069
Sst$^{tm2.1(cre)Zjh}$/J(SOM-Cre)	Jackson	RRID: Jax:013044
Gt(ROSA)26Sor$^{tm95.1(CAGGCaMP6f)Hze}$/J	Jackson	RRID: Jax:024105
B6.FVB-Tg(Camk2acre)2Gsc/Cnrm Mus musculus	EMMA	RRID:IMSR_EM:01153
Software and Algorithms		
MATLAB	MathWorks	2016a & 2014b; RRID:SCR_001622
fieldtriptoolbox	www.fieldtriptoolbox.org	RRID: SCR_004849
SleepSign for Animals	Kissei Comtech, Japan	Version 3.2

Table S2. Used resources.

Movie S1. Mean f_{norm} signal of the 36 ROIs during all solitary slow oscillations. Bottom trace indicates corresponding EEG recording (speed x 0.25).

References

1. Neckelmann, D., Olsen, O.E., Fagerland, S., and Ursin, R. (1994). The reliability and functional validity of visual and semiautomatic sleep/wake scoring in the Møll-Wistar rat. Sleep *17*, 120–131.

2. Oyanedel, C.N., Kelemen, E., Scheller, J., Born, J., and Rose-John, S. (2015). Peripheral and central blockade of interleukin-6 trans-signaling differentially affects sleep architecture. Brain. Behav. Immun. *50*, 178–185.

3. David, F., Schmiedt, J.T., Taylor, H.L., Orban, G., Di Giovanni, G., Uebele, V.N., Renger, J.J., Lambert, R.C., Leresche, N., and Crunelli, V. (2013). Essential thalamic contribution to slow waves of natural sleep. J. Neurosci. *33*, 19599–19610.

4. Mölle, M., and Born, J. (2011). Slow oscillations orchestrating fast oscillations and memory consolidation. Progr. Brain Res. *193*, 93–110.

5. Mölle, M., Eschenko, O., Gais, S., Sara, S.J., and Born, J. (2009). The influence of learning on sleep slow oscillations and associated spindles and ripples in humans and rats. Eur. J. Neurosci. *29*, 1071–1081.

6. Mölle, M., Bergmann, T., Marshall, L., and Born, J. (2011). Fast and slow spindles during the sleep slow oscillation: disparate coalescence and engagement in memory processing. Sleep *34*, 1411–1421.

7. Eschenko, O., Ramadan, W., Molle, M., Born, J., and Sara, S.J. (2008). Sustained increase in hippocampal sharp wave ripple activity during SWS after learning. Learn. Mem. *15*, 222–228.

8. Mölle, M., Marshall, L., Gais, S., and Born, J. (2002). Grouping of spindle activity during slow oscillations in human non-rapid eye movement sleep. J. Neurosci. *22*, 10941–10947.

9. English, D.F., Peyrache, A., Stark, E., Roux, L., Vallentin, D., Long, M. A., and Buzsáki, G. (2014). Excitation and inhibition compete to control spiking during hippocampal ripples: Intracellular study in behaving mice. J. Neurosci. *34*, 16509–16517.

10. Niethard, N., Hasegawa, M., Itokazu, T., Oyanedel, C.N., Born, J., and Sato, T.R. (2016). Sleep-stage-specific regulation of cortical excitation and inhibition. Curr. Biol. *26*, 2739–2749.

11. Pologruto, T. A., Sabatini, B.L., and Svoboda, K. (2003). ScanImage: flexible software for operating laser scanning microscopes. Biomed. Eng. Online *2*, 13.

2.4 Study III: How sleep balances cortical circuit activity

Author contributions study III

Author	Author position	Scientific ideas %	Data generation %	Analysis & interpretation %	Paper writing %
Niels Niethard	1st Corresponding.	47.5	100	47.5	47.5
Svenja Brodt	2nd	5	0	5	5
Jan Born	Last Corresponding.	47.5	0	47.5	47.5
Title of paper:	How sleep balances cortical circuit activity				
Status in publication process	submitted				

How sleep balances cortical circuit activity

Niels Niethard[1*],Svenja Brodt[1] and Jan Born[1,2*]

[1] Institute of Medical Psychology and Behavioral Neurobiology, University of Tübingen, 72076 Tübingen, Germany.

[2] Center for Integrative Neuroscience, University of Tübingen, 72076 Tübingen, Germany.

* Correspondence: niels.niethard@uni-tuebingen.de or jan.born@uni-tuebingen.de

Institute of Medical Psychology and Behavioral Neurobiology, University of Tuebingen

Ottfried-Mueller-Str. 25, 72076 Tuebingen, Germany

Telephone: +49-7071-29-88923

Fax: +49-7071-29-25016

Abstract

Sleep concurrently contributes to the homeostatic down-regulation of synapses as well as to mnemonic synaptic up-regulation. Here we used in-vivo two-photon calcium imaging of layer 2/3 neuron somas in mice, to show how these seemingly opposing functions are established in cortical networks. Pyramidal (Pyr) cells representing the major cortical population of excitatory cells, decreased activity during both epochs of slow wave sleep (SWS) and rapid-eye-movement (REM) sleep. During SWS, but not REM sleep epochs, activity of parvalbumin-positive inhibitory interneurons (PV-In) simultaneously increased, suggesting that down-regulation of Pyr activity during SWS reflects increased somatic inhibition, rather than synaptic down-scaling, of these cells. We moreover identified subpopulations of Pyr cells with highest activity during sleep spindles, which up-regulated activity during SWS epochs, consistent with an involvement of these cells in mnemonic processing. During succeeding REM sleep epochs these spindle-active Pyr cells showed a profound decrease in activity that was maintained into the following SWS epoch, and was paralleled by a decrease in activity of spindle-active PV-In. The pattern suggests that REM sleep generally produces synaptic down-scaling that even captures the spindle-active neurons engaging in mnemonic processing.

Introduction

In order to efficiently adapt to environmental conditions, the brain needs to accomplish two seemingly opposing tasks. On the one hand, it needs to encode and store relevant information in a long-lasting and stable way, which is assumed to be achieved by the strengthening of synaptic connections among the neurons representing the encoded information. On the other hand, persisting encoding and storing of new information would saturate the network's limited capacities of encoding and storing which makes necessary processes that down-regulate synaptic connections in a homeostatic manner [1,2]. Sleep has been identified as a brain state that might support these two functions in an integrated manner, although the underlying mechanisms are far from being clear. There is ample evidence supporting that sleep serves a global homeostatic process in cortical networks that down-scales and renormalizes synaptic connections that have been strengthened during prior wake phases [3–6]. Both core sleep stages, slow wave sleep (SWS) and rapid eye movement (REM) sleep possibly contribute to this down-regulation. Initially, it was thought to be particularly promoted by the <1 Hz slow oscillation (SO) as neuronal substrate underlying EEG slow wave activity (SWA) that hallmarks SWS [1,7]. However, recent findings [8] suggest that global down-scaling could also be conveyed by the 4-7 Hz theta rhythm that originates from septal-hippocampal circuits [9,10] and is a hallmark of REM sleep. Beyond down-scaling an renormalizing cortical activity, sleep is known to promote long-term memory formation and underlying strengthening of synaptic connections [7,11,12]. Again, both core sleep stages, SWS and REM sleep appear to be implicated in this process. Enhancing SOs during SWS enhances long-term memory formation [13–15], although this effect could primarily reflect the driving force of SOs on thalamic spindles [16]. Spindles are waxing and waning oscillations in the 10-15 Hz range that often nest into the upstate of the SO, and appear to provide optimal conditions for synaptic plastic processes underlying memory formation in cortical microcircuits [17,18]. Finally, there are also studies indicating that memory formation profits from REM sleep and accompanying theta activity [19].

Although SWS and REM sleep have been connected to both homeostatic synaptic down-regulation as well as to the up-regulation of synapses underlying memory formation, little is known about how these sleep stages and associated oscillatory phenomena concurrently establish the two functions in cortical networks. Here, we used in vivo two-

photon calcium imaging in mice in order to assess the temporal activity dynamics in large populations of cortical layer 2/3 cells across epochs of SWS and REM sleep, with the aim to dissociate neuronal subpopulations whose activity is down-scaled or up-scaled during sleep. Two-photon calcium imaging additionally allowed us to differentiate activity changes in the major population of excitatory cells, i.e., pyramidal cells, and the two major populations of inhibitory interneurons, i.e., parvalbumin-positive interneurons (PV-In) and somatostatin-positive interneurons (SOM-In). We found that Pyr, representing ~80 % of cortical neurons, indeed significantly decreased activity in the course of SWS and REM sleep epochs. The decrease during SWS, but not during REM sleep, was accompanied by an increase in activity of PV-In. Importantly, contrasting with the general down-regulation of Pyr activity during SWS, a subpopulation of these cells showing highest activity during spindles, up-regulated activity in the course of SWS. Surprisingly, these spindle active cells possibly involved in memory formation, also underwent profound down-regulation during succeeding REM sleep.

Results

Sleep reduces calcium activity of Pyr cells and simultaneously widens the activity distribution

We used in vivo two-photon calcium imaging of layer 2/3 soma of neurons within sensorimotor cortex in PV-Cre or SOM-Cre transgenic mice. To discriminate activity of PV-In and SOM-In, respectively, we injected two different virus types. First, we injected GCaMP6f to express a genetically encoded calcium indicator. Second, for discriminating the interneurons from other cells, we injected a virus expressing tdTomato Cre-de-pendently (AAV-FLEX-tdTomato). After 10-14 days, almost all neurons around the injection site (~200 µm) expressed GCaMP6f, whereas tdTomato expression was selective for the specific interneuron type. The majority (~80 %) of unlabeled cells in this setup consist of pyramidal cells; we, therefore, considered this population as putative pyramidal cells (Pyr). Once the GCaMP6f expression was strong enough for sufficient image quality, the animals were habituated to head fixation and then repeatedly recorded during epochs of wakefulness, SWS and REM sleep.

We characterized the activity dynamics of the neuron populations of interest (Pyr, PV-In, SOM-In) during epochs of SWS and REM sleep, by comparing activity during the first and last third of the individual epochs (Fig. 1). In these analyses, the mean activity of an individual cell during all wake epochs (set to 100 %) was used to normalize calcium activity. Pyr cells showed a decrease in calcium activity during both, SWS and REM sleep, from the first to the last third of an epoch ($P < 0.05$; SWS: $t = -2.33$; $df = 254$; REM: $t = -2.25$; $df = 144$). PV-In cells increased their activity in the course of SWS epochs ($P < 0.05$; $t = 2.32$; $df = 131$) but activity did not distinctly differ between the first and last third of REM sleep epochs ($P > 0.07$). SOM-In cells showed an opposing pattern of significantly decreasing calcium activity during SWS ($P < 0.01$; $t = -7.21$; $df = 122$) whereas during REM, activity levels remained unchanged ($P > 0.47$). As previously reported [20] activity of Pyr and SOM-In cells was generally higher during SWS than REM sleep, whereas PV-In activity was distinctly higher during REM sleep than SWS.

Changes in calcium activity during SWS did not correlate with SWA energy (i.e., power integrated over time) or changes in SWA during these epochs SWS for any of the three cell types ($P > 0.11$). Decreases in Pyr activity during REM sleep were negatively correlated with EEG theta energy ($P < 0.01$, $r < -0.25$). Changes in PV-In activity were

likewise negatively correlated with theta energy during REM sleep ($P < 0.01$, $r < -0.37$). Moreover, decreases in Pyr and PV-In activity were the more pronounced the longer the duration was of a REM epoch (Pyr: $P < 0.001$ $r = -0.35$; PV-In: $P < 0.001$, $r = -0.43$).

That Pyr cells, i.e., the major population of cortical neurons, on average, decrease in activity over SWS and REM sleep epochs is consistent with the view that sleep globally down-regulates cortical activity [2,21]. However, given that sleep serves twofold functions, to homeostatically down-regulate circuit activity but enhance circuits involved memory formation, we hypothesized, that sleep would not equally affect cells. To test this hypothesis, in a first approach, we compared the standard deviation of the ΔF/F calcium signal level for the different cell types between the first and last third of SWS and REM sleep epochs. We found that the variability in activity of the Pyr cell population, indeed, robustly increased from the first to the last third of both, SWS and REM sleep epochs ($P < 0.01$; SWS: $z = 4.83$; REM: $z = 3.86$; Wilcoxon's test, Fig. 1c). PV-In populations showed increases in variability of the ΔF/F calcium signal level only during SWS epochs ($P < 0.001$; $z = 3.45$), and SOM-In only during REM epochs ($P < 0.001$; $z = 2.97$).

Does prior wake activity predict the cell's activity during subsequent sleep?

Which neurons do and which do not down-regulate activity during sleep? To answer this question, in a first analysis we correlated activity dynamics during wake epochs with that during succeeding sleep epochs, assuming that cells strongly increasing their activity over a wake epoch would be implicated in information encoding. We found, particularly for Pyr and PV-In, positive correlations between the calcium activity changes during a wake epoch (ΔF/F calcium signal level during last third minus level during first third of a wake epoch) and activity changes during the subsequent SWS epoch (Pyr: $r = 0.43$, $P < 0.001$; PV-In: $r = 0.52$, $P < 0.001$; SOM-In: $r = 0.10$, $P < 0.001$, Fig. 2a). Thus, cells showing pronounced increases in activity over a wake epoch tend to increase their activity during subsequent SWS and vice versa.

Of note, different correlations were revealed for the *mean activity level* the cells showed during the prior wake epoch. Here, Pyr cells with higher activity during the wake epoch displayed greater decreases during subsequent SWS ($r = -0.21$; $P < 0.001$, Fig 2b). Likewise, the comparison of wake-active cells (i.e., the 20 % most active cells across *all* wake epochs) with wake-inactive cells (lowest 20 % of cells) revealed that wake-active

Pyr diminished activity in the course of SWS epochs ($P < 0.001$; $t = -5.01$; $df = 254$) while wake-inactive Pyr increased activity ($P < 0.05$; $t = 2.28$, $df = 254$; $F = 28.45$, $P < 0.001$, for 1st/3rd x Active/inactive ANOVA interaction).

Spindle-active Pyr cells increase activity during SWS

Spindles are well-known to be involved in sleep-dependent memory formation and underlying cortical synaptic plasticity [22]. We therefore hypothesized that neurons active during spindles are the ones that are spared from down-regulation or even show increasing activity during SWS. To discriminate spindle-active and spindle-inactive cells we calculated for each cell and SWS epoch the difference between the mean calcium activity in the presence of spindles and the mean activity during the remaining time without spindles. The 20% of cells (of the respective cell type) with the largest positive difference were considered spindle-active cells, whereas cells with small activity differences within the lowest 20% were considered spindle-inactive. We then analyzed activity changes across each SWS epoch. Indeed, spindle-active Pyr and also spindle-active PV-In cells increased their activity level from the first to the last third of a SWS epoch ($P < 0.01$; Pyr: $t = 3.48$, $df = 254$;PV-In: $t = 3.25$, $df = 131$), while spindle-active SOM-In decreased activity within SWS episodes ($P < 0.05$, $t = -2.06$, $df = 122$, Fig. 3). During REM sleep epochs, spindle-active Pyr and PV-In decreased activity ($P < 0.01$; Pyr: $t = -3.74$, $df = 144$; PV-In: $t = -3.52$, $df = 70$), while SOM-In changes remained non-significant.

Spindle-inactive Pyr displayed calcium dynamics opposite to those of spindle-active Pyr cells, i.e., they reduced activity during SWS epochs ($P < 0.01$, $t = -4.64$ $df = 254$) and increased activity during REM sleep epochs ($P < 0.01$, $t = 2.23$, $df = 144$;, $F = 45.17$, $P < 0.001$, for SWS/REM x Active/inactive ANOVA interaction). Dynamics of spindle-inactive PV-In during SWS or REM sleep epochs remained non-significant ($P > 0.1$) and spindle-inactive SOM-In followed the same activity pattern as spindle-active SOM-In with decreasing calcium activity during SWS ($P < 0.01$, $t = -5.07$ $df = 122$), but not REM sleep epochs ($F = 5.89$, $P < 0.05$, for SWS/REM ANOVA main effect). In additional analyses we clustered spindle-active and inactive cells separately according to whether or not the spindle occurred in the presence of a slow oscillation (SO) upstate. Analyses of these cell clusters revealed essentially similar activity changes within SWS and REM

sleep epochs, indicating that the observed dynamics are independent of the additional presence of SOs.

Both, spindle density and power in the 7–15 Hz spindle frequency band significantly increased from the first to the last third of all SWS episodes ($P < 0.001$; $d.f. = 254$; $t = -5.45$; $t = -7.27$ respectively, Fig. 3d). The increase spindle band power during SWS correlated with both the parallel increase in calcium activity of spindle-active Pyr cells ($r = 0.48$; $P < 0.001$) and with the decrease in activity of spindle-inactive Pyr cells ($r = -0.26$; $P < 0.001$, Fig. 3e).

In supplementary analyses, we found for all three cell types that, compared with spindle-inactive cells, the spindle-active cells also showed increased activity during the immediately preceding wake epoch ($P < 0.001$, Pyr: t = 59.26, df = 6704; PV-In: $t = 50.82$, $df = 3510$; SOM-In: $t = 22.72$, $df = 3192$). Yet, activity of spindle-active Pyr cells and SOM-In (but not PV-In) during this wake epoch was still significantly lower than that of the wake-active cell populations of this type, as defined by a generally enhanced activity (top 20 % of all cells) across *all* wake epochs ($P < 0.001$, Pyr: $t = -10.72$ $df = 6704$; SOM: $t = -23.06$ $df = 3192$). In contrast to spindle-active Pyr – these wake-active Pyr show a clear decrease in activity during SWS epochs (Supplementary Fig 1).

Pyr cells active during slow oscillations show stable activity during SWS

Like spindles, slow oscillations (SOs) have also been implicated in memory formation [14,23,24]. However, SOs are also thought to mediate processes of synaptic downscaling [1,2,25]. Often, spindles nest into the excitable upstate of the SO. Therefore, to dissociate regulatory functions of SO from those of spindles, here we concentrated on SOs that did not nest spindles. Analog to our approach to spindles, we clustered cells based on their activity during all SO upstates identified in an SWS epoch, subtracted by their activity during the remaining time of the SWS epoch. The top 20% cells were considered SO-active cells whereas the lowest 20% were considered SO-inactive cells. Neither SO-active nor SO-inactive Pyr cells showed any significant change in activity within SWS epochs ($P > 0.32$, Fig. 4). As to the interneuron populations, both SO-active and inactive PV-In increased activity during SWS epochs (P < 0.05; active: t = 2.65, df = 143; inactive: t = 2.18, df = 143), while SO-active and inactive SOM-In decreased activity during SWS epochs ($P < 0.01$; active: $t = -5.33$, $df = 133$; inactive: $t = -3.40$, $df = 133$). Over the course

of REM sleep epochs, SO-active Pyr and PV-In decreased activity (Pyr: $P < 0.01$, $t = -2.95$, $df = 144$; $F = 8.72$, $P < 0.05$, for $1^{st}/3^{rd}$ x Active/inactive ANOVA interaction, PV-In: $P < 0.001$, $t = -3.43$, $df = 70$, $F = 6.61$, $P < 0.05$, for $1^{st}/3^{rd}$ x Active/inactive interaction), whereas SO-active and inactive SOM-In did not express REM sleep related modulations.

The density of SOs (without nesting spindles) decreased during SWS epochs ($P < 0.001$; $t = 6.47$, $df = 254$), and there was also a parallel decrease in slow wave activity (SWA, power in the 0.1-4 Hz band) from the first to the last third of SWS episodes ($P < 0.001$; $t = 3.97$; $df = 254$). These decreases were not significantly correlated with the dynamics of any of SO-active and SO-inactive cell populations during SWS.

REM sleep renormalizes calcium activity of spindle-active cells

We found that during REM sleep epochs, spindle-active Pyr as well as the general population of Pyr cells decreased their activity. However, REM sleep also produced an enhanced variance in activity of the general Pyr cell population (Fig.1) which led us to suspect that the population of spindle-active Pyr might include a subset of cells that is most strongly implicated in memory formation and would, hence, be spared from down-regulation during REM sleep [26]. Overall, our analyses did not support this hypothesis. First, variability of activity among spindle-active Pyr did not change from the first to the last third of REM epochs ($P > 0.1$) consistent with homogenous temporal dynamics in this cell population. Second, comparing the 20% of spindle-active Pyr cells showing the strongest up-regulation of activity during the prior SWS epoch with those 20 % showing the weakest up-regulation, did not reveal a differential down-regulation of activity between these cell subsets during subsequent REM sleep ($P > 0.4$, for $1^{st}/3^{rd}$ x Active/inactive interaction). Finally, assuming that enhanced involvement in spindle-associated memory processing increases the cell's likelihood to escape down-regulation during subsequent REM sleep, we tested whether increases in spindle-active Pyr during SWS to go along with diminished decreases or even increases in activity during subsequent REM epochs. However, we did not find such correlation for spindle-active Pyr ($P > 0.08$, $r = 0.04$).

We finally examined whether the down-regulation of activity in spindle-active Pyr during REM sleep epochs represents a persistent change that is carried over to the next

SWS epoch. To this end, we compared ΔF/F calcium signals of spindle-active and inactive cells between two consecutive SWS epochs (SWS_n vs. SWS_{n+1}) which were interrupted by a REM sleep epoch. A comparison of activity during the first thirds of the SWS epochs revealed that spindle-active Pyr cells indeed exhibited a strong decrease in activity between these consecutive SWS epochs ($P < 0.001$, $t = 5.2$, $df = 115$, Fig. 5). No such decrease was observed for spindle-inactive cells ($P > 0.15$, $F = 17.10$, $P < 0.001$, for SWS-1/SWS-2 x Active/inactive interaction) or, in a further comparison with activity during consecutive SWS epochs interrupted by a single wake rather than REM sleep epoch ($P > 0.11$, $F = 6.71$, $P < 0.01$, for SWS-1/SWS-2 x REM/wake ANOVA interaction). Notably, with a REM sleep epoch intervening between the SWS epochs, the ΔF/F signals from spindle-active cells during the second SWS epoch fell on average even below the initial level of activity during the preceding wake epoch (Fig. 5c). PV-In spindle active and inactive cell clusters showed no difference between two consecutive SWS epochs ($P > 0.17$ for all analyses). Altogether, these data indicate spindle-active Pyr cells that show unique up-regulation of activity during SWS episodes, undergo robust down-regulation of activity during subsequent REM sleep.

Discussion

This study was based on the concept that sleep serves seemingly two opposing functions, i.e., to globally down-scale cortical synaptic networks and network activity and, on the other side, to protect from down-scaling or even up-scale those networks representing memories to be consolidated during sleep [1,27]. We used in-vivo calcium imaging of cortical circuits of naturally sleeping mice, with the aim to dissociate neuron populations whose activity undergo down-regulation across sleep from those, which were not down-regulated or even up-regulated. In fact, we found that during both epochs of SWS and REM sleep the variability in calcium activity levels increased in the population of excitatory Pyr cells representing the great majority of cortical neurons. This finding supports the view that sleep does not uniformly regulate activity in this cell population. On average, the increase in variability of activity was accompanied by a decrease in Pyr cell activity in the course of both SWS and REM sleep epochs, which is consistent with the notion that globally, sleep down-scales cortical synaptic networks. On the other side, we identified Pyr cells characterized by high activity during sleep spindles, which opposing

to the average trend, distinctly increased activity in the course of SWS epochs. Because spindles are known to promote synaptic plasticity underlying memory formation [17,18,22,28,29], this finding concurs with the notion that sleep up-scales subpopulations of Pyr cells involved in memory formation. Surprisingly, the same subpopulation of spindle active Pyr cells underwent profound down-regulation of activity during subsequent REM sleep epochs.

Our finding that both SWS and REM sleep epochs produce a robust increase in the variability of calcium activity levels in the Pyr cell population contrasts with electrophysiological findings indicating a shrinking rather than widening of firing rate distributions across sleep [30,31]. Specifically, those studies found that neurons with high firing rates show a strong decrease in spiking activity particularly in the course of SWS whereas neurons with low firing rates slightly increase spiking activity during this time. Indeed, this more specific picture was confirmed in the present study, when we focused on Pyr cells that in a trait-like manner were most active across *all* wake epochs, and compared them with cells generally showing minor activity during wake. The wake-active cells showed a pronounced decrease in calcium activity during SWS epochs whereas the wake-inactive cells increased in activity (supplementary Fig 1). Considering these analyses, we assume that the SWS-related increase in the variability of calcium activity which we observed here for the global population of Pyr cells, reflects an acute regulation of cell activity associated with sleep/wake-related information processing rather than processes that capture the cell's trait-like activity level. However, further factors need to be considered when comparing the present findings based on calcium imaging with previous electrophysiological findings of a global decrease in spike rate variability across sleep. Thus, imaging of calcium activity also includes the proportion of neurons with very low spiking activity which is typically missed in electrophysiological recordings [32]. Moreover, cortical activity dynamics might be layer specific. We focused on activity of layer 2/3 cells whereas spiking activity was studied mainly in layer 5 neurons. Finally, our measurement of calcium activity in the cell soma is not an immediate reflection of the neuron's spiking activity in terms of action potentials, but integrates spatially extended activity over time with a lower temporal resolution.

The average decrease in activity of Pyr cells during SWS and REM sleep epochs well fits the notion that sleep serves a global synaptic down-scaling of cortical networks

[1,2,26]. Yet, the mechanisms underlying the decrease might differ between SWS and REM sleep. As to SWS, previous work has linked slow wave activity (SWA) to a down scaling in synaptic networks [2,25,33] . However, in the present study, no consistent correlations were found between measures of SWA and changes in Pyr cell activity over SWS epochs. Rather than a consequence of weakened and decreased synaptic inputs, the decrease in activity of excitatory Pyr cells appeared to be a consequence of increased inhibitory inputs to these cells. In fact, PV-In cells displayed a strong increase in activity across SWS epochs. These cells effectively inhibiting the soma of Pyr cells, could themselves well account for the down-regulation of Pyr cell activity in the course of SWS. Hence, whether SWS actually contributes to down-scaling synapses remains to be scrutinized in morphological studies [5]. Synaptic down-scaling might have rather caused the decrease in Pyr cell activity accompanying REM sleep epochs, because activity of the major inhibitory neurons did not concurrently increase during these epochs, but remained unchanged (PV-In) or decreased (SOM-In) from the first to the last third of these epochs. The REM-sleep related decrease in Pyr cell activity was positively correlated with theta energy (i.e. theta power integrated over time). Similar hints at a contribution of theta activity to the down-regulation of network activity have been derived from correlational analyses of hippocampal spike activity across triplets of SWS-REM-SWS epochs [8]. However, evidence for an involvement of theta activity in processes of down-scaling is otherwise scarce and indirect [34,35].

We could identify a subpopulation of Pyr neurons showing highest activity during spindles, which - opposite to the global deactivation across SWS - displayed a substantial increase in activity during SWS. This is a central finding of the study which supports the idea that during sleep and particularly during SWS an up-regulation of specific assemblies putatively involved in memory processing is established while network activity is globally down-regulated. The up-regulation of activity during SWS was specific to spindle-active Pyr and PV-In, and was not seen in wake-active cells that down-regulated activity in the course of SWS. Only SOs that did not nest a spindle were considered in these analyses, which allowed to clearly discriminate the function of spindles from that of SOs. Spindles have been shown to promote the formation of memory and underlying synaptic plastic processes, like long-term potentiation [17]. At the level of cortical microcircuits, they are characterized by increased activity of pyramidal cells in the presence of distinctly

enhanced somatic inhibition of these cells via PV-In, i.e., a constellation facilitating plastic synaptic changes in response to afferent inputs to the distal dendrites of these cells [18,28]. Fittingly, the present study reveals a parallel increase in activity for spindle-active PV-In in the course of SWS. Moreover, the increase in Pyr cell activity was paralleled by an increase in spindle density across SWS. This increase in spindle activity in the course of SWS is well known from previous studies [36]. Spindles generated in thalamic networks with thalamo-cortical projections to both PV-INs and Pyr [37–39], could represent the driving force up-regulating activity of these circuits during memory processing [40,41].

Unexpectedly, calcium activity of spindle-active Pyr cells was uniformly down-regulated in the course of REM sleep epochs. The down-regulation was specific to the spindle-active Pyr, and not seen in spindle-inactive cells. Moreover, it persisted into subsequent SWS epochs which excludes that this down-regulation of activity originated from a REM sleep-associated increase in inhibitory inputs, e.g., from PV+ interneurons [20]. In fact, spindle-active PV-In likewise showed a distinct decrease in activity during REM sleep epochs, and activity levels of spindle-active SOM-In remained unchanged. Against this backdrop the persisting down-regulation of Pyr cell activity during REM sleep most likely reflects reduced excitatory input as a result of synaptic down-scaling. This interpretation well concurs with evidence from structural imaging of mice layer 5 pyramidal cells, indicating that REM sleep prunes postsynaptic dendritic spines of these neurons, that were newly formed during prior motor learning [42]. In light of the present data, the pyramidal cells with newly formed synapses following motor learning would be expected to constitute the population of spindle-active cells. However, that study also showed that REM sleep simultaneously maintains and strengthens a fraction of the newly formed synapses which was critical for motor improvement see after sleep. Diverging from this finding, here we were unable to identify a subgroup of spindle-active cells that did not undergo down-regulation during sleep which might be explained by reasons: first, focusing on the soma of pyramidal cells, we only measured the integrated activity of the entire neuron. Yet, REM sleep-associated strengthening of synapses might only occur in neurons with synapses that are simultaneously eliminated and, thereby, mask any enhancing effects on overall activity levels in these cells. Second, because in the present study the mice were not trained on a novel task before sleep, all newly formed synapses were down-scaled. This second explanation implicates that, beyond spindles, another mechanism exists that decides, e.g., based on the novelty of the encoded information, about whether a

newly formed representation is maintained or eliminated during REM sleep [34,35], which is a promising hypothesis to be tested in future research.

Methods

Animals

For the experiments two different strains of transgenic mice, PV-Cre mice [RRID:IMSR_JAX:008069 (n = 4)] and SOM-Cre mice [RRID:IMSR_JAX:013044 (n = 4)] were used. All mice were housed in groups of up to five animals under temperature and humidity controlled conditions (22 ± 2 ºC; 45 – 65 %) and a 12h/12h light dark cycle. All recordings started during the first hour of the light phase and only male mice older than eight weeks were recorded. Procedures were similar to those described previously [18,20], and also data collection relied on mice used in these previous studies. All experiments were approved by the local institutions in charge of animal welfare (Regierungspräsidium Tübingen, State of Baden-Wuerttemberg, Germany).

Surgery

All animals were anesthetized with 0.1 mg/g ketamine and 0.008 mg/g xylazine with a supplement of isoflurane. For topical anesthesia lidocain was applied. Afterwards the animals were mounted on a stereotaxic frame. Body temperature was continuously monitored and maintained at 37ºC. A custom-made head post was glued to the skull and subsequently cemented with dental acrylic (Kulzer Palapress, Germany).

Virus injection and the implantation of the imaging window followed headpost implantation. To this end, a craniotomy above the sensorimotor cortex (1.1 mm caudal and 1–1.3 mm lateral from the bregma) with a size of 1.2 mm x 2 mm was made. Afterwards, two viruses (AAV2/1-syn-GCaMP6f 2.96 × 1012 genomes/mL and AAV2/1-Flex-tdTomato 1.48 × 1011genomes/mL) were injected into multiple sites of the area of craniotomy (10–20 nL/site; 3–5 min/injection). The injection depth was between 130 and 300 μm. Virus injection was followed by the implantation of the imaging window (1 mm x 1.5 mm). The space between the skull and the imaging window was filled with agarose (1.5 - 2 %) and then the imaging window was cemented with dental acrylic.

EEG electrodes were implanted on the cortical surface of the contralateral hemisphere relative to the imaging window (−2.5 mm, lateral +2.5 mm from bregma). The reference elctrodes was implanted on the brain surface 1mm relative to lambda. Two wire electrodes were implanted into the neck muscle for EMG recordings (Science Products,

Germany). After the surgery, all animals were brought back to their home cage and were single-housed for the rest of the experiments. They had at least 10 days of recovery from surgery before imaging sessions started.

Head fixation procedure

After handling the animals 10 min per day for 1 week, the animal was habituated to the head fixation. Habituation consisted of four sessions per day for one week with increasing fixation durations (30 s, 3 min, 10 min, and 30 min) interleaved by 10-min rest intervals. Habituation was conducted until 24 hours prior to the first imaging session during the early light phase.

EEG and EMG Recordings

Sleep stages were identified based on EEG and EMG recordings during the imaging sessions. EEG and EMG signals were amplified, filtered (EEG: 0.01–300 Hz; EMG: 30–300 Hz), and sampled at a rate of 1,000 Hz (amplifier: model 15A54; Grass Technologies, USA). Based on EEG/EMG signals for succeeding 10-s epochs, the brain state of the mouse was classified into wake, SWS, and REM sleep stages [43,44]. Sleep stage classification was supported using the software SleepSign for animals (Kissei Comtech, Japan).

Offline detection of sleep slow oscillations and spindles.

To detect discrete slow oscillation (SO) events during SWS, offline algorithms were adopted from previously described procedures [45–47]. In brief, the EEG was bandpass filtered between 0.2 - 4.5 Hz and then, all positive-to-negative zero crossings of the signal as well as the local minimum and maximum between each two successive crossings were marked. Intervals between two succeeding positive-to-negative zero-crossings were identified as a SO event when the length of this interval was between 0.4 - 2 s and when the minimum amplitude and minimum-to-maximum amplitude was greater than 66.6 % of the average of the respective amplitude values across the whole recording. For these remaining events the enclosing zero-crossings represent the onset and end of the corresponding SO cycle.

Detection of discrete spindles was performed following an algorithm described by [48]: The EEG signal was band pass filtered between 7 - 15 Hz, rectified and, subsequently, all maxima were interpolated to yield the envelope for this frequency band. A spindle event was identified whenever the envelope exceeded an individual threshold for a duration of 0.5 to 3.0 s, whereby the threshold was defined by the standard deviation of the filtered signal during all SWS epochs of an individual mouse multiplied by a factor of 1.5. Thus, the positive and subsequent negative threshold crossing represented the onset and end of a spindle event. Detected spindle events were then characterized by their onset. For analyses, the root mean square signal (RMS) during identified spindle events was averaged time-locked to the spindle onset. The analyses of accompanying calcium signal centered – as for SO events – on an interval -2 to +3 s around the spindle event. The same procedure was applied to separately identify slow and fast spindles, after pre-filtering the EEG signal in the 7 - 15 Hz band.

To discriminate spindle-active and spindle inactive cells mean $\Delta F/F$ signals during spindles and during SWS without spindles were subtracted. This differences was calculated for each SWS episodes independently. The top 20% cells with highest difference between $\Delta F/F$ signals

Two-photon imaging

In vivo imaging was performed using a two-photon microscope based on the MOM system (Sutter, USA) controlled by ScanImage software [49]. The light source was a pulsed Ti:sapphire laser ($\lambda = 980$ nm; Chameleon; Coherent, USA). Red and green fluorescence photons were collected with an objective lens (Nikon; 16×; 0.80 numerical aperture [NA]), separated by a 565-nm dichroic mirror (Chroma; 565dcxr) and barrier filters (green: ET525/70 m-2p; red: ET605/70 m-2p), and measured using photomultiplier tubes (Hamamatsu Photonics; H10770PA-40). The imaging frame consisted of 1,024 × 256 pixels, and the frame rate was 5.92 Hz (169 ms per frame). Images were collected in layer 2/3 at a depth of 150–250 μm. All subsequent analyses were performed on the original data or after high-pass pre-filtering at 0.1 Hz to eliminate slower changes possibly originating from metabolic and blood flow changes. As both analyses yielded essentially the same results, and also because of the lower sensitivity to changes in blood flow of

two-photon imaging, this report is restricted to analyses based on unfiltered two-photon imaging data.

Two-photon image analysis

Lateral motion was corrected in two steps [50]. A cross-correlation-based image alignment (Turboreg) was performed, followed by a line-by-line correction using an algorithm based on a hidden Markov model [51]. ROIs containing individual neurons were drawn manually, and the pixel values within each ROI were summed to estimate the fluorescence of this neuron. PV-INs and SOM-INs were manually detected by red fluorescence signal expressed by AAV2/1-Flex-tdtomato. The individual cell traces were calculated as the average pixel intensity within the ROIs for each frame. The cell traces were transformed into the percent signal change ($\Delta F/F$), in which the baseline for each cell was defined as the 20th percentile value of all frames. We confirmed that the neuropil signal did not affect our results by performing neuropil subtraction. The neuropil signal was estimated for each ROI as the average pixel value within two pixels around the ROI (excluding adjacent cells). The true signal was estimated as $F(t) = FinROI - r \times FaroundROI$, where $r = 0.7$.

Statistics

All analyses based on differences within the different brain states (SWS, REM, wake epochs). $\Delta F/F$ signals of each detected cell were normalized by dividing the signal value by the cell's mean activity during all episodes scored as wakefulness. Cell clustering and comparisons of activity during wake epochs themselves was based on $\Delta F/F$ signals that were not normalized. Average activity was calculated for each cell during the 1st, 2nd and 3rd third of each epoch of SWS, REM sleep and wakefulness. For analyses of the temporal activity dynamics within epochs, analyses of variance were performed, including the repeated measures factor "1st/3rd Third" (representing activity during the first and last third of an epoch), and the group factors "SWS/REM" (representing the different sleep stages) and "Active/inactive" (representing the cell clusters formed on the basis of different activity levels). ANOVAs run on neighboring SWS epochs contained a repeated measures factor SWS-1/SWS-2. Significant ANOVA effects were followed by post-hoc

(two-sided, paired) Student's *t*-test for comparing wake normalized ΔF/F signals between the first and last thirds of SWS, REM sleep or wakefulness and for the comparison of calcium activity between neighboring SWS epochs. For comparing non-normal distributed standard deviations of population activity during SWS and REM sleep Wilcoxon's signed rank test was used. For correlation analyses, Pearson product-moment correlation coefficients were calculated. Respective *P*-values were Bonferroni corrected.

Acknowledgements

Author contributions

N.N. and J.B. designed the study. N.N. performed experiments, N.N. and S.B. analyzed the data. N.N., S.B. and J.B. wrote the manuscript.

Competing interests

The authors declare no competing interest.

References

1.   Tononi, G. & Cirelli, C. Sleep and the price of plasticity: from synaptic and cellular homeostasis to memory consolidation and integration. *Neuron* **81**, 12–34 (2014).

2.   Tononi, G. & Cirelli, C. Sleep and synaptic down-selection. *Eur. J. Neurosci.* (2019). doi:10.1111/ejn.14335

3.   Vyazovskiy, V. V, Cirelli, C., Pfister-Genskow, M., Faraguna, U. & Tononi, G. Molecular and electrophysiological evidence for net synaptic potentiation in wake and depression in sleep. *Nat. Neurosci.* **11**, 200–208 (2008).

4.   Diering, G. H. *et al.* Homer1a drives homeostatic scaling-down of excitatory synapses during sleep. *Science (80-.).* **355**, 511–515 (2017).

5.   de Vivo, L. *et al.* Ultrastructural evidence for synaptic scaling across the wake/sleep cycle. *Science (80-.).* **355**, 507–510 (2017).

6.   Spano, G. M. *et al.* Sleep deprivation by exposure to novel objects increases synapse density and axon-spine interface in the hippocampal CA1 region of adolescent mice. *J. Neurosci.* 0380–19 (2019). doi:10.1523/JNEUROSCI.0380-19.2019

7.   Rasch, B. & Born, J. About sleep's role in memory. *Physiol. Rev.* **93**, 681–766 (2013).

8.   Grosmark, A. D., Mizuseki, K., Pastalkova, E., Diba, K. & Buzsáki, G. REM sleep reorganizes hippocampal excitability. *Neuron* **75**, 1001–7 (2012).

9.   Kang, D., Ding, M., Topchiy, I., Shifflett, L. & Kocsis, B. Theta-rhythmic drive between medial septum and hippocampus in slow-wave sleep and microarousal: a Granger causality analysis. *J. Neurophysiol.* **114**, 2797–803 (2015).

10.   Buzsáki, G. Theta Oscillations in the Hippocampus. *Neuron* **33**, 325–340 (2002).

11.   Yang, G. *et al.* Sleep promotes branch-specific formation of dendritic spines after learning. *Science (80-.).* **344**, 1173–1178 (2014).

12.   Sawangjit, A. *et al.* The hippocampus is crucial for forming non-hippocampal long-term memory during sleep. *Nature* **564**, 109–113 (2018).

13. Marshall, L., Helgadóttir, H., Mölle, M. & Born, J. Boosting slow oscillations during sleep potentiates memory. *Nature* **444**, 610–613 (2006).

14. Ngo, H. V. V, Martinetz, T., Born, J. & Mölle, M. Auditory closed-loop stimulation of the sleep slow oscillation enhances memory. *Neuron* **78**, 545–553 (2013).

15. Chauvette, S., Seigneur, J. & Timofeev, I. Sleep oscillations in the thalamocortical system induce long-term neuronal plasticity. *Neuron* **75**, 1105–1113 (2012).

16. Latchoumane, C.-F. V., Ngo, H.-V. V., Born, J. & Shin, H.-S. Thalamic spindles promote memory formation during sleep through triple phase-locking of cortical, thalamic, and hippocampal rhythms. *Neuron* **95**, 424-435.e6 (2017).

17. Rosanova, M. & Ulrich, D. Pattern-specific associative long-term potentiation induced by a sleep spindle-related spike train. *J. Neurosci.* **25**, 9398–405 (2005).

18. Niethard, N., Ngo, H.-V. V, Ehrlich, I. & Born, J. Cortical circuit activity underlying sleep slow oscillations and spindles. *Proc. Natl. Acad. Sci. U. S. A.* **115**, E9220–E9229 (2018).

19. Boyce, R., Glasgow, S. D. & Williams, S. Causal evidence for the role of REM sleep theta rhythm in contextual memory consolidation. **352**, 812–817 (2016).

20. Niethard, N. *et al.* Sleep-stage-specific regulation of cortical excitation and inhibition. *Curr. Biol.* **26**, 2739–2749 (2016).

21. Niethard, N., Burgalossi, A. & Born, J. Plasticity during sleep is linked to specific regulation of cortical circuit activity. *Front. Neural Circuits* **11**, 1–9 (2017).

22. Puentes-Mestril, C., Roach, J., Niethard, N., Zochowski, M. & Aton, S. J. How rhythms of the sleeping brain tune memory and synaptic plasticity. *Sleep* (2019). doi:10.1093/sleep/zsz095

23. Binder, S. *et al.* Transcranial slow oscillation stimulation during sleep enhances memory consolidation in rats. *Brain Stimul.* **7**, 508–515 (2014).

24. Wei, Y., Krishnan, G. P. & Bazhenov, M. Synaptic mechanisms of memory consolidation during sleep slow oscillations. *J. Neurosci.* **36**, 4231–47 (2016).

25. González-Rueda, A., Pedrosa, V., Feord, R. C., Clopath, C. & Paulsen, O. Activity-dependent

downscaling of subthreshold synaptic inputs during slow-wave-sleep-like activity in vivo. *Neuron* **97**, 1244-1252.e5 (2018).

26.   Niethard, N. & Born, J. Back to baseline: sleep recalibrates synapses. *Nat. Neurosci.* 1 (2019). doi:10.1038/s41593-018-0327-6

27.   Diekelmann, S. & Born, J. The memory function of sleep. *Nat Rev Neurosci* **11**, 114–126 (2010).

28.   Seibt, J. *et al.* Cortical dendritic activity correlates with spindle-rich oscillations during sleep in rodents. *Nat. Commun.* **8**, 684 (2017).

29.   Steriade, M. & Timofeev, I. Neuronal plasticity in thalamocortical networks during sleep and waking oscillations. *Neuron* **37**, 563–76 (2003).

30.   Levenstein, D., Watson, B. O., Rinzel, J. & Buzsáki, G. Sleep regulation of the distribution of cortical firing rates. *Curr. Opin. Neurobiol.* **44**, 34–42 (2017).

31.   Clawson, B. C. *et al.* Sleep promotes, and sleep loss inhibits, selective changes in firing rate, response properties and functional connectivity of primary visual cortex neurons. *Front. Syst. Neurosci* **12**, 40 (2018).

32.   Brecht, M., Roth, A. & Sakmann, B. Dynamic receptive fields of reconstructed pyramidal cells in layers 3 and 2 of rat somatosensory barrel cortex. *J. Physiol.* **553**, 243–265 (2003).

33.   Gulati, T., Guo, L., Ramanathan, D. S., Bodepudi, A. & Ganguly, K. Neural reactivations during sleep determine network credit assignment. *Nat. Neurosci.* **20**, 1277–1284 (2017).

34.   Poe, G. R., Nitz, D. A., McNaughton, B. L. & Barnes, C. A. Experience-dependent phase-reversal of hippocampal neuron firing during REM sleep. *Brain Res.* **855**, 176–180 (2000).

35.   Poe, G. R. Sleep is for forgetting. *J. Neurosci.* **37**, 464 LP – 473 (2017).

36.   Dijk, D.-J., Hayes, B. & Czeisler, C. A. Dynamics of electroencephalographic sleep spindles and slow wave activity in men: effect of sleep deprivation. *Brain Res.* **626**, 190–199 (1993).

37.   Bruno, R. M. & Simons, D. J. Feedforward mechanisms of excitatory and inhibitory cortical receptive fields. *J. Neurosci.* **22**, 10966–75 (2002).

38. Schubert, D., Kötter, R., Zilles, K., Luhmann, H. J. & Staiger, J. F. Cell type-specific circuits of cortical layer IV spiny neurons. *J. Neurosci.* **23**, 2961–70 (2003).

39. Porter, J. T., Johnson, C. K. & Agmon, A. Diverse types of interneurons generate thalamus-evoked feedforward inhibition in the mouse barrel cortex. *J. Neurosci.* **21**, 2699–710 (2001).

40. Jiang, X. *et al.* Replay of large-scale spatio-temporal patterns from waking during subsequent NREM sleep in human cortex. *Sci. Rep.* **7**, 17380 (2017).

41. Schönauer, M. *et al.* Decoding material-specific memory reprocessing during sleep in humans. *Nat. Commun.* **8**, 15404 (2017).

42. Li, W., Ma, L., Yang, G. & Gan, W.-B. REM sleep selectively prunes and maintains new synapses in development and learning. *Nat. Neurosci.* 1–16 (2017). doi:10.1038/nn.4479

43. Neckelmann, D., Olsen, O. E., Fagerland, S. & Ursin, R. The reliability and functional validity of visual and semiautomatic sleep/wake scoring in the Møll-Wistar rat. *Sleep* **17**, 120–131 (1994).

44. Oyanedel, C. N., Kelemen, E., Scheller, J., Born, J. & Rose-John, S. Peripheral and central blockade of interleukin-6 trans-signaling differentially affects sleep architecture. *Brain. Behav. Immun.* **50**, 178–185 (2015).

45. David, F. *et al.* Essential thalamic contribution to slow waves of natural sleep. *J. Neurosci.* **33**, 19599–19610 (2013).

46. Mölle, M. & Born, J. Chapter 7 – Slow oscillations orchestrating fast oscillations and memory consolidation. in *Progress in Brain Research* **193**, 93–110 (2011).

47. Mölle, M., Eschenko, O., Gais, S., Sara, S. J. & Born, J. The influence of learning on sleep slow oscillations and associated spindles and ripples in humans and rats. *Eur. J. Neurosci.* **29**, 1071–1081 (2009).

48. Mölle, M., Marshall, L., Gais, S. & Born, J. Grouping of spindle activity during slow oscillations in human non-rapid eye movement sleep. *J. Neurosci.* **22**, 10941–10947 (2002).

49. Pologruto, T. a, Sabatini, B. L. & Svoboda, K. ScanImage: flexible software for operating laser scanning microscopes. *Biomed. Eng. Online* **2**, 13 (2003).

50. Komiyama, T. *et al.* Learning-related fine-scale specificity imaged in motor cortex circuits of behaving mice. *Nature* **464**, 1182–6 (2010).

51. Dombeck, D. a., Khabbaz, A. N., Collman, F., Adelman, T. L. & Tank, D. W. Imaging Large-Scale Neural Activity with Cellular Resolution in Awake, Mobile Mice. *Neuron* **56**, 43–57 (2007).
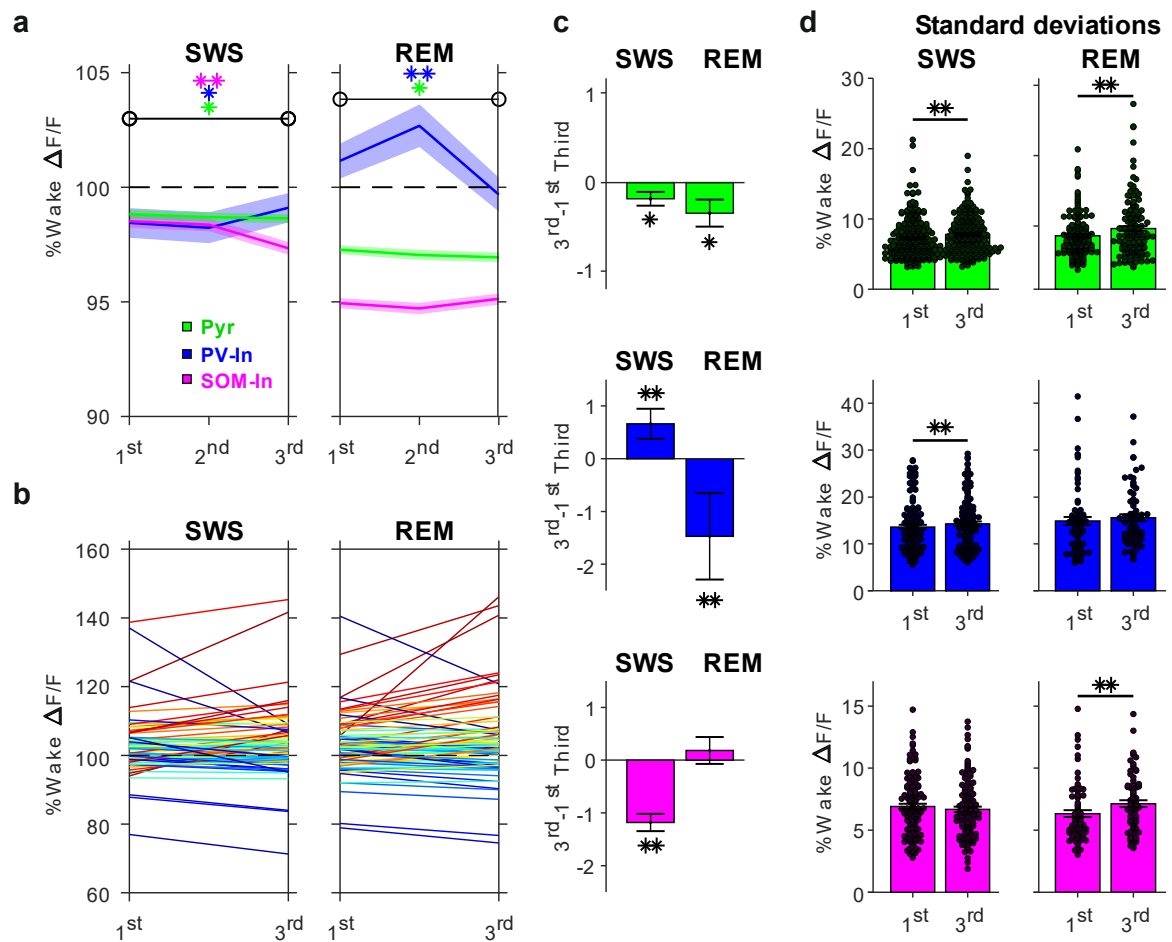
Fig. 1 Cortical calcium activity decreases and disperses during sleep.

a, Mean ± SEM wake-normalized ΔF/F calcium signals of Pyr (green), PV-In (blue) and SOM-In (pink) during thirds of SWS (n: Pyr 255, PV-In 132, SOM-In 123) and REM sleep epochs (n: Pyr 145, PV-In 71, SOM-In 74). Significant changes from first to last third of SWS and REM epochs are indicated by asterisks in the respective color (** $P < 0.01$; * $P < 0.05$). **b**, Wake normalized ΔF/F calcium signals of Pyr cells during the first (1st) and third (3rd) third of an example SWS and subsequent REM epoch. Increasing or decreasing courses for each recorded cell are color coded from red to blue, respectively. **c**, Mean difference (± SEM) in activity of Pyr, PV-In and SOM-In from first to last third (3rd - 1st Third) of SWS (left) and REM sleep (right) epochs (** $P < 0.01$; * $P < 0.05$). **d**, Mean ± SEM of standard deviations of calcium activity during first and last third of SWS (left) and REM sleep epochs (right) for Pyr (green), PV-In (blue) and SOM-In (** $P < 0.01$; * $P < 0.05$, Wilcoxon's test). In all panels the wake-normalized ΔF/F calcium signal is indicated (in %) with the signal across all wake epochs set to 100 %.
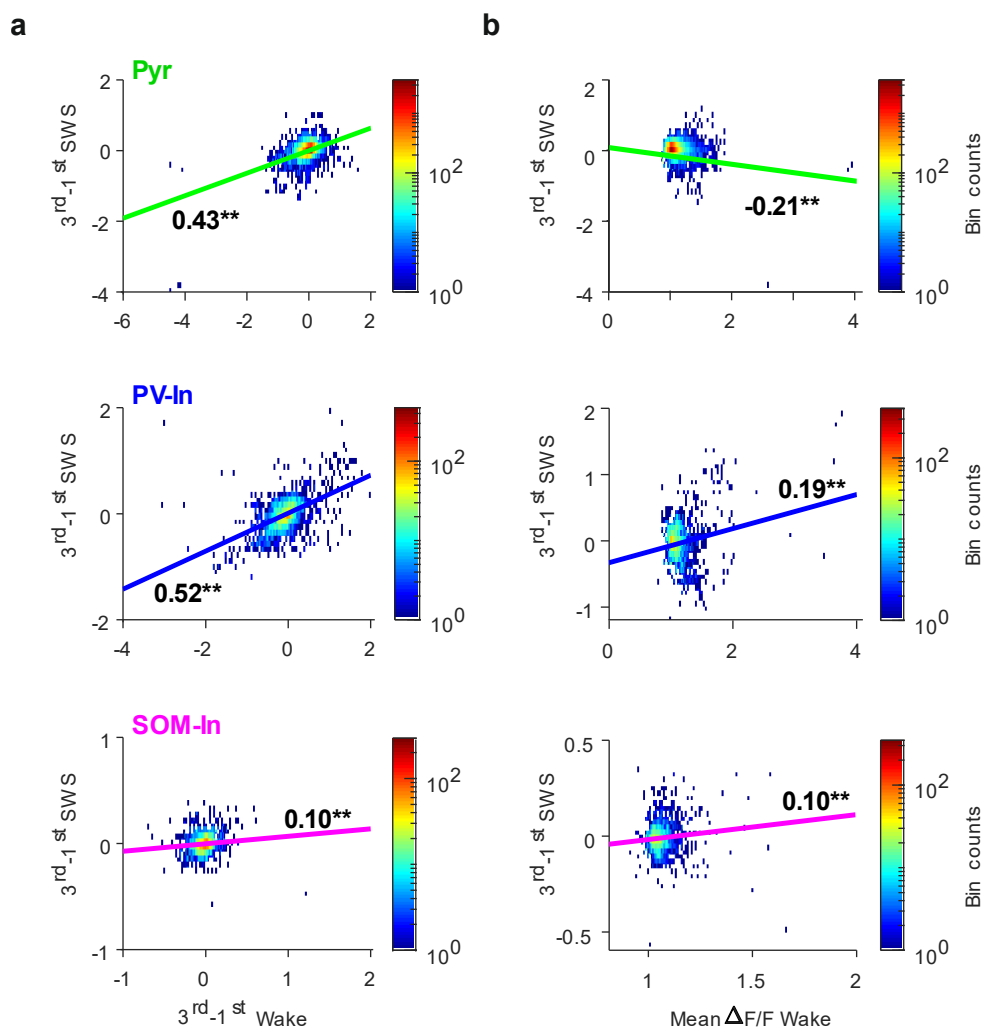
Fig. 2 Changes in the cell's activity during SWS correlate with activity during prior wake epoch.

Density plots for correlations between the change in a cell's activity during a SWS epoch (3rd - 1st Third) and **a.** the *change* in activity during the preceding wake epoch (3rd - 1st Third), and **b,** the *mean* activity level during the preceding wake epoch for (from top to bottom) Pyr, PV-In and SOM-In. r-values and significances are indicated (** $P < 0.01$; * $P < 0.05$). Note, increases in Pyr and PV-In during SWS epochs show robust correlations with increases in activity of these cells during the prior wake epochs.
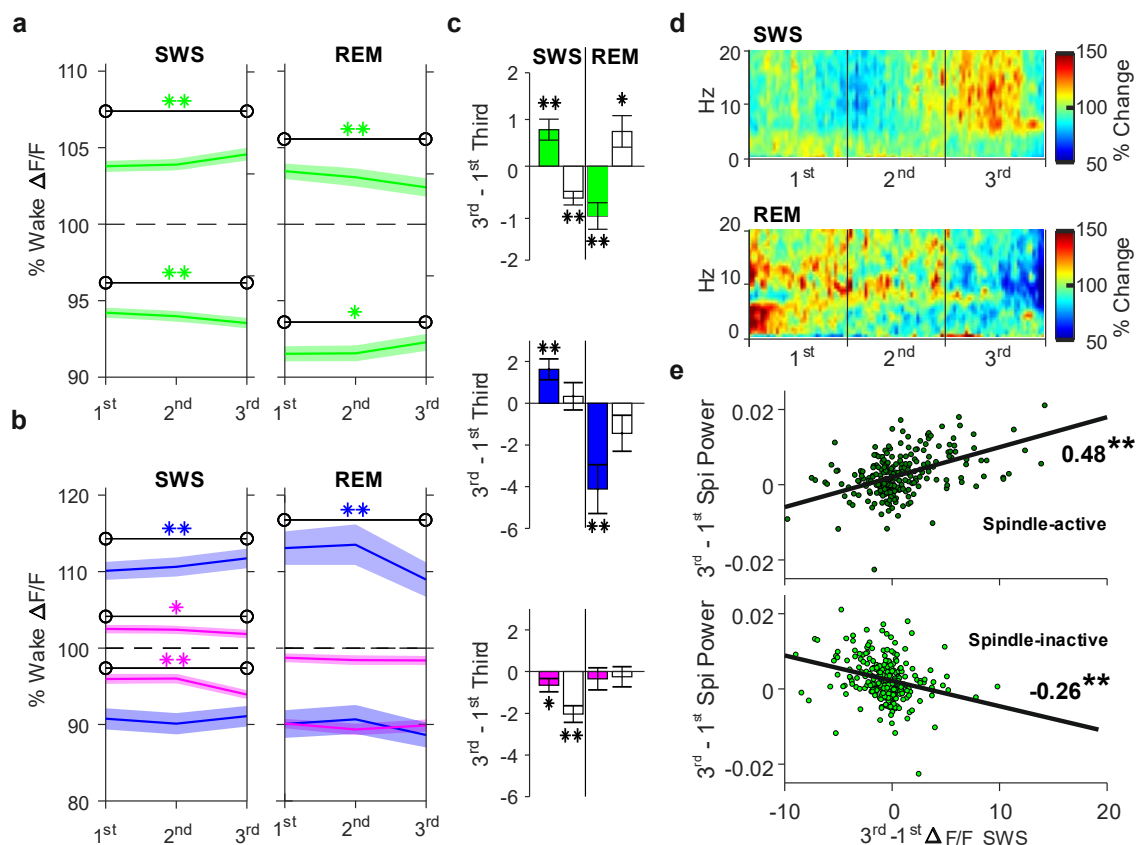
Fig. 3 Spindle-active Pyr cells show increased calcium activity during SWS.

a, Mean ± SEM wake-normalized ΔF/F calcium signals of spindle-active (upper traces) and spindle-inactive (lower traces) Pyr cells (green) during thirds of SWS (n: Pyr 255, PV-In 132, SOM-In 123) and REM sleep epochs (n: Pyr 145, PV-In 71, SOM-In 74). Significant changes from first to last third of SWS and REM epochs are indicated by asterisks (** $P < 0.01$; * $P < 0.05$). **b**, As in a, but for spindle-active PV-In (upper lines, blue) and SOM-In (pink) and spindle-inactive PV-In and SOM-In (lower blue and pink lines, respectively). **c**, Mean difference (± SEM) in activity of spindle active (filled bars) and spindle inactive (empty bars) Pyr, PV-In and SOM-In from first to last third (3rd - 1st Third) of SWS (left) and REM sleep (right) epochs (** $P < 0.01$; * $P < 0.05$). Note, spindle-active Pyr and PV-In significantly increase calcium activity over SWS epochs and significant decrease over REM sleep epochs. **d,** Time frequency plots of EEG power (0.1-20 Hz) across all SWS (top) and REM sleep (bottom) epochs. Color code indicates

change (in %) in power with reference to the mean power during an epoch in the respective frequency. **e**, Density plots for correlations between calcium activity changes during SWS (3rd – 1st Third) and changes in the spindle band (7-15 Hz) power for spindle-active (top) and spindle in-active (bottom). r-values and significances are indicated (** $P < 0.01$).
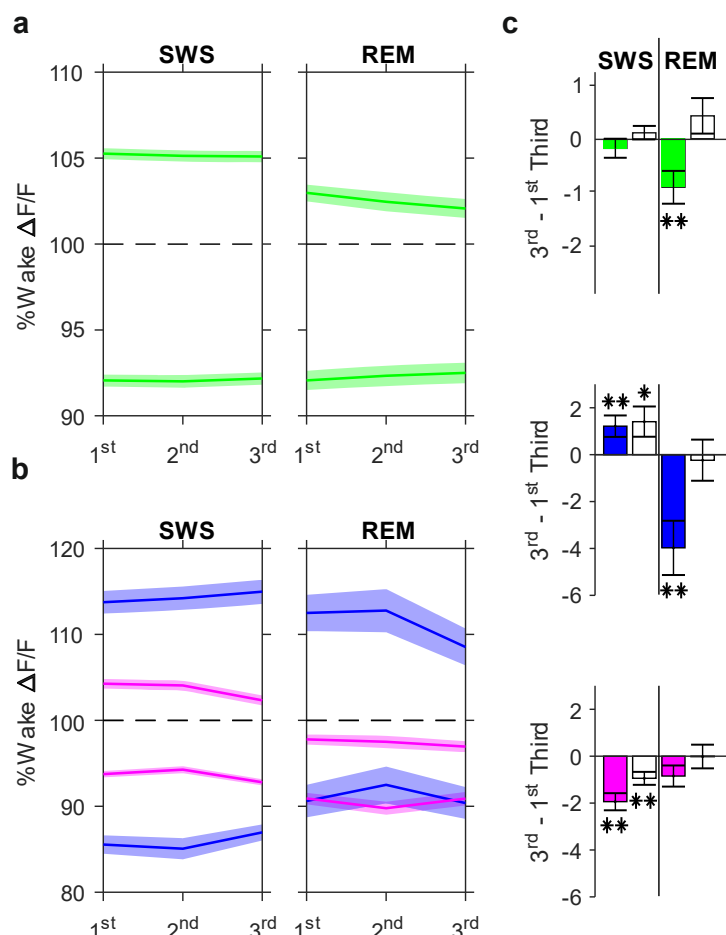
Fig. 4: Pyr cells active during SO upstates show stable activity during SWS.

a, Mean ± SEM wake-normalized ΔF/F calcium signals of SO-active (upper traces) and SO-inactive (lower traces) Pyr cells (green) during thirds of SWS (n: Pyr 255, PV-In 132, SOM-In 123) and REM sleep epochs (n: Pyr 145, PV-In 71, SOM-In 74). Significant changes from first to last third of SWS and REM epochs are indicated by asterisks (** P < 0.01; * P < 0.05). **b**, As in a, but for SO-active PV-In (upper lines, blue) and SOM-In (pink) and SO-inactive PV-In and SOM-In (lower blue and pink lines, respectively). **c**, Mean difference (± SEM) in activity of SO-active (filled bars) and SO-inactive (empty bars) Pyr, PV-In and SOM-In from first to last third (3rd - 1st Third) of SWS (left) and REM sleep (right) epochs. (** P < 0.01; * P < 0.05).
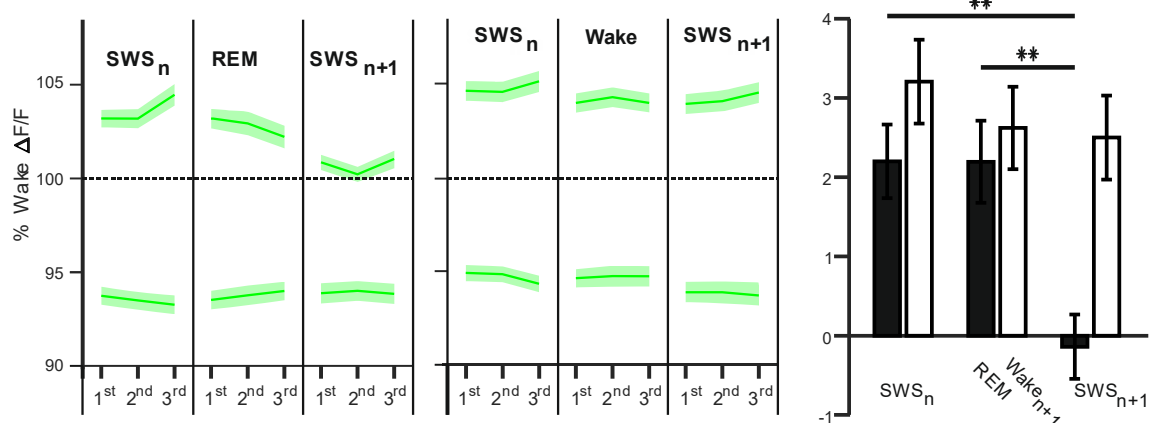
Fig. 5: REM sleep down-regulates activity of spindle-active Pyr cells.

Mean ± SEM wake-normalized ΔF/F calcium signals of spindle-active (upper traces) and spindle-inactive (lower traces) Pyr cells **a.** during a sequences of sleep epochs comprising **a.** a SWS epoch (SWS_n) followed by a REM sleep epoch and another SWS epoch (SWS_{n+1}) and **b.** during a control sequences where the two SWS epochs, SWS_n and SWS_{n+1}, are interrupted by a single Wake epoch. Calcium activity ± SEM is indicated for thirds of the epochs. **c**. Mean ± SEM activity in epoch sequences containing two succeeding SWS epochs (SWS_n SWS_{n+1}) epochs that are either interrupted by a REM sleep epoch (black bars) or a Wake epoch (empty bars). Activity levels for the first third of the respective epochs are indicated (normalized by subtracting the level during the prior wake epoch). ** $P < 0.01$, * $P < 0.05$, for pairwise comparisons between conditions). Note, REM sleep intervening between the SWS epochs induces a persisting down-regulation of Pyr cell activity. This finding was confirmed in control analyses accounting for differences in the duration of intervening REM and Wake epochs (Supplementary Fig. 2).

Supplementary Figures
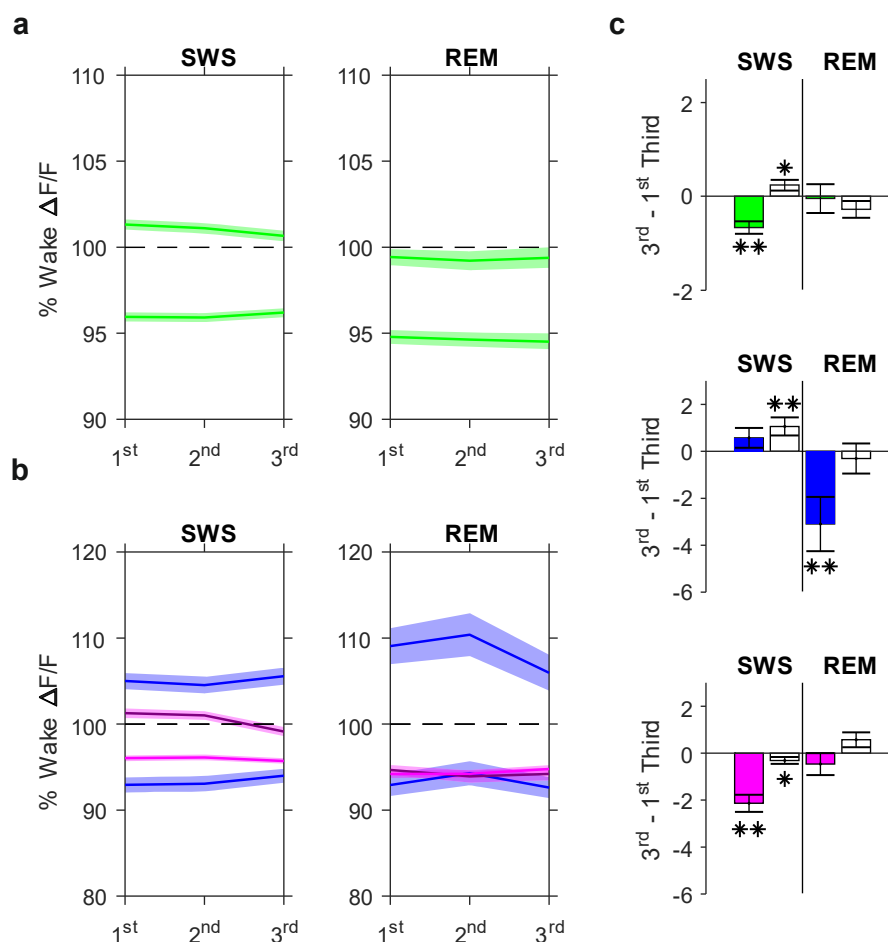
Supplementary Figure 1: Pyr cells showing generally high activity during wakefulness reduce their activity during SWS.

a, Mean ± SEM wake-normalized ΔF/F calcium signals of wake-active (upper lines) and wake-inactive (lower lines) Pyr cells (green) during thirds of SWS (n: Pyr 255, PV-In 132, SOM-In 123) and REM sleep epochs (n: Pyr 145, PV-In 71, SOM-In 74). Significant changes from first to last third of SWS and REM epochs are indicated by asterisks (** $P < 0.01$; * $P < 0.05$). **b**, As in a, but for wake-active PV-In (upper lines, blue) and SOM-In (pink) and wake-inactive PV-In and SOM-In (lower blue and pink lines, respectively). **c**, Mean difference (± SEM) in activity of wake-active (filled bars) and wake-inactive (empty bars) Pyr, PV-In and SOM-In from first to last third (3rd - 1st Third) of SWS (left) and REM sleep (right) epochs (** $P < 0.01$; * $P < 0.05$). Wake-active Pyr include the top 20 % Pyr with the highest average calcium activity across *all* wake episodes.
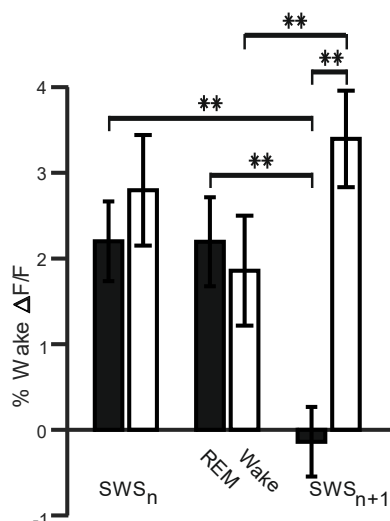
Supplementary Figure 2: **REM sleep down-regulates activity of spindle-active Pyr cells.**

This figure extends Fig. 5c of the main text comparing calcium activity in sequences of sleep epochs comprising two succeeding SWS epochs that are either interrupted by a REM sleep epoch or a single wake epoch. Note, in the SWS-REM-SWS sequences the REM sleep epoch is typically followed by a more or less extended wake epoch, because mice very rarely directly shift from REM sleep into SWS. Moreover, the total duration of the intervening interval between the succeeding SWS epochs differed for the SWS-REM-SWS and SWS-Wake-SWS sequences (18.49 ± 1.96 vs 9.91 ± 0.91 min, $P < 0.001$). To account for these possible confounds, in a further control analysis only SWS-Wake-SWS sequences with similar durations as the intervening REM sleep epoch were included (1.34 ± 0.08 vs 1.35 ± 0.01 min, n = 117 vs n = 76). The figure shows mean $\pm$ SEM activity in the beginning, i.e., during the first third of the respective epoch for the SWS-REM-SWS sequence (black bars) and the SWS-Wake-SWS sequence (empty bars). Activity levels are normalized by subtracting the level during the prior wake epoch. ** $P < 0.01$, * $P < 0.05$, for pairwise comparisons between conditions. Note, results confirm that REM sleep intervening between the SWS epochs induces a persisting down-regulation of Pyr cell activity.

3   Conclusions and general discussion

The present work examined the calcium activity of cortical circuits during sleep to gain insight into how sleep affects neuronal plasticity. The fact that sleep architecture is defined by changes in the prevalent brain rhythms fits nicely with findings of study I that interneurons display very specific activity patterns during the different sleep stages. This study is the first investigating calcium activity levels of SOM-In and PV-In during sleep and it revealed changes of the E/I balance during REM sleep, which might be associated with the pruning observed on apical dendrites during REM sleep (Li et al., 2017). Surprisingly this study also showed that during REM sleep the excitatory activity is reduced across the entire imaging area of the dorsal cortex. Previous work has suggested REM sleep as an active state with cortical activity levels comparable to wakefulness. One potential explanation for this discrepancy might be the employed techniques. While former studies used cell-unspecific techniques, we were the first to record calcium activity separately from excitatory pyramidal cells as well as inhibitory PV-In and SOM-In to overcome this important disadvantage of electrophysiological recordings. Electrophysiological studies have an increased risk of only considering particularly active cells, since rarely active cells are very difficult to detect. PV-In belong to the most active cells and therefore electrophysiological studies likely overestimate average global firing rates. We also performed additional wide field experiments showing similar overall activity reduction during REM sleep in deeper cortical layers to make our results more comparable with those of other experiments.

Study II focused on the investigation of local calcium activity changes during SWS specific oscillatory events. We showed that calcium influx into excitatory pyramidal cells is threefold higher during spindles occurring in the upstate of SOs than during solitary spindles or solitary SOs likely facilitating synaptic potentiation during such co-occurring events. This fits well with findings from behavioral experiments showing strong correlations between SO-spindle coupling and memory performance after sleep (Helfrich et al., 2017). In addition, we found that SOs, regardless of whether they occurred alone or coupled with a spindle, are associated with an increase in SOM-In activity prior to their downstate. A recent study nicely complements this result by selectively manipulating the activity of SOM-In for the induction of slow oscillations (Funk et al., 2017). Our finding that spindles are always accompanied by increased PV-In activity and a simultaneous

reduction of SOM-In activity suggests that the resulting low dendritic inhibition opens a time window for enhanced dendritic plasticity. This hypothesis is supported by findings that dendritic calcium is increased during spindles without necessarily reaching the cell's soma (Seibt et al., 2017). We showed that especially when spindles co-occur with SOs the increased calcium influx into pyramidal cells together with the reduced dendritic inhibition might serve as a key mechanism for synaptic plasticity during sleep.

In study III we directly addressed the question whether both synaptic downscaling and upscaling processes can be observed simultaneously during sleep and how this is related to sleep-specific oscillations. First, we showed that SWS and REM sleep are both characterized by an overall reduction in pyramidal cell activity accompanied by a diversification of the network's activity, i.e. an increase in variability. This supports the idea of opposing synaptic scaling dynamics during sleep. Based on the results of study II we then investigated whether those cells that are activated during sleep spindles also show changes in their excitability. Indeed, we found that spindle-active cells increased their activity, while spindle-inactive cells decreased their activity during SWS. Complementary analyses in which cells were clustered based on their activity during the SO upstate and the mean activity during wakefulness showed that the increase in activity over the course of SWS was specific for spindle-active cells. Our hypothesis that these cells also show a relative increase in activity over the course of REM sleep was not confirmed. Instead, we found that spindle-active cells decreased their activity during REM sleep while spindle-inactive cells increased their activity. The decrease in activity of spindle active cells as well as the decrease of the average activity across all cells during REM sleep correlated with the duration of REM sleep epochs.

3.1 Sleep stages and synaptic plasticity

Although, the observed global synaptic downregulation speaks primarily to a general homeostatic regulatory function of sleep, it is unlikely to suffice as an explanation for the active contribution of sleep to memory consolidation, as this requires an intricate balance between a specific downregulation of some synaptic connections and sparing of downregulation (Tononi and Cirelli, 2014) or upregulation of yet other synaptic connections (Niethard and Born, 2019). Indeed, it has been shown that synaptic rescaling during sleep

is not restrained to the reduction of synaptic connectivity but includes also the augmentation of synaptic connections (for review see Raven et al., 2018).

Additionally, those two opposing dynamics during sleep seem to be differently regulated by SWS and REM sleep (Niethard et al., 2017). Several studies have shown that cortical and hippocampal activity is mainly reduced during REM sleep (Grosmark et al., 2012; Watson et al., 2016). Study I also showed that the synaptic scaling processes during sleep are diverse and not only dependent on the specific sleep stage but also on the cell type of interest. We found that REM sleep is characterized by a relatively high cortical inhibition through PV-In, which is in turn accompanied by increased postsynaptic GABA levels and it was shown that postsynaptic GABA can induce spine shrinkage within one to two hours (Hayama et al., 2013) – a time scale that corresponds well to durations of typical sleep epochs. Therefore, REM sleep-dependent-GABA release could be one of the reasons for the synaptic pruning observed during REM sleep. However, the mechanism how selective cells and their synapses can be protected from pruning or even undergo a strengthening is still elusive. Importantly, recent evidence suggests that in 30 % of REM sleep to SWS transitions the hippocampus enters REM sleep before cortical areas (Durán et al., 2018; Emrick et al., 2016) making it impossible to draw a precise temporal line between those two brain states. Therefore, sleep stages cannot be regarded as uniform phenomena throughout the whole brain.

Also, the findings from study III point towards a major role of REM sleep in reducing synaptic strength and a select sleep spindle dependent increase of synaptic strength during SWS. However, within the same cell both synaptic strengthening and weakening can occur during SWS and REM sleep, probably depending on synapse size (de Vivo et al., 2017) and AMPA receptor densities (Diering et al., 2017). Therefore, it is unlikely that the synaptic turnover in one cell is uniform during sleep, but rather that opposing dynamics can take place in the same cell. In fact, the morphology of excitatory cortical neurons and their widespread dendritic trees suggest dendritic branches as a computational element mediating between synaptic and cellular plasticity. Anatomical and functional clustering of synaptic inputs on those branches has far-reaching consequences for signal processing within the cell (Moore et al., 2017) and branch-specific changes in dendritic excitability primes neighboring synapses for synaptic potentiation allowing the compart-

mentalization of a neuron's information storage (Kastellakis et al., 2015). Therefore, beside the assumption that changes in synaptic strength encode memories, this suggests synaptic clusters as the major cellular compartment where information could be stored. A remaining question is what features determine which circuits should undergo synaptic strengthening to consolidate memories. One potential mechanism for this could be the reactivation of memory traces during sleep, more precisely the specific reactivation of select cell ensembles during a certain oscillatory phase of the network.

3.2   Sleep oscillations and synaptic plasticity

As already mentioned, reactivation is a well-described and replicable phenomenon facilitating memory consolidation during sleep. However, the timing of reactivation is pivotal to determine whether the reactivated circuits undergo strengthening or weakening. Oscillations are a crucial factor for mediating activity timing within a neural network, guiding communication between cells and inducing synaptic plasticity. As mentioned before several characteristic oscillations can be observed during sleep. They are comprised of a variety of frequencies ranging from low to high frequency bands, each providing unique time windows for synaptic plasticity and the consolidation of memories during sleep (Puentes-Mestril et al., 2019). Based on those findings Study II and study III investigated the impact of sleep-specific oscillations on cortical circuit activity.

Recent studies on memory consolidation during sleep have revealed that the local distribution of SOs predicts memory improvements after sleep (Heib et al., 2013; Tamaki et al., 2013). Their causal role for memory consolidation during sleep is further supported by studies showing better memory performance after applying non-invasive brain stimulation to induce SOs (Ngo et al., 2013b; Perrault et al., 2019). The results from study II showed that SOs are accompanied by a distinct modulation of SOM-In. Interestingly, the transition to the SO downstate was the only time point that was characterized by increased dendritic inhibition through SOM-In. This constellation is very powerful in blocking dendritic calcium spikes and their propagation to the cell's soma and therefore also the formation of new synapses. Indeed recent research showed that stimulating SOM-In cells during learning reduces spine formation and memory performance (Chen et al., 2015). In Study III we showed that the cell reactivation during the SO upstate leads to a significant

reduction of pyramidal cell activity during subsequent REM sleep. These findings are supported by a recent study showing that cells that are activated during the upstate of SOs are more likely to show synaptic depression while their activation during the downstates leads to synaptic potentiation (González-Rueda et al., 2018). In summary, it appears that the precise time point/phase during which the previously encoded memory is re-activated within the SO determines its fate.

Sleep spindles have been shown to occur more frequently in areas active during encoding and their density correlates with memory consolidation (Cox et al., 2014). As described before, the induction of synaptic potentiation or depotentiation is dependent on intra-cellular calcium concentrations and during sleep spindles apical dendrites show increased local calcium influx in mice (Seibt et al., 2017). This together with the finding of branch-specific spine formation during SWS (Yang et al., 2014) indicates that spindles mediate the plasticity of synaptic clusters through localized dendritic calcium influx. Our data from study III fit nicely with the idea that reactivation during sleep spindles induces synaptic potentiation because only spindle active cells but not SO active cells underwent an upscaling of their activity over the course of the respective SWS epoch.

Importantly, the before mentioned positive effect of induced SOs on memory consolidation is accompanied by an increased number of SO-coupled spindles (Ngo et al., 2013b, 2013a) and it is known that sleep spindles tend to nest in the upstate of SOs (Cox et al., 2018; Klinzing et al., 2016; Mölle et al., 2006; Staresina et al., 2015). In line with this, it was speculated that the beneficial effect on memory performance is mainly due to the increase in SO-spindle coupling rather than SO density alone (Ngo et al., 2013b). Study II indeed showed that the calcium influx in cortical pyramidal cells is more than threefold higher during spindles nesting in the upstate of SOs compared to solitary spindles or solitary SOs suggesting that this constellation provides optimal conditions for inducing synaptic plasticity. Therefore, the timing between SOs and spindles appears as a key mechanism for synaptic plasticity and memory consolidation during sleep.

The temporal relation between spindles and SOs is of special interest because also hippocampal ripples (high frequency oscillations in the range of 100 - 300 Hz) tend to occur time-locked to the negative trough of spindles. In rats the encoding of an object-place recognition task results in higher coupling between cortical SOs, spindles and hippocampal ripples during the following SWS episode (Maingret et al., 2016). Importantly the

beneficial effect of ripples on memory consolidation during sleep does not appear to stem from potentiation of hippocampal synapses because the blockade of hippocampal ripples prevents their downregulation (Norimoto et al., 2018). Instead, hippocampal ripples seem to facilitate stronger cortical representations. Our results support this view. First, the reduced dendritic inhibition during spindles increases the impact of excitatory inputs onto dendrites. Second, the increased excitatory cortical activity during spindles nesting in the SO upstate could be the result of the excitation through increased hippocampal inputs during ripple activity. It makes sense that blocking ripples also suppresses the hippocampal cortical input, which induces the actual strengthening of the cortical memory representation. Indeed, replay of place cells that previously were activated during the encoding of a spatial environment is known to occur during hippocampal ripples (Chen and Wilson, 2017)) and blocking ripples during sleep results in impaired memory performance (Ego-Stengel and Wilson, 2010; Girardeau and Zugaro, 2011; Norimoto et al., 2018). This together with their high frequency turns hippocampal ripples into a good candidate for the oscillatory mechanism that synchronizes the reactivation of memory relevant hippocampal and cortical circuits. Altogether, during SWS the co-occurrence of SOs, spindles and ripples orchestrates a hippocampal - cortical loop that times hippocampal and cortical memory reactivations. The unique constellation of cortical excitation and inhibition during those oscillations seems to play a major role in opening a time window for synaptic plasticity on apical dendrites in cortical pyramidal cells to facilitate cortical memory representations and their uncoupling might explain memory impairments during aging (Helfrich et al., 2017; Muehlroth et al., 2019).

The dominating EEG-rhythm during REM sleep is theta activity. In humans, the theta power during REM sleep correlates with better memory in emotional memories (Hutchison and Rathore, 2015; Nishida et al., 2009). Also in animals, REM theta activity is important for the consolidation of cued fear memories and object-place recognition tasks (Boyce et al., 2016). Furthermore, optogenetic stimulation of hippocampal theta activity through PV-In can compensate the negative effects of sleep deprivation on the consolidation of fear memories (Ognjanovski et al., 2018). Those results together with our findings from study I suggests that PV-In activity is essential for synaptic plasticity during REM sleep. Interestingly, hippocampal place cells that encode a location in a novel environment tend to reactivate during the peak of REM theta, but once the environment becomes familiar, they change their reactivation time point to the REM theta trough (Poe

et al., 2000). This indicates that the novelty of the engram affects the precise phasing properties of the reactivation of the involved cells during REM sleep.

Together, these findings suggest an important role of oscillatory events during SWS and REM sleep for the coordinated reactivation of memory engrams during sleep. The order in which SWS always occurs before REM sleep may be due to the fact that SWS must first perform a basic memory stabilization before the permanent reduction of dendritic inhibition can occur during REM sleep without compromising memory content. Although this already explains some of the underlying mechanisms, it seems unlikely that the timing windows provided by specific oscillatory events alone orchestrate the complex process of determining which cells need to be strengthened, maintained or removed.

3.3 E/I balance and disease

While the present work focused on providing insights into basic research questions, the findings can be related to several pathological phenomena. Diseases such as schizophrenia, autism, epilepsy or Alzheimer's disease (AD) all share alterations of sleep and E/I balance as common features. In the following, potential implications for AD are briefly highlighted.

Since decades, AD has been under intensive investigation by researchers and clinicians. Emerging evidence points towards a major role of an altered cortical E/I balance in patients with AD (Frere and Slutsky, 2018; Palop and Mucke, 2016; Palop et al., 2006). Especially the loss and malfunction of SOM-In is a well-known phenomenon in AD mice models (Moreno-Gonzalez et al., 2009; Ramos et al., 2006). Even though there is a study using two-photon imaging in mice showing that the number of hippocampal SOM-In was similar in an AD model compared with wild type mice this study also showed that SOM-In undergo dramatic morphological changes, including the loss of entire axons (Schmid et al., 2016). Additionally, in human tissue it was shown that in tissue from AD patients the number of PV-In is reduced (Takahashi et al., 2010) further underlining the AD related changes of inhibitory cells.

Beside the altered morphology of inhibitory neurons, disrupted sleep is a risk factor for developing AD and AD patients' sleep architecture has been shown to change even before

clinical symptoms are present (Ju et al., 2014; Roh et al., 2014). In AD mice models, increased periods of wakefulness and decreased sleep duration accompanies the beginning of amyloid plaque accumulation in the hippocampus and a strongly disrupted sleep pattern can be observed once plaques become widespread (Roh et al., 2012). Therefore, positive feedback loops between amyloid plaques, sleep and AD exist and it appears that it is rather the reoccurring sequence of sleep loss and amyloid plaque accumulation causing the manifestation of AD than disrupted sleep or the accumulation of plaques alone. Especially, the finding that spindle duration, count and density correlate negatively with extracellular markers of AD (Kam et al., 2019) suggests a role of PV-In in AD related changes of sleep. The present work supports this view and repeating study II in an AD mouse model would provide insights in how the cortical circuit activity in AD is altered during sleep.

Furthermore, AD is also associated with an impaired neurogenesis and the adult neurogenesis within the dentate gyrus is closely linked to GABAergic inputs (Kempermann et al., 2015; Ming and Song, 2011; De Toni et al., 2008). Experiments using transgenic mice expressing an APOE ε4gene as a model for AD disease showed that the gene expression not only causes a reduction of GABAergic cells and synapses but also a reduced maturation of adult born granule cells (Li et al., 2009). Therefore, the specific regulation of cortical inhibition during sleep might play an important role for neurogenesis. Especially the relatively high inhibition during REM sleep found in study I suggests REM sleep as a regulator of adult neurogenesis via increased GABAergic inputs from PV-In. Future work that records the activity of PV-In in the dentate gyrus during REM sleep in both wild type and AD model mice would clarify whether and how sleep might affect neurogenesis in health and disease.

Another factor that points towards a major role of an altered inhibitory cell function in AD is the finding that AD patients also have an increased risk for developing epilepsy, which is known to be accompanied by enhanced synaptic excitation (Pandis and Scarmeas, 2012; Stief et al., 2007). Interestingly epileptic patients almost never show seizures during REM sleep and study I suggests that this is due to the increased cortical inhibition through PV-In. This hypothesis is further supported by a study showing that epileptic seizures can be induced by silencing PV-In (Drexel et al., 2017).

These and our findings together suggest an altered E/I balance during sleep as a potential factor of AD. However, future studies are needed to investigate whether and how this could provide a potential treatment.

3.4 Future directions

The research of inhibitory circuits during sleep is still in its infancy. However, our results showed that both SWS and REM sleep are characterized by distinct changes of excitation and inhibition. These results, together with the new methods available, will enable the investigation of the specific underlying mechanisms and the resulting morphological changes.

First, in the present work we investigated the calcium activity of the two major inhibitory cell types. However, cortical circuits include several other inhibitory cell types and it is very likely that they not only affect overall excitatory activity but also mediate activity between PV-In and SOM-In. Another cell type that is a good candidate for mediating between inhibitory and excitatory cell activity are astrocytes. However, their interaction with neurons is still poorly understood. Newly available genetic vectors and transgenic mouse lines will allow to reliably image their calcium activity during sleep. So far, evidence already shows that they are crucially involved in neuronal plasticity and memory formation (Haydon and Nedergaard, 2015; De Pittà et al., 2016).

Second, the used microscope allowed a sampling of the calcium signal with acquisition rates up to 6 Hz. Modern resonant scanning systems will allow to dramatically increase the temporal resolution or to image an entire three dimensional cortical column (0.5 mm x 0.5 mm x 0.5 mm) instead of a two dimensional plane (Prevedel et al., 2016). This, together with newly available fluorescent calcium indicators, makes it possible to analyze calcium activity of distinct cell types even for single oscillatory cycles of spindles during SWS and theta activity during REM sleep within entire cortical columns.

Third, all our studies only recorded spontaneous activity of different cell types. Therefore, we cannot draw any causal relations between sleep specific phenomena such as oscillations and the activity of certain cell types. Based on our results the selective manipulation of SOM-In during sleep could be used to directly proof their influence on synaptic plasticity during sleep.

Lastly, even though we complemented our two-photon data with wide field calcium imaging of almost the entire dorsal surface of the brain we were not able to investigate the activity of subcortical structures such as the hippocampus and the thalamus. Future studies combining memory tasks with subcortical electrophysiological recordings and cortical calcium imaging will allow untangling temporal relationships between the different areas, which is needed to investigate whether and how the reactivation of a memory representation finally leads to a stable cortical representation.

3.5   Concluding remarks

In our work, we showed that sleep is characterized by unique calcium activity changes of excitatory and inhibitory circuits and that those changes of the E/I balance are essential for our brains to remain plastic. This together with the current state of research suggests sleep as an active state, which allows the brain to further process information it has acquired during wakefulness and the disconnection from the outer world during sleep is most likely necessary to not interfere with this process. To get back to the beginning of this thesis, therefore instead of considering sleep as the brother of the death probably the best matching deity of roman antiquity would be Genius, the personal guardian, granting intellect and strength.

4   Reference list

Antony, J.W., Gobel, E.W., O'Hare, J.K., Reber, P.J., and Paller, K. a (2012). Cued memory reactivation during sleep influences skill learning. Nat. Neurosci. *15*, 1114–1116.

Aserinsky, E., and Kleitman, N. (1953). Regularly occurring periods of eye motility, and concomitant phenomena, during sleep. Science (80-.). *118*, 273–274.

Averkin, R.G., Szemenyei, V., Bordé, S., and Tamás, G. (2016). Identified Cellular Correlates of Neocortical Ripple and High-Gamma Oscillations during Spindles of Natural Sleep. Neuron *92*, 916–928.

Berridge, M.J., Bootman, M.D., and Lipp, P. (1998). Calcium - a life and death signal. Nature *395*, 645–648.

Binder, S., Berg, K., Gasca, F., Lafon, B., Parra, L.C., Born, J., and Marshall, L. (2014). Transcranial slow oscillation stimulation during sleep enhances memory consolidation in rats. Brain Stimul. *7*, 508–515.

Bonjean, M., Baker, T., Lemieux, M., Timofeev, I., Sejnowski, T., and Bazhenov, M. (2011). Corticothalamic feedback controls sleep spindle duration in vivo. J. Neurosci. *31*, 9124–9134.

Borbely, A.A. (1982). Two process model of sleep regulation. Hum Neurobiol *1*, 195–204.

Boyce, R., Glasgow, S.D., and Williams, S. (2016). Causal evidence for the role of REM sleep theta rhythm in contextual memory consolidation. *352*, 812–817.

Cairney, S.A., Durrant, S.J., Hulleman, J., and Lewis, P.A. (2014). Targeted memory reactivation during slow wave sleep facilitates emotional memory consolidation. Sleep *37*, 701–707.

Cantero, J.L., Atienza, M., Stickgold, R., Kahana, M.J., Madsen, J.R., and Kocsis, B. (2003). Sleep-dependent theta oscillations in the human hippocampus and neocortex. J. Neurosci. *23*, 10897–10903.

Chen, Z., and Wilson, M.A. (2017). Deciphering neural codes of memory during sleep. Trends Neurosci. *40*, 260–275.

Chen, S.X., Kim, A.N., Peters, A.J., and Komiyama, T. (2015). Subtype-specific plasticity of inhibitory circuits in motor cortex during motor learning. Nat. Neurosci. *18*, 1109–1115.

Cirelli, C., and Tononi, G. (2008). Is sleep essential? *6*, 1605–1611.

Clawson, B.C., Durkin, J., Suresh, A.K., Pickup, E.J., Broussard, C.G., and Aton, S.J. (2018). Sleep promotes, and sleep loss inhibits, selective changes in firing rate, response properties and functional connectivity of primary visual cortex neurons. Front. Syst. Neurosci *12*, 40.

Contreras, D., Steriade, M., Neurophysiologie, L. De, Medecine, F. De, and Laval, U. (1996). Spindle oscillation in cats: the role of corticothalamic feedback in a thalamically generated rhythm. J. Physiol. *490 (Pt 1*, 159–179.

Cox, R., Hofman, W.F., de Boer, M., and Talamini, L.M. (2014). Local sleep spindle

modulations in relation to specific memory cues. Neuroimage *99*, 103–110.

Cox, R., Mylonas, D.S., Manoach, D.S., and Stickgold, R. (2018). Large-scale structure and individual fingerprints of locally coupled sleep oscillations. Sleep *41*, 1–15.

Debellemaniere, E., Chambon, S., Pinaud, C., Thorey, V., Dehaene, D., Léger, D., Chennaoui, M., Arnal, P.J., and Galtier, M.N. (2018). Performance of an ambulatory dry-EEG device for auditory closed-loop stimulation of sleep slow oscillations in the home environment. Front. Hum. Neurosci. *12*, 88.

Diekelmann, S., and Born, J. (2010). The memory function of sleep. Nat Rev Neurosci *11*, 114–126.

Diering, G.H., Nirujogi, R.S., Roth, R.H., Worley, P.F., Pandey, A., and Huganir, R.L. (2017). Homer1a drives homeostatic scaling-down of excitatory synapses during sleep. Science (80-.). *355*, 511–515.

Douglas, R.J., and Martin, K. a. C. (2004). Neuronal circuits of the neocortex. Annu. Rev. Neurosci. *27*, 419–451.

Drexel, M., Romanov, R.A., Wood, J., Weger, S., Heilbronn, R., Wulff, P., Tasan, R.O., Harkany, T., and Sperk, G. (2017). Selective silencing of hippocampal parvalbumin interneurons induces development of recurrent spontaneous limbic seizures in mice. J. Neurosci. *37*, 8166–8179.

Durán, E., Oyanedel, C.N., Niethard, N., Inostroza, M., and Born, J. (2018). Sleep stage dynamics in neocortex and hippocampus. Sleep *41*, 1–11.

Durkin, J., and Aton, S.J. (2016). Sleep-dependent potentiation in the visual system Is at odds with the synaptic homeostasis hypothesis. Sleep *39*, 155–159.

Ego-Stengel, V., and Wilson, M.A. (2010). Disruption of ripple-associated hippocampal activity during rest impairs spatial learning in the rat. Hippocampus *20*, 1–10.

Emrick, J.J., Gross, B.A., Riley, B.T., and Poe, G.R. (2016). Different simultaneous sleep states in the hippocampus and neocortex. Sleep *39*, 2201–2209.

Fino, E., Packer, A.M., and Yuste, R. (2012). The logic of inhibitory connectivity in the neocortex.

Frere, S., and Slutsky, I. (2018). Alzheimer's disease: from firing instability to homeostasis network collapse. Neuron *97*, 32–58.

Funk, C.M., Peelman, K., Bellesi, M., Marshall, W., Cirelli, C., and Tononi, G. (2017). Role of somatostatin-positive cortical interneurons in the generation of sleep slow waves. J. Neurosci. *37*, 9132–9148.

Gennaro, L. De, and Ferrara, M. (2003). lJ Sleep spindles : an overview. Sleep Med. *7*, 422–440.

Genzel, L., Kroes, M.C.W., Dresler, M., and Battaglia, F.P. (2014). Light sleep versus slow wave sleep in memory consolidation: a question of global versus local processes? Trends Neurosci. *37*, 10–19.

Girardeau, G., and Zugaro, M. (2011). Hippocampal ripples and memory consolidation. Curr. Opin. Neurobiol. *21*, 452–459.

Giuditta, A., Ambrosini, M.V., Montagnese, P., Mandile, P., Cotugno, M., Zucconi, G.G., and Vescia, S. (1995). The sequential hypothesis of the function of sleep. Behav. Brain

Res. *69*, 157–166.

González-Rueda, A., Pedrosa, V., Feord, R.C., Clopath, C., and Paulsen, O. (2018). Activity-dependent downscaling of subthreshold synaptic inputs during slow-wave-sleep-like activity in vivo. Neuron *97*, 1244-1252.e5.

Grosmark, a. D., and Buzsaki, G. (2016). Diversity in neural firing dynamics supports both rigid and learned hippocampal sequences. Science (80-.). *351*, 1440–1443.

Grosmark, A.D., Mizuseki, K., Pastalkova, E., Diba, K., and Buzsáki, G. (2012). REM sleep reorganizes hippocampal excitability. Neuron *75*, 1001–1007.

Hartse, K.M. (2011). The phylogeny of sleep. Handb. Clin. Neurol. *98*, 97–109.

Hayama, T., Noguchi, J., Watanabe, S., Takahashi, N., Hayashi-Takagi, A., Ellis-Davies, G.C.R., Matsuzaki, M., and Kasai, H. (2013). GABA promotes the competitive selection of dendritic spines by controlling local Ca2+ signaling. Nat. Neurosci. *16*, 1409–1416.

Haydon, P.G., and Nedergaard, M. (2015). How do astrocytes participate in neural plasticity? Cold Spring Harb. Perspect. Biol. *7*, a020438.

Heib, D.P.J., Hoedlmoser, K., Anderer, P., Zeitlhofer, J., Gruber, G., Klimesch, W., and Schabus, M. (2013). Slow oscillation amplitudes and up-state lengths relate to memory improvement. PLoS One *8*, e82049.

Helfrich, R.F., Mander, B.A., Jagust, W.J., Knight, R.T., and Walker, M.P. (2017). Old brains come uncoupled in sleep: slow wave-spindle synchrony, brain atrophy, and forgetting. Neuron 1–10.

Hengen, K.B., Torrado Pacheco, A., McGregor, J.N., Van Hooser, S.D., and Turrigiano, G.G. (2016). Neuronal firing rate homeostasis is inhibited by sleep and promoted by wake. Cell *165*, 180–191.

Hensch, T.K. (2005). Critical period plasticity in local cortical circuits. Nat. Rev. Neurosci. *6*, 877–888.

Higley, M.J. (2006). Balanced excitation and inhibition determine spike timing during frequency adaptation. J. Neurosci. *26*, 448–457.

Huber, R., Hill, S.L., Holladay, C., Biesiadecki, M., Tononi, G., and Cirelli, C. (2004). Sleep homeostasis in drosophila melanogaster. Sleep *27*, 628–639.

Hutchison, I.C., and Rathore, S. (2015). The role of REM sleep theta activity in emotional memory. Front. Psychol. *6*, 1439.

Isaacson, J.S., and Scanziani, M. (2011). How inhibition shapes cortical activity. Neuron *72*, 231–243.

Ju, Y.S., Brendan, P., and Holtzman, D.M. (2014). Sleep and Alzheimer disease pathology —a bidirectional relationship.

Kales, A., and Rechtschaffen, A. (1968). A manual of standardized terminology, techniques and scoring system for Sleep Stages of Human Subjects: Allan Rechtschaffen and Anthony Kales, Editors (Bethesda, Md., U. S. National Institute of Neurological Diseases and Blindness, Neurological Information Network, 1968.).

Kam, K., Parekh, A., Sharma, R.A., Andrade, A., Lewin, M., Castillo, B., Bubu, O.M., Chua, N.J., Miller, M.D., Mullins, A.E., et al. (2019). Sleep oscillation-specific associations with Alzheimer's disease CSF biomarkers: novel roles for sleep spindles and

tau. Mol. Neurodegener. *14*, 10.

Kastellakis, G., Cai, D.J., Mednick, S.C., Silva, A.J., and Poirazi, P. (2015). Synaptic clustering within dendrites: an emerging theory of memory formation. Prog. Neurobiol. *126*, 19–35.

Kawamoto, E.M., Vivar, C., and Camandola, S. (2012). Physiology and pathology of calcium signaling in the brain. *3*, 1–17.

Kempermann, G., Song, H., and Gage, F.H. (2015). Neurogenesis in the adult hippocampus. Cold Spring Harb. Perspect. Biol. *7*, a018812.

Klinzing, J.G., Mölle, M., Weber, F., Supp, G., Hipp, J.F., Engel, A.K., and Born, J. (2016). Spindle activity phase-locked to sleep slow oscillations. Neuroimage *134*, 607–616.

Kubota, Y., Karube, F., Nomura, M., and Kawaguchi, Y. (2016). The diversity of cortical inhibitory synapses. Front. Neural Circuits *10*, 1–15.

Laughlin, S.B., and Sejnowski, T.J. (2003). Communication in neuronal networks. Science *301*, 1870–1874.

Lemieux, M., Chen, J.-Y., Lonjers, P., Bazhenov, M., and Timofeev, I. (2014). The impact of cortical deafferentation on the neocortical slow oscillation. J. Neurosci. *34*, 5689–5703.

Levelt, C.N., and Hübener, M. (2012). Critical-period plasticity in the visual cortex. Annu Rev Neurosci *35*, 309–330.

Li, G., Bien-Ly, N., Andrews-Zwilling, Y., Xu, Q., Bernardo, A., Ring, K., Halabisky, B., Deng, C., Mahley, R.W., and Huang, Y. (2009). GABAergic interneuron dysfunction impairs hippocampal neurogenesis in adult apolipoprotein E4 knockin mice. Cell Stem Cell *5*, 634–645.

Li, W., Ma, L., Yang, G., and Gan, W.-B. (2017). REM sleep selectively prunes and maintains new synapses in development and learning. Nat. Neurosci. 1–16.

Liguz-Lecznar, M., Urban-Ciecko, J., and Kossut, M. (2016). Somatostatin and somatostatin-containing neurons in shaping neuronal activity and plasticity. Front. Neural Circuits *10*, 48.

Lohmann, C., and Wong, R.O.L. (2005). Regulation of dendritic growth and plasticity by local and global calcium dynamics. Cell Calcium *37*, 403–409.

Lovett-Barron, M., Turi, G.F., Kaifosh, P., Lee, P.H., Bolze, F., Sun, X.-H., Nicoud, J.-F., Zemelman, B. V, Sternson, S.M., and Losonczy, A. (2012). Regulation of neuronal input transformations by tunable dendritic inhibition. Nat. Neurosci. *15*, 423–430.

Lovett-Barron, M., Kaifosh, P., Kheirbek, M., Danielson, N., Zaremba, J., Reardon, T., Turi, G., Hen, R., Zemelman, B., and Losonczy, A. (2014). Dendritic inhibition in the hippocampus supports fear learning. Science (80-.). *343*, 857–863.

Luczak, A., Barthó, P., Marguet, S.L., Buzsáki, G., and Harris, K.D. (2007). Sequential structure of neocortical spontaneous activity in vivo. Proc. Natl. Acad. Sci. U. S. A. *104*, 347–352.

Lüthi, A. (2013). Sleep spindles: where they come from, what they do. Neuroscientist *20*, 243–256.

Maingret, N., Girardeau, G., Todorova, R., Goutierre, M., and Zugaro, M. (2016). Hippocampo-cortical coupling mediates memory consolidation during sleep. Nat. Neurosci. *19*, 959–964.

Markram, H., Toledo-Rodriguez, M., Wang, Y., Gupta, A., Silberberg, G., and Wu, C. (2004). Interneurons of the neocortical inhibitory system. Nat. Rev. Neurosci. *5*, 793–807.

Marshall, L., Helgadóttir, H., Mölle, M., and Born, J. (2006). Boosting slow oscillations during sleep potentiates memory. Nature *444*, 610–613.

Massimini, M. (2004). The sleep slow oscillation as a traveling wave. J. Neurosci. *24*, 6862–6870.

Michaelsen, K., and Lohmann, C. (2010). Calcium dynamics at developing synapses: mechanisms and functions. Eur. J. Neurosci. *32*, 218–223.

Ming, G., and Song, H. (2011). Adult neurogenesis in the mammalian brain: significant answers and significant questions. Neuron *70*, 687–702.

Miyawaki, H., and Diba, K. (2016). Regulation of hippocampal firing by network oscillations during sleep. Curr. Biol. *26*, 893–902.

Mölle, M., Marshall, L., Gais, S., and Born, J. (2002). Grouping of spindle activity during slow oscillations in human non-rapid eye movement sleep. J. Neurosci. *22*, 10941–10947.

Mölle, M., Yeshenko, O., Marshall, L., Sara, S.J., and Born, J. (2006). Hippocampal sharp wave-ripples Linked to slow oscillations in rat slow-wave sleep. J. Neurophysiol. *96*, 62–70.

Moore, J.J., Ravassard, P.M., Ho, D., Acharya, L., Kees, A.L., Vuong, C., and Mehta, M.R. (2017). Dynamics of cortical dendritic membrane potential and spikes in freely behaving rats. Science. *355*, eaaj1497.

Moreno-Gonzalez, I., Baglietto-Vargas, D., Sanchez-Varo, R., Jimenez, S., Trujillo-Estrada, L., Sanchez-Mejias, E., del Rio, J.C., Torres, M., Romero-Acebal, M., Ruano, D., et al. (2009). Extracellular amyloid-β and cytotoxic glial activation induce significant entorhinal neuron loss in young PS1M146L/APP751SL mice. J. Alzheimer's Dis. *18*, 755–776.

Muehlroth, B.E., Sander, M.C., Fandakova, Y., Grandy, T.H., Rasch, B., Shing, Y.L., and Werkle-Bergner, M. (2019). Precise slow oscillation–spindle coupling promotes memory consolidation in younger and older adults. Sci. Rep. *9*, 1940.

Né Dicte Amilhon, B., Huh, C.Y.L., Dé, F., Manseau, R., Ducharme, G., Nichol, H., Adamantidis, A., and Williams, S. (2015). Parvalbumin interneurons of hippocampus tune population activity at theta frequency. Neuron *86*, 1277–1289.

Ngo, H.V. V, Claussen, J.C., Born, J., and Mölle, M. (2013a). Induction of slow oscillations by rhythmic acoustic stimulation. J. Sleep Res. *22*, 22–31.

Ngo, H.V. V, Martinetz, T., Born, J., and Mölle, M. (2013b). Auditory closed-loop stimulation of the sleep slow oscillation enhances memory. Neuron *78*, 545–553.

Niethard, N., and Born, J. (2019). Back to baseline: sleep recalibrates synapses. Nat. Neurosci. 1.

Niethard, N., Hasegawa, M., Itokazu, T., Oyanedel, C.N., Born, J., and Sato, T.R. (2016).

Sleep-stage-specific regulation of cortical excitation and inhibition. Curr. Biol. *26*, 2739–2749.

Niethard, N., Burgalossi, A., and Born, J. (2017). Plasticity during sleep is linked to specific regulation of cortical circuit activity. Front. Neural Circuits *11*, 1–9.

Niethard, N., Ngo, H.-V. V, Ehrlich, I., and Born, J. (2018). Cortical circuit activity underlying sleep slow oscillations and spindles. Proc. Natl. Acad. Sci. U. S. A. *115*, E9220–E9229.

Nishida, M., Pearsall, J., Buckner, R.L., and Walker, M.P. (2009). REM sleep, prefrontal theta, and the consolidation of human emotional memory. Cereb. Cortex *19*, 1158–1166.

Norimoto, H., Makino, K., Gao, M., Shikano, Y., Okamoto, K., Ishikawa, T., Sasaki, T., Hioki, H., Fujisawa, S., and Ikegaya, Y. (2018). Hippocampal ripples downregulate synapses. Science. *0702*, 1–9.

Ognjanovski, N., Schaeffer, S., Wu, J., Mofakham, S., Maruyama, D., Zochowski, M., and Aton, S. (2017). Parvalbumin-expressing interneurons coordinate hippocampal network dynamics required for memory consolidation. Nat. Commun. *In Press*, 1–13.

Ognjanovski, N., Broussard, C., Zochowski, M., and Aton, S.J. (2018). Hippocampal network oscillations rescue memory consolidation deficits caused by sleep loss. Cereb. Cortex *28*, 3711–3723.

Oudiette, D., and Paller, K.A. (2013). Upgrading the sleeping brain with targeted memory reactivation. Trends Cogn. Sci. *17*, 142–149.

Palop, J.J., and Mucke, L. (2016). Network abnormalities and interneuron dysfunction in Alzheimer disease. Nat. Rev. Neurosci. *17*, 777–792.

Palop, J.J., Chin, J., and Mucke, L. (2006). A network dysfunction perspective on neurodegenerative diseases. Nature *443*, 768–773.

Pandis, D., and Scarmeas, N. (2012). Seizures in alzheimer disease: clinical and epidemiological data. Epilepsy Curr. *12*, 184–187.

Perrault, A.A., Khani, A., Quairiaux, C., Kompotis, K., Franken, P., Muhlethaler, M., Schwartz, S., and Bayer, L. (2019). Whole-night ontinuous rocking entrains spontaneous neural oscillations with benefits for sleep and memory. Curr. Biol. *29*, 402-411.e3.

Peyrache, A., Battaglia, F.P., and Destexhe, A. (2011). Inhibition recruitment in prefrontal cortex during sleep spindles and gating of hippocampal inputs. Proc. Natl. Acad. Sci. U. S. A. *108*, 17207–17212.

Piantoni, G., Astill, R.G., Raymann, R.J.E.M., Vis, J.C., Coppens, J.E., and Van Someren, E.J.W. (2013). Modulation of gamma and spindle-range power by slow oscillations in scalp sleep EEG of children. Int. J. Psychophysiol. *89*, 252–258.

De Pittà, M., Brunel, N., and Volterra, A. (2016). Astrocytes: Orchestrating synaptic plasticity? Neuroscience *323*, 43–61.

Poe, G.R. (2017). Sleep is for forgetting. J. Neurosci. *37*, 464 LP – 473.

Poe, G.R., Nitz, D.A., McNaughton, B.L., and Barnes, C.A. (2000). Experience-dependent phase-reversal of hippocampal neuron firing during REM sleep. Brain Res. *855*, 176–180.

Prevedel, R., Verhoef, A.J., Pernía-Andrade, A.J., Weisenburger, S., Huang, B.S.,

Nöbauer, T., Fernández, A., Delcour, J.E., Golshani, P., Baltuska, A., et al. (2016). Fast volumetric calcium imaging across multiple cortical layers using sculpted light. Nat. Methods *13*, 1021–1028.

Puentes-Mestril, C., Roach, J., Niethard, N., Zochowski, M., and Aton, S.J. (2019). How rhythms of the sleeping brain tune memory and synaptic plasticity. Sleep.

Raizen, D.M., Zimmerman, J.E., Maycock, M.H., Ta, U.D., You, Y., Sundaram, M. V., and Pack, A.I. (2008). Lethargus is a Caenorhabditis elegans sleep-like state. Nature *451*, 569–572.

Ramos, B., Baglietto-Vargas, D., Rio, J.C. del, Moreno-Gonzalez, I., Santa-Maria, C., Jimenez, S., Caballero, C., Lopez-Tellez, J.F., Khan, Z.U., Ruano, D., et al. (2006). Early neuropathology of somatostatin/NPY GABAergic cells in the hippocampus of a PS1 × APP transgenic model of Alzheimer's disease. Neurobiol. Aging *27*, 1658–1672.

Rasch, B., and Born, J. (2013). About sleep's role in memory. Physiol. Rev. *93*, 681–766.

Rasch, B., Büchel, C., Gais, S., and Born, J. (2007). Odor cues during slow-wave sleep prompt declarative memory consolidation. Science *315*, 1426–1429.

Raven, F., Van der Zee, E.A., Meerlo, P., and Havekes, R. (2018). The role of sleep in regulating structural plasticity and synaptic strength: Implications for memory and cognitive function. Sleep Med. Rev. *39*, 3–11.

Roh, J.H., Huang, Y., Bero, A.W., Kasten, T., Stewart, F.R., Bateman, R.J., and Holtzman, D.M. (2012). Disruption of the sleep-wake cycle and diurnal fluctuation of -amyloid in mice with alzheimer's disease pathology. Sci. Transl. Med. *4*, 150ra122-150ra122.

Roh, J.H., Jiang, H., Finn, M.B., Stewart, F.R., Mahan, T.E., Cirrito, J.R., Heda, A., Snider, B.J., Li, M., Yanagisawa, M., et al. (2014). Potential role of orexin and sleep modulation in the pathogenesis of Alzheimer's disease. J. Exp. Med. *211*, 2487–2496.

Royer, S.E.B., Zemelman, B. V, Losonczy, A., Kim, J., Chance, F., Magee, J.C., and Ki, G.O.R.B.A. (2012). Control of timing, rate and bursts of hippocampal place cells by dendritic and somatic inhibition. Nat. Neurosci. *15*, 1–10.

Rudy, B., Fishell, G., Lee, S., and Hjerling-Leffler, J. (2011). Three groups of interneurons account for nearly 100% of neocortical GABAergic neurons. Dev. Neurobiol. *71*, 45–61.

Sabatini, B.L., Maravall, M., and Svoboda, K. (2001). Ca 2 + signaling in dendritic spines. 349–356.

Scheyltjens, I., and Arckens, L. (2016). The current status of somatostatin-interneurons in inhibitory control of brain function and plasticity. Neural Plast. *2016*.

Schmid, L.C., Mittag, M., Poll, S., Steffen, J., Wagner, J., Geis, H.-R., Schwarz, I., Schmidt, B., Schwarz, M.K., Remy, S., et al. (2016). Dysfunction of somatostatin-positive interneurons associated with memory deficits in an alzheimer's disease model. Neuron *92*, 114–125.

Seibt, J., Richard, C.J., Sigl-Glöckner, J., Takahashi, N., Kaplan, D.I., Doron, G., de Limoges, D., Bocklisch, C., and Larkum, M.E. (2017). Cortical dendritic activity correlates with spindle-rich oscillations during sleep in rodents. Nat. Commun. *8*, 684.

Sejnowski, T.J., and Destexhe, a (2000). Why do we sleep? Brain Res. *886*, 208–223.

Shein-Idelson, M., Ondracek, J.M., Liaw, H.-P., Reiter, S., and Laurent, G. (2016). Slow waves, sharp waves, ripples, and REM in sleeping dragons. Science *352*, 590–595.

Staresina, B.P., Ole Bergmann, T., Bonnefond, M., van der Meij, R., Jensen, O., Deuker, L., Elger, C.E., Axmacher, N., and Fell, J. (2015). Hierarchical nesting of slow oscillations, spindles and ripples in the human hippocampus during sleep. Nat. Neurosci. *18*, 1679–1686.

Steriade, M. (1995). Thalamic origin of sleep spindles: Morison and Bassett (1945). J. Neurophysiol. *73*, 921–922.

Steriade, M., McCormick, D.A., and Sejnowski, T.J. (1993). Thalamocortical oscillations in the sleeping and aroused brain. Science *262*, 679–685.

Stief, F., Zuschratter, W., Hartmann, K., Schmitz, D., and Draguhn, A. (2007). Enhanced synaptic excitation – inhibition ratio in hippocampal interneurons of rats with temporal lobe epilepsy. *25*, 519–528.

Takahashi, H., Brasnjevic, I., Rutten, B.P.F., Kolk, N. Van Der, Perl, D.P., Bouras, C., Steinbusch, H.W.M., Schmitz, C., Hof, P.R., and Dickstein, D.L. (2010). Hippocampal interneuron loss in an APP/PS1 double mutant mouse and in Alzheimer's disease. Brain Struct. Funct. *214*, 145.

Tamaki, M., Huang, T.-R., Yotsumoto, Y., Hämäläinen, M., Lin, F.-H., Náñez, J.E., Watanabe, T., and Sasaki, Y. (2013). Enhanced spontaneous oscillations in the supplementary motor area are associated with sleep-dependent offline learning of finger-tapping motor-sequence task. J. Neurosci. *33*, 13894–13902.

Timofeev, I., and Steriade, M. (1996). Low-frequency rhythms in the thalamus of intact-cortex and decorticated cats. J. Neurophysiol. *76*, 4152–4168.

De Toni, A., Zbinden, M., Epstein, J.A., Ruiz i Altaba, A., Prochiantz, A., and Caille, I. (2008). Regulation of survival in adult hippocampal and glioblastoma stem cell lineages by the homeodomain-only protein HOP. Neural Dev. *3*, 13.

Tononi, G., and Cirelli, C. (2003). Sleep and synaptic homeostasis: a hypothesis. Brain Res. Bull. *62*, 143–150.

Tononi, G., and Cirelli, C. (2014). Sleep and the price of plasticity: from synaptic and cellular homeostasis to memory consolidation and integration. Neuron *81*, 12–34.

Tremblay, R., Lee, S., and Rudy, B. (2016). GABAergic interneurons in the neocortex: from cellular properties to circuits. Neuron *91*, 260–292.

Ulrich, D. (2016). Sleep spindles as facilitators of memory formation and learning. Neural Plast. *2016*, 1–7.

van Versendaal, D., and Levelt, C.N. (2016). Inhibitory interneurons in visual cortical plasticity. Cell. Mol. Life Sci. *73*, 3677–3691.

Vijayan, S., Lepage, K.Q., Kopell, N.J., and Cash, S.S. (2017). Frontal beta-theta network during REM sleep. Elife *6*.

Villa, K.L., Berry, K.P., Subramanian, J., Cha, J.W., Oh, W.C., Kwon, H.B., Kubota, Y., So, P.T.C., and Nedivi, E. (2016). Inhibitory synapses are repeatedly assembled and removed at persistent sites in vivo. Neuron *89*, 756–769.

de Vivo, L., Bellesi, M., Marshall, W., Bushong, E. a., Ellisman, M.H., Tononi, G., and

Cirelli, C. (2017). Ultrastructural evidence for synaptic scaling across the wake/sleep cycle. Science. *355*, 507–510.

Vorster, A.P., and Born, J. (2015). Sleep and memory in mammals, birds and invertebrates. Neurosci. Biobehav. Rev. *50*, 103–119.

Vyazovskiy, V., Olcese, U., and Lazimy, Y. (2009). Cortical firing and sleep homeostasis. Neuron *63*, 865–878.

Vyazovskiy, V. V, Cirelli, C., Pfister-Genskow, M., Faraguna, U., and Tononi, G. (2008). Molecular and electrophysiological evidence for net synaptic potentiation in wake and depression in sleep. Nat. Neurosci. *11*, 200–208.

Watson, B.O., Levenstein, D., Greene, J.P., Gelinas, J.N., and Buzsáki, G. (2016). Network homeostasis and state dynamics of neocortical sleep. Neuron *90*, 839–852.

Wehr, M.S., and Zador, a. M. (2003). Balanced inhibition underlies tuning and sharpens spike timing in auditory cortex. Nature *426*, 442–446.

Yang, G., Lai, C.S.W., Cichon, J., Ma, L., Li, W., and Gan, W.-B. (2014). Sleep promotes branch-specific formation of dendritic spines after learning. Science. *344*, 1173–1178.

Yavorska, I., and Wehr, M. (2016). Somatostatin-expressing inhibitory interneurons in cortical circuits. Front. Neural Circuits *10*, 76.

Zucker, R.S. (1999). Calcium- and activity-dependent synaptic plasticity. Curr. Opin. Neurobiol. *9*, 305–313.

Acknowledgements

First, I have to thank my research supervisor, Prof. Jan Born. Without his assistance and dedicated involvement in every step during the last seven years, this work would have never been accomplished. I am especially grateful to Jan for giving me all the freedom I needed to develop my own line of research with simultaneously making sure that I did not get lost. His patience, motivation, and immense knowledge together with his continuous support made it a pleasure to work at his institute. He has been a great boss and our discussions at the Boulanger were priceless. I would also like to thank Prof. Hartmut Leuthold for being my second supervisor and his help, support and advice to hand in this thesis.

I thank all my colleagues for the stimulating discussions, for all the shared sweets and for all the fun we have had in Sardinia and Blaubeuren during the last years. Thanks to all the former and current members of the jungle office, it was fantastic to share the office with all of you. In particular, I would like to thank Carlos for always supporting me and our crazy chancho ideas and for our endless bike trips around Europe.

Finally, I would like to thank my friends and family, especially my mother for supporting me throughout all the years. Most importantly, thank you Svenja for all your help, for being with me, for all the moments we shared already and for those that will come.

A   Curriculum Vitae

Personal Information

Name	Niels Alwa Niethard
Date of birth	22. 05. 1985
Place of birth	Kirchheimbolanden
Nationality	German
Office address	Institute of Medical Psychology and Behavioural Neurobiology
	Eberhard Karls Universitat Tubingen
	Ottfried-Muller-Str. 25, 72076 Tubingen
	Phone +49 7071 29889-29
Mail	niels.niethard@uni-tuebingen.de

Education

2006–2012	Diploma in psychology ('with distinction'), University of Innsbruck

Professional and Research experience

Since 09/2012	PhD student, Institute of Medical Psychology and Behavioral Neurobiology, University of Tubingen
2011-2012	Research assistant, Institute of Psychology, University of Innsbruck

Teaching

Since 2016	Seminars in Medical Psychology, University of Tubingen

Awards

09/2017	Trainee Professional Development Award by the Society for Neuroscience, Washington D.C., USA.
03/2015	Stipend awardee: The Brain Conferences; The Brain in Focus: New Approaches to Imaging Neurons and Neural Circuits, Rungstedgaard, Denmark (2016).

B   List of publications

Puentes-Mestril, C., Roach, J., **Niethard, N.**, Zochowski, M., & Aton, S. J. (2019). How rhythms of the sleeping brain tune memory and synaptic plasticity. Sleep, 42(7), 1–14. https://doi.org/10.1093/sleep/zsz095

Niethard, N., & Born, J. (2019). Back to baseline: sleep recalibrates synapses. Nature Neuroscience, 22(2), 149–151. https://doi.org/10.1038/s41593-018-0327-6

Niethard, N., Ngo, H.-V. V, Ehrlich, I., & Born, J. (2018). Cortical circuit activity underlying sleep slow oscillations and spindles. Proceedings of the National Academy of Sciences of the United States of America, 115(39), E9220–E9229. https://doi.org/10.1073/pnas.1805517115

Sawangjit, A., Oyanedel, C. N., **Niethard, N.**, Salazar, C., Born, J., & Inostroza, M. (2018). The hippocampus is crucial for forming non-hippocampal long-term memory during sleep. Nature, 564(7734), 109–113. https://doi.org/10.1038/s41586-018-0716-8

Durán, E., Oyanedel, C. N., **Niethard, N.**, Inostroza, M., & Born, J. (2018). Sleep stage dynamics in neocortex and hippocampus. Sleep, 41(6), 1–11. https://doi.org/10.1093/sleep/zsy060

Niethard, N., Burgalossi, A., & Born, J. (2017). Plasticity during sleep is linked to specific regulation of cortical circuit activity. Frontiers in Neural Circuits, 11, 65. https://doi.org/10.3389/fncir.2017.00065

Niethard, N., Hasegawa, M., Itokazu, T., Oyanedel, C. N., Born, J., & Sato, T. R. (2016). Sleep-stage-specific regulation of cortical excitation and inhibition. Current Biology, 26(20), 2739–2749. https://doi.org/10.1016/j.cub.2016.08.035